CHALMERS
UNIVERSITY OF TECHNOLOGY

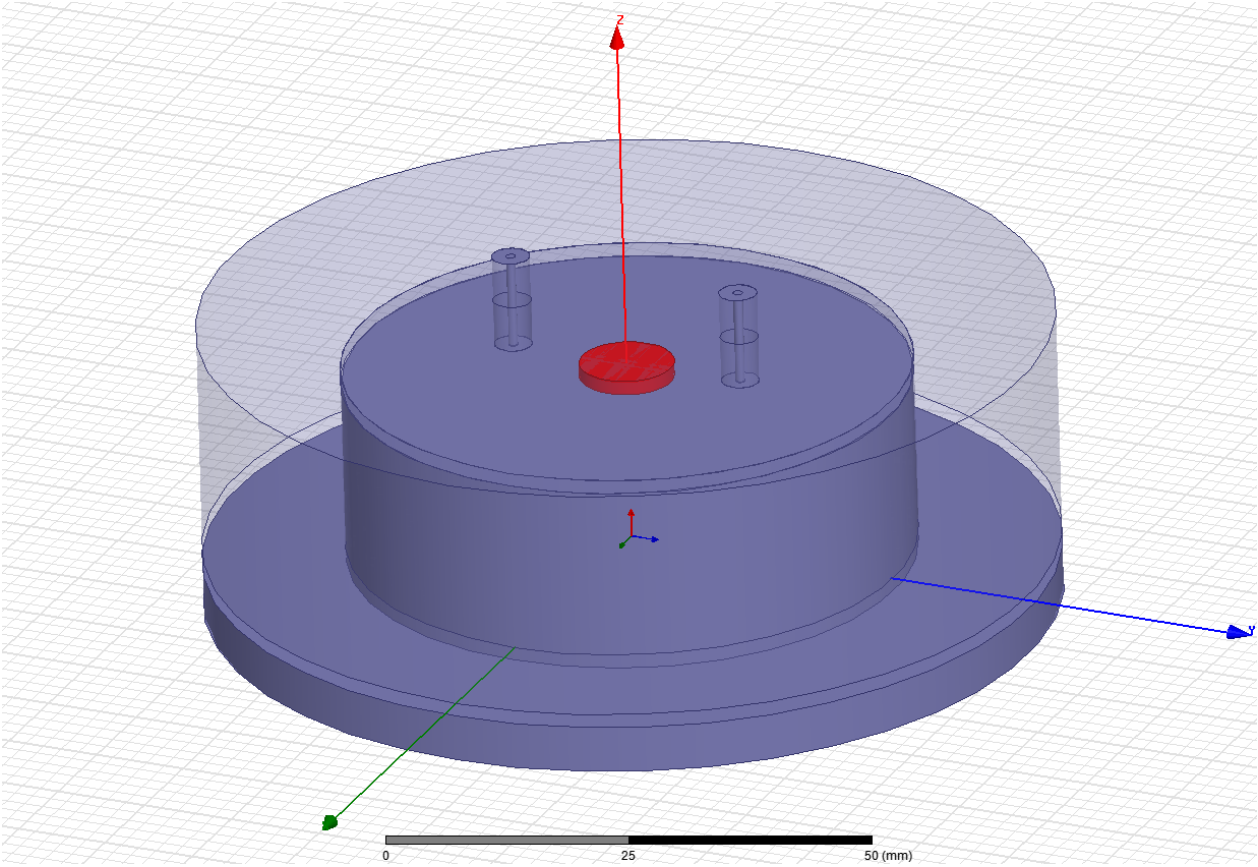

Measurement of Complex Permittivity and Permeability Through a Cavity-Perturbation Method

Master's Thesis in Applied Physics

TOMAS RYDHOLM

Department of Applied Physics
CHALMERS UNIVERSITY OF TECHNOLOGY
Gothenburg, Sweden 2015

Measurement of Complex Permittivity and Permeability Through a Cavity-Perturbation Method

By

Tomas Rydholm

Supervisor:
Joakim Johansson
Antenna Product Unit
RUAG Space AB
Gothenburg, Sweden

Examiner:
Philippe Tassin
Depertment of Applied Physics
Chalmers University of Technology
Gothenburg, Sweden

CHALMERS

Measurement of Complex Permittivity and Permeability
Through a Cavity-Perturbation Theory
Tomas Rydholm

©Tomas Rydholm, 2015

Printed at Chalmers Reproservice
Sven Hultins gata 12
412 96 Gothenburg, Sweden 2015
Telephone: 031-772 8011

This master's degree project was conducted at RUAG Space in Gothenburg, Sweden.

Cover: The cavity resonator designed in this project as it appears in ANSYS HFSS, the program used for simulations. The red disc in the middle of the cavity represents the sample.

Measurement of Complex Permittivity and Permeability Through a Cavity-Perturbation Method

Tomas Rydholm
Department of Applied Physics
Chalmers University of Technology

Abstract

Fabrication of antenna and microwave devices demands good knowledge of certain material parameters such as permittivity and permeability, including their corresponding losses. The project presented in this master's degree thesis aims to develop an experimental setup to measure these properties at microwave frequencies. A cylindrical cavity resonator was designed for a cavity perturbation method. In this method, it is studied how the resonance frequencies shift as a sample is inserted into the cavity resonator. The permittivity and permeability can be determined from this frequency shift and the loss parameters can be obtained from the broadening of the resonance peaks in the spectrum.
An alternative method is developed, in which the measurements are compared to data obtained from simulations. A set of curves or contour lines, describing the resonance frequency of a specified mode, is plotted as function of the permittivity and permeability. By performing two measurements where the sample is placed at two different positions in the cavity, the material properties can be determined from the point where the two curves cross each other. We refer to this new method as the "curve-set method".
Simulations indicate that the cavity-perturbation method can be used together with the designed cavity resonator to measure the permittivity and dielectric loss tangent accurately for nonmagnetic materials. However, it seems difficult to measure the permeability and magnetic loss tangent. On the other hand, the curve-set method appears to be a possible way to determine both the permittivity and the permeability, given that the simulations represent experiments accurately.

Keywords: permittivity, permeability, dielectric loss, magnetic loss, cavity resonator, resonance frequency, cavity-perturbation method

Contents

Notation and abbreviations

α	Attenuation constant
β	Phase constant
γ	Propagation constant
ε	Permittivity
$\boldsymbol{\Phi}$	ϕ-dependent part of separable field
ϕ	Azimuthal coordinate
μ	Permeability
χ_e	Electric susceptibility
χ_m	Magnetic susceptibility
ω	Angular frequency
A	Calibration parameter
a	Cavity radius
$\boldsymbol{B}$	Magnetic flux density
B	Calibration parameter
C	Arbitrary field amplitude
C	Calibration parameter
c	Speed of light
$\boldsymbol{D}$	Electric displacement field
$\boldsymbol{E}$	Electric field
$\boldsymbol{e}$	z-independent part of electric field
f	Frequency
FEM	Finite element method
$\boldsymbol{H}$	Magnetic field
$\boldsymbol{h}$	z-independent part of magnetic field
$J_n(x)$	Bessel function of the first kind and order n
j	Imaginary unit
k_c	cutoff wavenumber
l	Cavity length

$\boldsymbol{M}$	Magnetization field
$\boldsymbol{P}$	Polarization field
$\mathcal{P}$	Cauchy principal value
P	Average dissipation of energy
PCB	Printed circuit board
R	r-dependent part of separable field
r	Radial coordinate
Q	Quality factor (Q-factor)
S	Scattering parameter (S-parameter)
SUT	Sample under test
$\tan\delta_e$	Dielectric loss tangent
$\tan\delta_m$	Magnetic loss tangent
TE	Transverse electric
TEM	Transverse electromagnetic
TM	Transverse magnetic
u_{nm}	m^{th} root of the Bessel function of order n
V	Voltage
V_C	Cavity volume
V_S	Sample volume
W	Total electromagnetic energy
$Y_n(x)$	Bessel function of second kind and order n
z	Longitudinal coordinate

Chapter 1

Introduction

This master's degree project has been carried out at Ruag Space AB in Gothenburg. Ruag is a manufacturer of satellite equipment such as antennas and microwave electronics. Within antenna and microwave technology, it is important to have good knowledge of certain material parameters to obtain products of high quality. Accurately known parameter values may also shorten the product development time by eliminating the "trial-and-error" phase of the system optimization procedure. Examples of such parameters are the complex valued permittivity ε and permeability μ. These parameters are often provided with an undesirably high uncertainty by the supplier and it is in the interest of Ruag to construct an experimental setup to measure these parameters accurately.

1.1 Problem formulation

The purpose of this project is to design an experimental setup that can be used to measure the permittivity and permeability accurately. The goal is to to determine the real part of the relative permittivity ε_r to the first decimal place and to determine the order of magnitude of the dielectric loss tangents. Preferably, the relative permeability μ_r and magnetic loss tangent should be possible to measure with the same accuracy as well. The frequency range of interest is 0.4–40 GHz, although it is unlikely that a single setup can cover the entire interval.

1.1.1 Limitations

The project is limited to dielectric materials. Metals will thus not be considered. We also restrict ourselves to homogeneous and isotropic materials.

In addition, there are some practical restrictions. For example, the materials of interest are often provided in sheets. Samples are therefore most easily shaped like

discs. These cannot be fabricated arbitrarily small, and a radius no less then 5 mm is recommended. The experimental setup itself should also be of "appropriate" dimensions. Reasonable dimensions are around 100 mm.

1.2 Measurement methods

The relative permittivity and dielectric loss of a material can be measured in a vast number of ways [1, 2]. In a rough generalization, they can be divided into resonant and non-resonant methods [2]. In resonant methods these parameters are determined by either studying the resonance frequency of the sample itself or by observing how the resonance of the system is shifted by introducing a sample of the material into the experimental setup. In non-resonant methods on the other hand, the parameters are obtained directly from studying the reflections and transmissions of an incoming signal. The parameters of interest can then be determined from the coefficients of reflection and transmission. In general, resonator methods are more accurate but lack the ability of frequency sweeps [2]. They are thus limited to discrete frequencies.

The experimental setups may also be categorized after their physical appearance. Measurements can, for example, be performed by introducing the sample into a cavity, by fabrication of microstrips/stripline or by open-air wave reflection. Below, a few different techniques that have been considered in this project are presented.

1.2.1 Hakki-Coleman resonator

The Hakki-Coleman resonator was developed in 1960 [3] and further developed by Courtney in 1970 [4]. It is therefore also referred to as the Courtney resonator. The sample under test (or SUT for short) takes the role of a dielectric resonator and is placed between two shorted and in theory infinitely large conducting planes. Two probes are also introduced to excite and measure an electromagnetic field, see Figure 1.1.

This setup has the advantage that even though air gaps may be present between the conductors and the sample, which in general affect the result, the TE_{011} mode may be used to eliminate this problem. This particular mode will not have an electric field directed normally to the sample-conductor interface and hence air gaps will not cause problems. There also exist analytical solutions to the permittivity. A drawback is that the measurements are limited to the resonance frequencies and thus a set of samples are needed to cover different frequencies. One might also argue that the non-closed system could give rise to radiation losses. However, by dimensioning the setup correctly, this may be avoided [4]. Furthermore, an

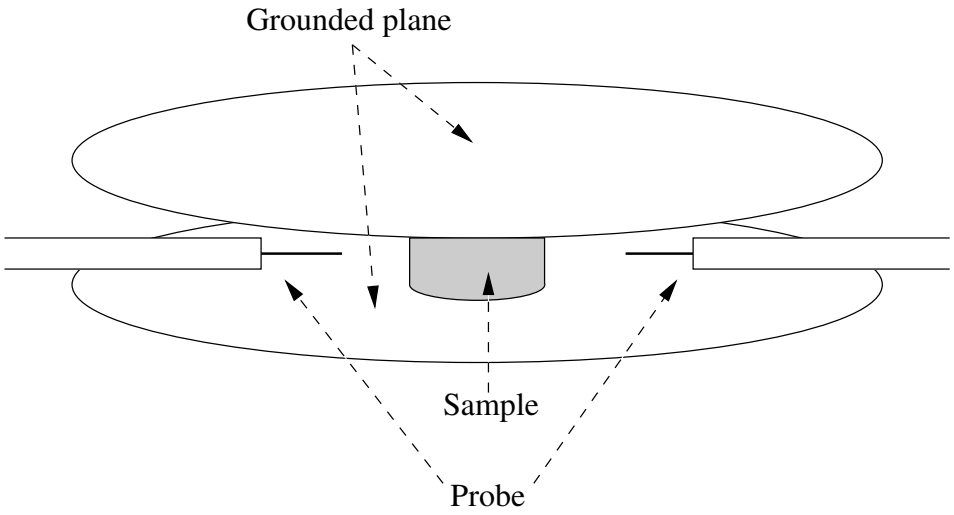

Figure 1.1: The Hakki-Coleman resonator.

accuracy better than one percent for the real parts of ε_r and μ_r as well as $5 \cdot 10^{-5}$ for the dielectric loss tangent has been obtained [4]. Values around 10^{-5} with an accuracy of one percent should be possible to measure for the imaginary part of μ_r [4]. A fact that speaks in favor of this technique is that it is an International Electrotechnical Commission (IEC) standard for dielectric measurements [5].

1.2.2 Cavity-perturbation methods

A somewhat similar technique utilizes closed cavities, often of cylindrical or rectangular shapes. An empty cavity has a certain resonance frequency. By inserting a dielectric sample, this resonance is shifted and the dielectric properties may be determined thereof.

These techniques are examples of cavity-perturbation methods and there exist a range of different implementations. The easier ones utilize an ordinary cavity and the sample properties are determined from the frequency shift. This is a common method for property measurements and often the TE_{011} or TM_{010} modes are used in the case of cylindrical cavity resonators [2]. In this method, the frequency is restricted to the resonance of the cavity. Either an adjustable cavity or many different cavities are needed to cover the whole spectrum.

As will be seen in the theoretical treatment below, the treatment used in these perturbation methods is only valid when measurements are performed at the same frequency before and after the introduction of the sample. Therefore, more advanced methods exist where the shape of the cavity is altered to cancel the frequency shift [2]. Such methods operate at quasi TE_{011} modes, often referred to

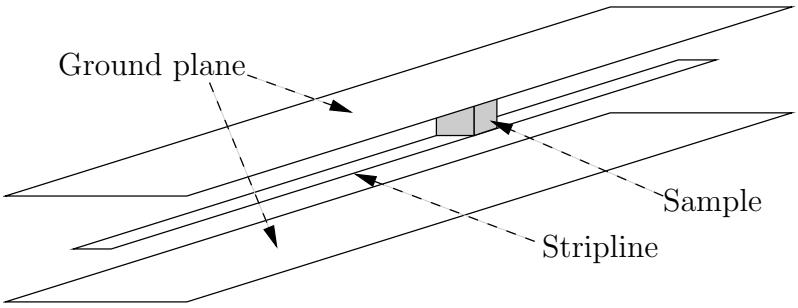

Figure 1.2: Schematic sketch of a stripline cavity.

as $TE_{01\delta}$ modes. However, these demand a rigorous numerical treatment [2] and an adjustable cavity length may introduce mechanical measurement errors. On the other hand, it is also stated to be more accurate than the Hakki-Coleman resonator [2]. The treatment is known to give accurate values for samples of low and medium losses [2]. Cavity-perturbation methods are known to be limited to samples of relative permittivity less than 10 [4].

1.2.3 Stripline

Perturbation measurements can also be performed by using an open stripline cavity [6, 7]. This is basically a planar transmission line placed between two other grounded conducting planes. Similarly, introduction of a dielectric sample will shift the resonance of the system and the material properties can be obtained from this frequency shift. The setup is presented in Figure 1.2.

The propagating wave will be a transverse electromagnetic (TEM) wave. Therefore, the electric field may be directed between the mid conductor and the grounded plane and thus normal to the sample-conductor interface. Hence, air gaps will not be as easy to avoid and might give rise to problems. A good property is, however, that the setup allows the use of harmonics and a single setup can be used to measure the properties at up to around ten different frequencies in a wide range [7]. Still, more than one setup is needed to cover the entire desired spectrum unless an adjustable setup can be fabricated.

1.2.4 Waveguide

Waveguides are examples of non-resonant techniques. Instead of studying how the resonance frequency shifts, the scattering parameters are directly studied to determine the material properties. The advantage is that a single setup can be used to measure a continuous spectrum, in an interval depending on the waveguide dimensions [2].

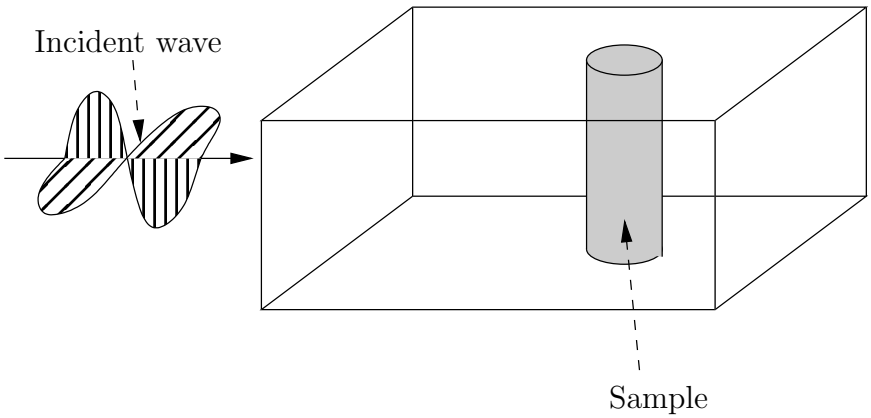

Figure 1.3: Schematic sketch of the waveguide setup.

The proposed technique would use rod shaped samples and TE_{01} modes to avoid the effects of air gaps, much like the Hakki-Coleman method discussed above, see Figure 1.3. However, this sample shape would not be easy to fabricate.

1.2.5 Microstrip

Another way to get around the problem of air gaps is to use microstrip lines etched directly onto the dielectric substrate. The properties of microstrips make them suitable for measurements in the range 100 MHz–12 GHz [8]. Studies of resonances in microstrips have resulted in accuracies of around one percent for the relative permittivity of the substrate [9].

The usability of this technique is related to how easy they are to fabricate. If many samples can be produced at a low cost, a wide frequency range would be possible to cover. On the other hand, a conductive surface has to be applied. This process might alter the material and its properties. Therefore, the microstrip methods are suitable for materials that are already covered by a metal layer, such as PCB (Printed circuit board) materials.

1.2.6 Other techniques

Other possible techniques involve interferometers [10, 11, 12, 13, 14], free-space reflection and transmission [15, 16, 17], and near-field microwave microscopes [18].

Interferometric methods have both shown the possibility of high accuracy [12] and wide frequency bands [14]. However, interferometric methods are sensitive to the mechanical settings and the setups are quite complicated compared to cavity, stripline and waveguide techniques. Hence, as a restriction to the project, these methods are not considered.

For similar reasons, the free-space methods are omitted. For example, tilting the sample will affect the reflections [15]. On the other hand, effects from air gaps are avoided [2].

Near-field microwave microscopes are quite complicated compared to other methods but have the advantage that materials with non-homogeneous properties can be characterized [18]. However, this lies outside the scope of this project and microscopes will therefore not be evaluated.

1.3 Choice of method

As seen in the descriptions above, different methods have different advantages and disadvantages. The choice of a suitable method is, therefore, based on a number of decisions. For example, if we want to measure a continuous spectrum the number of possible methods is quickly reduced compared to if a discrete number of frequencies can be regarded. In addition, the parameters that need to be measured also plays a role in the choice. For example, some methods are only suitable for measuring the permittivity, whereas others can be used for the permittivity as well as the permeability.

The spectrum of interest is 0.4–40 GHz. Finding a technique that can cover this interval is problematic. The dimensions of the setups will depend on the frequency studied, either to make sure that certain modes can be excited or that they *cannot* be excited. For example, a rectangular waveguide of width a has a cutoff frequency f_c given by equation (1.1), below which no frequencies will propagate [19].

$$f_c = \frac{c}{2a}, \tag{1.1}$$

where c is the speed of light. As a consequence, setups allowing for low frequencies tend to be quite large. As an example, we turn to the Cavity-perturbation method described in Section 1.2.2. The resonance frequency for the TE_{nmp} or TM_{nmp} mode is given by [19]

$$f_{nmp} = \frac{c}{2\pi\sqrt{\mu_r\varepsilon_r}}\sqrt{\left(\frac{u_{nm}}{a}\right)^2 + \left(\frac{p\pi}{l}\right)^2} \tag{1.2}$$

where a and l are the radius and length of the cavity; n, m and p determine the mode and u_{nm} is the m^{th} root of either the n^{th} ordered Bessel function (TM modes) or its derivative (TE modes). In Figure 1.4 we present the needed cavity length and radius in order to obtain certain resonance frequencies for the commonly used TE_{011} modes. As seen, the dimensions needed to reach the lower limit of interest are quite large whereas either the radius or the length has to be much smaller than the other to reach the upper limit. For this particular setup and mode, we could

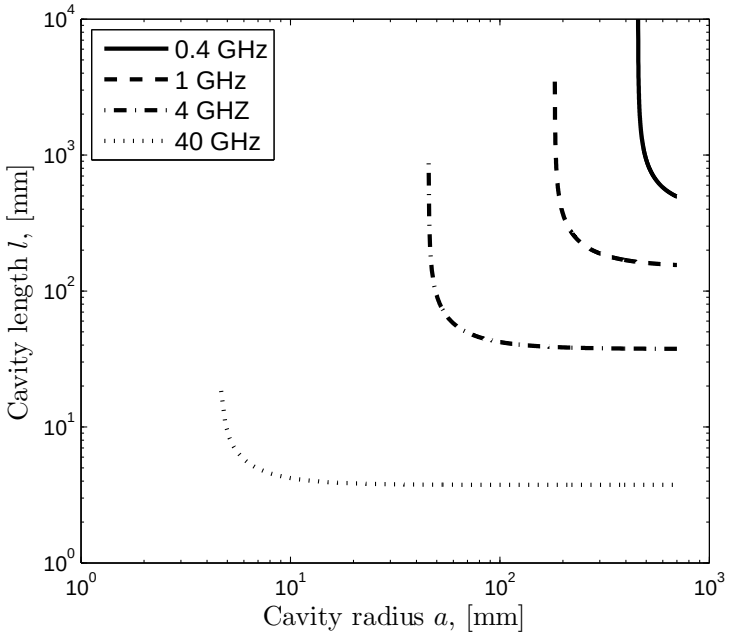

Figure 1.4: The cavity length as function of the radius in order to obtain a certain resonance frequency for the TE_{011} mode.

cover the whole interval by using a cavity of radius 600 mm and a length that can be varied between 3.7 and 580 mm. This is, of course, not a realistic scenario.

For the stripline setup, the frequencies are related to the length of the stripline and the distance between the stripline and ground planes. The length of the stripline equals half of the wavelength corresponding to the lowest frequency that can be studied. Simultaneously, the distance between the stripline and ground planes should not be larger than a quarter of the wavelength corresponding to the highest frequency to avoid excitations of unwanted modes [7]. The top frequency as function of this separation is presented in Figure 1.5 and the lower limit is presented in Figure 1.6. The dimensions of this setup become quite reasonable. In addition, one single setup can be used to measure up to ten different frequencies. Unfortunately, previous studies have shown that the errors can be fairly large [7].

The microstrip technique is common to use in the interval 100 MHz–12 GHz [8] and thus covers a large part of the interval of interest. On the other hand, these methods are suitable for PCB materials as discussed above. The properties of such materials are usually accurately provided by the supplier. These techniques will therefore not be considered further.

Hence, there are three methods that might be of interest; the Hakki-Coleman resonator, the cavity-perturbation method, and the waveguide containing a rod-

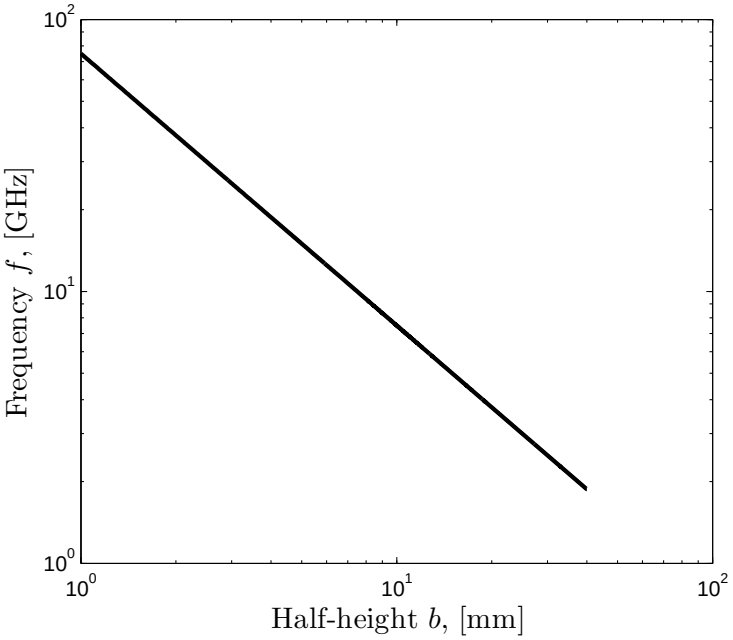

Figure 1.5: Upper frequency limit as function of the distance between the stripline and a grounded plane.

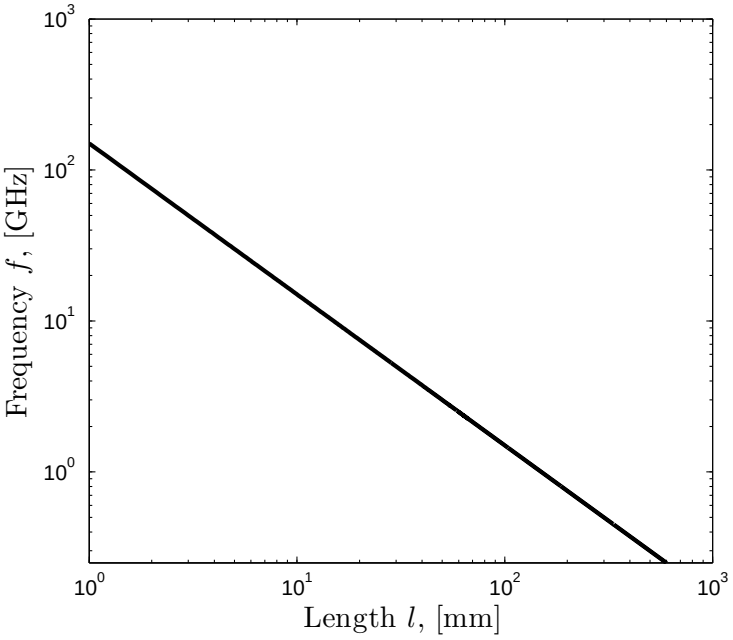

Figure 1.6: Lower frequency limit as function of the stripline length.

Table 1.1: Comparison of different techniques. "Anisotropic", "Inhomogeneous" and "Shape" refer to the properties and shapes of the sample one wants to test.

Method	Frequencies	Anisotropic	Inhomogeneous	Shape
Hakki-Coleman	Discrete	No	No	Disc/rod
Cavity-perturbation	Discrete	No	No	Disc/rod
Stripline	Discrete	Yes	No	Block
Waveguide	Continuous	No	No	Rod
Microstrip	Discrete	No	No	Sheet
Interferometer	Continuous	—	—	—
Microscopy	—	—	Yes	—

shaped sample. However, the latter of these will not be considered since it will not in general be possible to shape the samples as rods. A comparison of all presented techniques are summarized in Table 1.1.

A cavity resonator is a closed system, which will minimize the problem of radiation loss. As previously mentioned, it should be possible also in the Hakki-Coleman method to avoid this loss by a careful choice of dimensions. However, we will in this project restrict ourselves to the cavity-perturbation method and design a cavity resonator since it previously has proven to be the more accurate method.

1.4 Outline of the report

In this chapter, we have discussed some possible techniques that previously have been used to measure permittivity and permeability. We have determined that a cavity-perturbation method should be a suitable technique due to our interests and the restrictions made.

In this project, a cavity resonator has been designed to operate in the desired frequency range, although at discrete frequencies. Simulations were conducted with the Finite Element Method (FEM) solver Ansys HFSS as an aid in the design process. Simulation specifications are given in Section 1.5. The same program was then used to evaluate the resonator and to test the validity of the cavity-perturbation method. Finally, some experimental measurements were performed to investigate the validity of the method.

This report is divided as follows. The second chapter is devoted to the theoretical background. The focus of the chapter is on the description of the modes in a cylindrical cavity and how the resonances are shifted by insertion of a sample. We then move on to the third chapter which is divided into two parts. First, the design procedure is covered and we discuss the design of the cavity. The second part describes the measurement procedure of the cavity-perturbation method and

how it differs depending on what property we want to measure. The fourth chapter presents the results. Here, we present the results of the simulations and experiments and discuss the accuracy when measuring the different properties. Finally, we summarize the project in the concluding chapter. We discuss the results and problems of the project and give some suggestions for further development.

1.5 Simulation specifications

The simulations were performed in Ansys HFSS (version 15), which has a few different solution types. For frequency sweeps, the solution type was set to "Driven Terminal" with the following specifications:

- Maximum Number of Passes: 10
- Maximum Delta S: 0.02
- Maximum refinement per pass: 30%
- Minimum number of converged passes: 3
- First order basis functions
- Direct solver
- Sweep type: Discrete

For the eigenvalue simulations, the solution type was set to "Eigenmode" with the following specifications:

- Maximum number of Passes: 5
- Maximum Delta Frequency Per Pass: 10 %
- Maximum refinement per pass: 30%
- Minimum number of converged passes: 3
- First order basis functions

These choices resulted in converging solutions. One could of course generate an even finer mesh but this leads to longer computation times and does not necessarily improve the results. This was considered a suitable compromise between time and precision.

Chapter 2

Theory

In this chapter we will give a theoretical explanation of the method. We start by giving a brief discussion on the permittivity and permeability and what these parameters depend on. We then move on to a derivation of the resonant modes of a circular cavity resonator and how these modes are affected by introducing a dielectric or magnetic sample. In particular we investigate the case when this sample can be treated as a small perturbation. Finally, we give a short description of different coupling devices that can be used to excite the cavity resonator.

2.1 Material properties

In this project we are interested in how materials affect electromagnetic fields. The corresponding material parameters are the permittivity ε for electric fields and the permeability μ for magnetic fields.

2.1.1 Permittivity

For isotropic materials, the permittivity is related to the polarization of the material through

$$\begin{aligned} \boldsymbol{D} &= \varepsilon_0 \boldsymbol{E} + \boldsymbol{P} \\ &= \varepsilon_0 \boldsymbol{E} + \varepsilon_0 \chi_e \boldsymbol{E} \\ &= \varepsilon_0 (1 + \chi_e) \boldsymbol{E} \\ &= \varepsilon_0 \varepsilon_r \boldsymbol{E}, \end{aligned} \tag{2.1}$$

where $\boldsymbol{D}$ is the electric displacement field, $\boldsymbol{E}$ is the electric field, $\boldsymbol{P}$ is the polarization field, and χ_e is the dielectric susceptibility of the material [20]. Bold symbols here denote vectors. In addition, the permittivity of the material is related to the

vacuum permittivity ε_0 and the relative permittivity ε_r of the material through

$$\varepsilon = \varepsilon_0 \varepsilon_r. \tag{2.2}$$

Thus, it is possible in theory to determine the permittivity from the knowledge of how the material is polarized by an external field. We can relate the susceptibility to the molecular polarizability of the material. Displacement of free ions in the material or of the electron cloud of individual atoms contributes to this polarizability. In addition, some molecules have permanent dipole moments which is also a contributing factor [21]. We shall here only give a qualitative description of the phenomenon. For a further treatment, readers are referred to Ramo *et al.* [21].

For materials showing a lossy behavior, the permittivity becomes complex-valued.

$$\varepsilon_r = \varepsilon_r' - \mathrm{j}\varepsilon_r'' \tag{2.3}$$

It is the imaginary part ε_r'' that determines the dielectric losses. However, it is often more convenient to consider the ratio between these two terms. We therefore define the dielectric loss tangent as

$$\tan \delta_e = \frac{\varepsilon_r''}{\varepsilon_r'}. \tag{2.4}$$

When an electron cloud or single ions are shifted, a restoring force will act on it. The system can be compared to a mechanical system of weights connected with springs. Naturally, the resonant frequencies of the ions will be lower since the ions are heavier. These resonances also appear in the permittivity [21]. A qualitative graphical description adapted from Ramo *et al.* [21] is presented in Figure 2.1. The important thing to note here is that the permittivity is more or less constant for low frequencies. In general, it would be sufficient to measure the permittivity at a single frequency in the regime of interest and it will give a fairly good picture of the permittivity, maybe not for the entire interval 0.4–40 GHz but at least in the lower microwave regime.

There is an interesting relation between the real and imaginary parts of a complex-valued function $f(z)$, given that it is analytic on the real axis and in the upper half-plane, and that the function tends to zero sufficiently fast for large $|z|$, called the Kramers-Kronig relations [20, 22]:

$$\varepsilon'(\omega) = \varepsilon_0 + \frac{2}{\pi}\mathcal{P}\int_0^\infty \mathrm{d}\omega' \, \frac{\omega' \varepsilon''(\omega')}{\omega'^2 - \omega^2} \tag{2.5}$$

$$\varepsilon''(\omega) = -\frac{2\omega}{\pi}\mathcal{P}\int_0^\infty \mathrm{d}\omega' \, \frac{\varepsilon'(\omega') - \varepsilon_0}{\omega'^2 - \omega^2}. \tag{2.6}$$

Here, $\mathcal{P}$ denotes that one should take the Cauchy principal value of the integral. In other words, it is in theory sufficient to know either the real or imaginary part of the permittivity, given that we know it for all frequencies. This will not be the case in this project, but it is an interesting fact nonetheless.

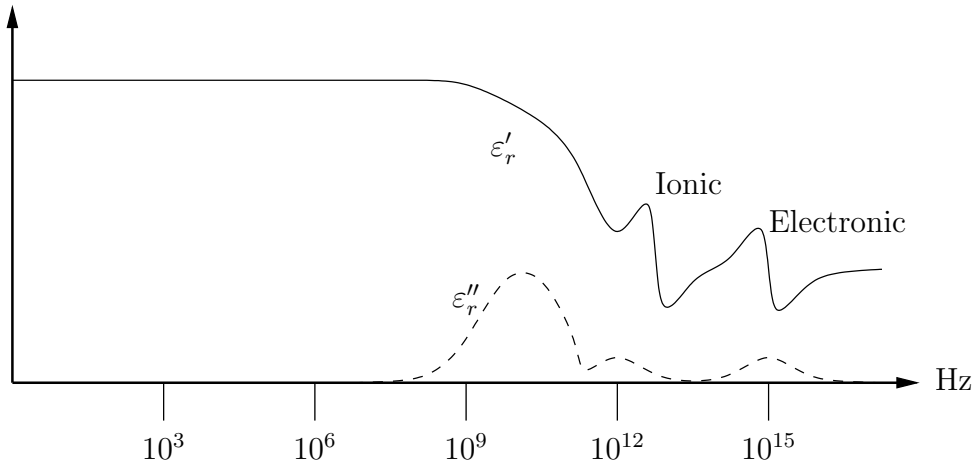

Figure 2.1: Qualitative description of the permittivity as function of frequency. Adapted from Ramo *et al.* [21].

2.1.2 Permeability

The corresponding property for magnetic fields is the magnetic permeability μ, related to the magnetization $\boldsymbol{M}$ of the material through

$$\begin{aligned} \boldsymbol{B} &= \mu_0(\boldsymbol{H} + \boldsymbol{M}) \\ &= \mu_0(\boldsymbol{H} + \chi_m \boldsymbol{H}) \\ &= \mu_0(1 + \chi_m)\boldsymbol{H} \\ &= \mu_0 \mu_r \boldsymbol{H}, \end{aligned} \tag{2.7}$$

where $\boldsymbol{B}$ is the magnetic flux density, $\boldsymbol{H}$ is the magnetic field, andχ_m is the *magnetic* susceptibility [20]. Just as for the permittivity, μ is the product of the vacuum permeability μ_0 and the relative permeability μ_r and is in general a complex parameter

$$\mu_r = \mu_r' - \mathrm{j}\mu_r''. \tag{2.8}$$

We may then define the magnetic loss tangent as

$$\tan \delta_m = \frac{\mu_r''}{\mu_r'}. \tag{2.9}$$

The permeability of a material depends on the atomic dipoles and a contributing factor is the spin of the electrons [23]. The value may vary strongly with the frequency and it is in general not possible to use the constant approximation utilized in the case of permittivity [2]. A qualitative graphical description adapted from Chen *et al.* [2] is presented Figure 2.2.

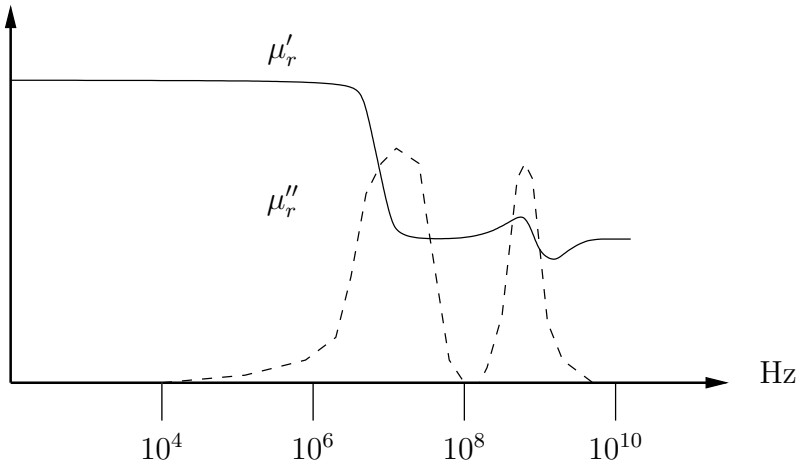

Figure 2.2: Qualitative description of the permeability as function of frequency. Adapted from Chen *et al.* [2].

2.2 Analytical treatment of a cylindrical cavity

We will here treat the field profiles of a cylindrical cavity of radius a and length l. For an empty cavity, it is possible to find analytical expressions for the field profiles, which will be derived in this section. In this project, we shall consider two types of modes: transverse electric (TE) modes and transverse magnetic (TM) modes. TE modes have no electric component in the direction of propagation whereas TM modes have no such magnetic component. There are also hybrid modes that do not fall into this categorization. However, these lie outside the scope of the project. The E- and H-fields can be separated into two factors, one independent on the direction of propagation and one dependent on the direction of propagation:

$$\boldsymbol{E}(r,\phi,z) = \boldsymbol{e}(r,\phi)\exp(\mp\gamma z) \tag{2.10}$$
$$\boldsymbol{H}(r,\phi,z) = \boldsymbol{h}(r,\phi)\exp(\mp\gamma z). \tag{2.11}$$

where γ is the propagation constant, given by

$$\gamma = \alpha + \mathrm{j}\beta. \tag{2.12}$$

α is known as the attenuation constant and β as the phase constant. The z-independent part of the fields can then be split into the transverse $\boldsymbol{e}_\perp$ and $\boldsymbol{h}_\perp$, as well as the longitudinal $\boldsymbol{e}_z$ and $\boldsymbol{h}_z$:

$$\boldsymbol{E}(r,\phi,z) = (\boldsymbol{e}_\perp(r,\phi) + \boldsymbol{e}_z(r,\phi))\exp(\mp\gamma z) \tag{2.13}$$
$$\boldsymbol{H}(r,\phi,z) = (\boldsymbol{h}_\perp(r,\phi) + \boldsymbol{h}_z(r,\phi))\exp(\mp\gamma z), \tag{2.14}$$

where

$$\boldsymbol{e}_\perp(r,\phi) = e_r(r,\phi)\hat{r} + e_\phi(r,\phi)\hat{\phi} \tag{2.15}$$
$$\boldsymbol{e}_z(r,\phi) = e_z(r,\phi)\hat{z} \tag{2.16}$$
$$\boldsymbol{h}_\perp(r,\phi) = h_r(r,\phi)\hat{r} + h_\phi(r,\phi)\hat{\phi} \tag{2.17}$$
$$\boldsymbol{h}_z(r,\phi) = h_z(r,\phi)\hat{z}. \tag{2.18}$$

We will omit the arguments where they are not necessary in the following derivation. Similarly, we can split the gradient into a transverse and a longitudinal part:

$$\nabla = \nabla_\perp + \hat{z}\partial_z. \tag{2.19}$$

Here we will derive the mode profiles in a cylindrical cavity filled with air. Air is essentially free from dielectric losses and we shall therefore assume that the attenuation constant $\alpha = 0$, i.e. the propagation constant γ is purely imaginary:

$$\gamma = \mathrm{j}\beta. \tag{2.20}$$

We also assume that the permittivity and permeability equal the values in vacuum, ε_0 and μ_0. Inspired by the work of Collin [24], we start from Maxwell's equations.

$$\begin{aligned}
\nabla \times \boldsymbol{E} &= -\partial_t \mu_0 \boldsymbol{H} \\
(\nabla_\perp + \hat{z}\partial_z) \times (\boldsymbol{e}_\perp + \boldsymbol{e}_z) \exp(\mp\mathrm{j}\beta z) &= -\mathrm{j}\omega\mu_0(\boldsymbol{h}_\perp + \boldsymbol{h}_z) \exp(\mp\mathrm{j}\beta z) \\
(\nabla_\perp \mp \mathrm{j}\beta\hat{z}) \times (\boldsymbol{e}_\perp + \boldsymbol{e}_z) &= -\mathrm{j}\omega\mu_0(\boldsymbol{h}_\perp + \boldsymbol{h}_z) \\
\nabla_\perp \times \boldsymbol{e}_\perp \mp \mathrm{j}\beta\hat{z} \times \boldsymbol{e}_\perp - \hat{z} \times \nabla_\perp e_z &= -\mathrm{j}\omega\mu_0(\boldsymbol{h}_\perp + \boldsymbol{h}_z)
\end{aligned}$$

Treating the perpendicular and axial components individually we can write this as

$$\nabla_\perp \times \boldsymbol{e}_\perp = -\mathrm{j}\omega\mu_0 \boldsymbol{h}_z \tag{2.21}$$
$$\mp\mathrm{j}\beta\hat{z} \times \boldsymbol{e}_\perp - \hat{z} \times \nabla_\perp e_z = -\mathrm{j}\omega\mu_0 \boldsymbol{h}_\perp. \tag{2.22}$$

We also have

$$\begin{aligned}
\nabla \cdot \mu_0 \boldsymbol{H} &= 0 \\
(\nabla_\perp + \hat{z}\partial_z) \cdot \mu_0(\boldsymbol{h}_\perp + \boldsymbol{h}_z) \exp(\mp\mathrm{j}\beta z) &= 0 \\
(\nabla_\perp \cdot \boldsymbol{h}_\perp \mp \mathrm{j}\beta\hat{z} \cdot \boldsymbol{h}_z)\mu_0 \exp(\mp\mathrm{j}\beta z) &= 0
\end{aligned}$$

yielding

$$\nabla_\perp \cdot \boldsymbol{h}_\perp = \pm\mathrm{j}\beta h_z \tag{2.23}$$

Analogously, using $\nabla \times \boldsymbol{H} = \partial_t \varepsilon_0 \boldsymbol{E}$ and $\nabla \cdot \varepsilon_0 \boldsymbol{E} = 0$, we get

$$\nabla_\perp \times \boldsymbol{h}_\perp = \mathrm{j}\omega\varepsilon_0 \boldsymbol{e}_z \tag{2.24}$$
$$\mp\mathrm{j}\beta\hat{z} \times \boldsymbol{h}_\perp - \hat{z} \times \nabla_\perp h_z = \mathrm{j}\omega\varepsilon_0 \boldsymbol{e}_\perp \tag{2.25}$$
$$\nabla_\perp \cdot \boldsymbol{e}_\perp = \pm\mathrm{j}\beta e_z. \tag{2.26}$$

2.2.1 Field profiles of TM modes in a cylindrical cavity

For TM modes, we set $h_z = 0$ and obtain the following equations:

$$\nabla_\perp \times \boldsymbol{e}_\perp = 0 \tag{2.27}$$
$$\mp \mathrm{j}\beta\hat{z} \times \boldsymbol{e}_\perp - \hat{z} \times \nabla_\perp e_z = -\mathrm{j}\omega\varepsilon_0 \boldsymbol{h}_\perp \tag{2.28}$$
$$\nabla_\perp \cdot \boldsymbol{h}_\perp = 0 \tag{2.29}$$
$$\nabla_\perp \times \boldsymbol{h}_\perp = \mathrm{j}\omega\varepsilon_0 \boldsymbol{e}_z \tag{2.30}$$
$$\mp \mathrm{j}\beta\hat{z} \times \boldsymbol{h}_\perp = \mathrm{j}\omega\mu_0 \boldsymbol{e}_\perp \tag{2.31}$$
$$\nabla_\perp \cdot \boldsymbol{e}_\perp = \pm \mathrm{j}\beta e_z. \tag{2.32}$$

We then seek the solution to the wave equation for the longitudinal electric field:

$$\nabla_\perp^2 e_z + k_c^2 e_z = 0, \tag{2.33}$$

where k_c is the cutoff wave number. Due to the cylindrical symmetry of the cavity, we can express this relation as

$$\frac{\partial^2 e_z}{\partial r^2} + \frac{1}{r}\frac{\partial e_z}{\partial r} + \frac{1}{r^2}\frac{\partial^2 e_z}{\partial \phi^2} + k_c^2 e_z = 0. \tag{2.34}$$

By using separation of variables, $e_z = \Phi(\phi)R(r)$, this can be rewritten as

$$\Phi(\phi)R''(r) + \frac{1}{r}\Phi(\phi)R'(r) + \frac{1}{r^2}\Phi''(\phi)R(r) + k_c^2\Phi(\phi)R(r) = 0 \tag{2.35}$$

$$r^2\frac{R''(r)}{R(r)} + r\frac{R'(r)}{R(r)} + r^2 k_c^2 = -\frac{\Phi''(\phi)}{\Phi(\phi)}, \tag{2.36}$$

where the primes now refer to derivatives with respect to the argument. Note that the left-hand side only depend on r, whereas the right-hand side only depends on ϕ. The equation is thus separable and we may conclude that both expressions are constant and we choose them to equal n^2 for reasons that will soon become clear. We may thus write

$$r^2 R''(r) + rR'(r) + (r^2 k_c^2 - n^2)R(r) = 0 \tag{2.37}$$
$$\Phi''(\phi) + n^2\Phi(\phi) = 0. \tag{2.38}$$

Equation (2.37) is solved by the Bessel functions of the first kind whereas Equation (2.38) is solved by sine and cosine functions:

$$R(r) = C_1 J_n(k_c r) + C_2 Y_n(k_c r) \tag{2.39}$$
$$\Phi(\phi) = C_3 \cos n\phi + C_4 \sin n\phi. \tag{2.40}$$

For physical reasons we may draw a few conclusions. First, the solution should be periodic in ϕ. Hence, n should be an integer. Second, the angle can be chosen arbitrarily up to a phase and we may choose to use just the cosine or the sine term. We thus set $C_4 = 0$. Third, $Y_n(k_c r)$ is singular at $r = 0$ and should, therefore, be omitted. Finally, the metallic boundary condition states that e_z should vanish at $r = a$. By denoting the m^{th} zero of $J_n(k_c r)$ as u_{nm}, the cutoff frequency can be written as

$$k_c = \frac{u_{nm}}{a}. \tag{2.41}$$

Combining all these conclusions, we can write e_z as

$$e_z = \tilde{C} \cdot J_n\left(\frac{u_{nm} r}{a}\right) \cos n\phi, \quad n = 0,1,2... \tag{2.42}$$

Now, we return to Equations (2.27) to (2.32) to obtain expressions for the transverse field components.

$$\begin{aligned} \nabla_\perp \times (\nabla_\perp \times e_\perp) = \nabla_\perp(\nabla_\perp \cdot \boldsymbol{e}) - \nabla_\perp^2 \boldsymbol{e}_\perp &\stackrel{!}{=} 0 \\ \nabla_\perp(\pm \mathrm{j}\beta e_z) + k_c^2 \boldsymbol{e}_\perp &= 0 \end{aligned}$$

resulting in

$$\boldsymbol{e}_\perp = \mp \frac{\mathrm{j}\beta}{k_c^2} \nabla_\perp e_z. \tag{2.43}$$

The magnetic fields are obtained by

$$\begin{aligned} \mp\beta \hat{z} \times \boldsymbol{h}_\perp &= \omega\varepsilon_0 \boldsymbol{e}_\perp \\ \mp\beta \hat{z} \times (\hat{z} \times \boldsymbol{h}_\perp) &= \omega\varepsilon_0 \hat{z} \times \boldsymbol{e}_\perp \\ \mp\beta((\hat{z} \cdot \boldsymbol{h}_\perp)\hat{z} - (\hat{z} \cdot \hat{z})\boldsymbol{h}_\perp) &= \omega\varepsilon_0 \hat{z} \times \boldsymbol{e}_\perp \\ \pm\beta \boldsymbol{h}_\perp &= \omega\varepsilon_0 \hat{z} \times \boldsymbol{e}_\perp, \end{aligned}$$

giving us the relation

$$\boldsymbol{h}_\perp = \pm \frac{\omega\varepsilon_0}{\mathrm{j}\beta} \hat{z} \times \boldsymbol{e}_\perp. \tag{2.44}$$

We can now express the total fields as

$$\boldsymbol{E}_z = \hat{z} e_z \exp(\mp \mathrm{j}\beta z) \tag{2.45}$$

$$\boldsymbol{E}_\perp = \boldsymbol{e}_\perp \exp(\mp \mathrm{j}\beta z) = \mp \frac{\mathrm{j}\beta}{k_c^2} \exp(\mp \mathrm{j}\beta z) \nabla_\perp e_z \tag{2.46}$$

$$\boldsymbol{H}_\perp = \boldsymbol{h}_\perp \exp(\mp \mathrm{j}\beta z) = \pm \frac{\omega\varepsilon_0}{\mathrm{j}\beta} \hat{z} \times \boldsymbol{e}_\perp \exp(\mp \mathrm{j}\beta z) \tag{2.47}$$

Using the relation

$$\begin{aligned}\nabla_\perp e_z &= \hat{r}\frac{\partial e_z}{\partial r} + \hat{\phi}\frac{1}{r}\frac{\partial e_z}{\partial \phi} \\ &= \hat{r}\tilde{C}\cdot k_c J_n'(k_c r)\cos n\phi - \hat{\phi}\frac{n}{r}\tilde{C}\cdot J_n(k_c r)\sin n\phi\end{aligned} \tag{2.48}$$

we end up with

$$E_r = \mp\tilde{C}\cdot\frac{\mathrm{j}\beta}{k_c}J_n'(k_c r)\cos n\phi\exp\left(\mp\mathrm{j}\beta z\right) \tag{2.49}$$

$$E_\phi = \pm\tilde{C}\cdot\frac{\mathrm{j}\beta}{k_c^2}\frac{n}{r}J_n(k_c r)\sin n\phi\exp\left(\mp\mathrm{j}\beta z\right) \tag{2.50}$$

$$E_z = \tilde{C}\cdot J_n(k_c r)\cos n\phi\exp\left(\mp\mathrm{j}\beta z\right) \tag{2.51}$$

$$H_r = -\tilde{C}\cdot\mathrm{j}\frac{\omega\varepsilon_0}{k_c^2}\frac{n}{r}J_n(k_c r)\sin n\phi\exp\left(\mp\mathrm{j}\beta z\right) \tag{2.52}$$

$$H_\phi = -\tilde{C}\cdot\mathrm{j}\frac{\omega\varepsilon_0}{k_c}J_n'(k_c r)\cos n\phi\exp\left(\mp\mathrm{j}\beta z\right) \tag{2.53}$$

$$H_z = 0. \tag{2.54}$$

These equations describe the fields in a cylindrical waveguide (although we have omitted the time dependence). To obtain the fields in a cavity, we start by considering two waves traveling in opposite directions:

$$E_\phi^+ + E_\phi^- = \frac{\mathrm{j}\beta}{k_c^2}\frac{n}{r}J_n(k_c r)\sin n\phi(\tilde{C}^+\exp\left(-\mathrm{j}\beta z\right) - \tilde{C}^-\exp\left(\mathrm{j}\beta z\right)). \tag{2.55}$$

To close the cavity, we impose boundary conditions for a perfect conductor, i.e., E_r and E_ϕ must vanish at $z = 0$ and $z = l$. Hence, we obtain

$$\tilde{C}^+ - \tilde{C}^- = 0 \tag{2.56}$$

$$\tilde{C}^+\exp\left(-\mathrm{j}\beta l\right) - \tilde{C}^-\exp\left(\mathrm{j}\beta l\right) = 0. \tag{2.57}$$

If we combine these expressions, we see that

$$\sin\beta l = 0 \tag{2.58}$$

and thus β can only take a set of discrete values given by

$$\beta = \frac{p\pi}{l}, \quad p = 0,1,2,... \tag{2.59}$$

We can now express the fields in terms of an arbitrary amplitude $C = 2\tilde{C}$.

$$E_r = C \cdot \frac{\beta}{k_c} J_n'(k_c r) \cos n\phi \sin \beta z \tag{2.60}$$

$$E_\phi = -C \cdot \frac{\beta}{k_c^2} \frac{n}{r} J_n(k_c r) \sin n\phi \sin \beta z \tag{2.61}$$

$$E_z = C \cdot J_n(k_c r) \cos n\phi \cos \beta z \tag{2.62}$$

$$H_r = -\mathrm{j}C \cdot \frac{\omega \varepsilon_0}{k_c^2} \frac{n}{r} J_n(k_c r) \sin n\phi \cos \beta z \tag{2.63}$$

$$H_\phi = -\mathrm{j}C \cdot \frac{\omega \varepsilon_0}{k_c} J_n'(k_c r) \cos n\phi \cos \beta z \tag{2.64}$$

$$H_z = 0 \tag{2.65}$$

2.2.2 Field profiles of TE modes in a cylindrical cavity

Analogously, we can perform the same series of calculations for the TE modes, i.e. $e_z = 0$. The result is the following set of equations.

$$E_r = C \frac{\omega \mu_0}{k_c^2} \frac{n}{r} J_n(k_c r) \sin n\phi \sin \beta z \tag{2.66}$$

$$E_\phi = C \frac{\omega \mu_0}{k_c} J_n'(k_c r) \cos n\phi \sin \beta z \tag{2.67}$$

$$E_z = 0 \tag{2.68}$$

$$H_r = -\mathrm{j}C \frac{\beta}{k_c} J_n'(k_c r) \cos n\phi \cos \beta z \tag{2.69}$$

$$H_\phi = \mathrm{j}C \frac{\beta}{k_c^2} \frac{n}{r} J_n(k_c r) \sin n\phi \cos \beta z \tag{2.70}$$

$$H_z = -\mathrm{j}C J_n(k_c r) \cos n\phi \sin \beta z \tag{2.71}$$

$$\tag{2.72}$$

k_c is now given by

$$k_c = \frac{u_{nm}'}{a}, \tag{2.73}$$

where u_{nm}' denotes the m^{th} zero of $J_n'(k_c r)$, i.e., k_c is defined similarly as in Equation (2.41) but is now related to the derivative of Bessel functions rather than the Bessel functions themselves. We should also note that in the case of TE modes, the integer p has to be strictly positive since $p = 0$ only yields trivial fields.

2.2.3 Mode distribution

An effective tool to visualize the resonant frequencies f as function of the cavity dimensions is the so-called mode chart. Such a diagram is presented in Figure 2.3,

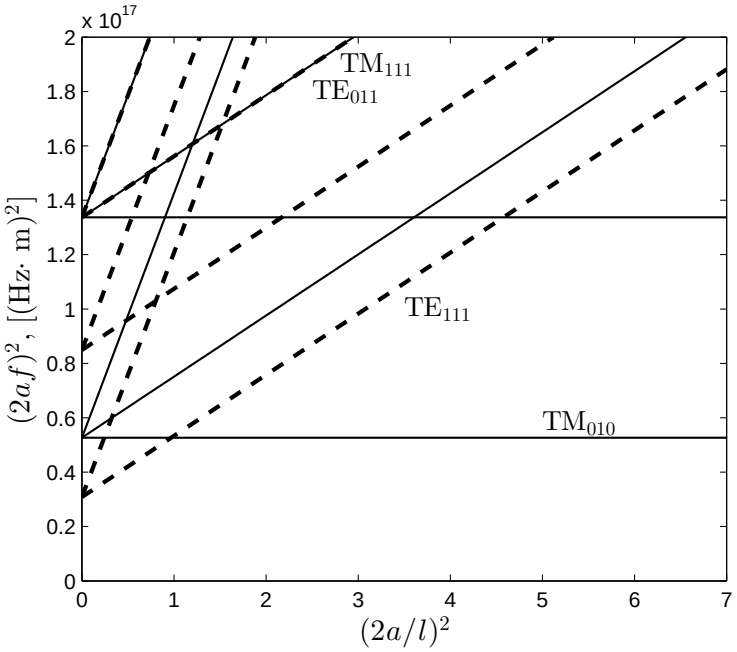

Figure 2.3: Mode chart with some different modes marked. Solid lines indicate TM modes and dashed lines indicate TE modes. Note the degeneracy of the TE_{011} and TM_{111} modes.

adapted from Chen *et al.* [2]. From this chart, we can observe a few things. First, the resonance frequencies of TM_{nm0} modes are independent of the cavity length. It then follows that the TM_{010} mode can be made the dominant one by choosing the ratio $a/l > 0.49$. One can also see that there are degenerate modes, for example the TE_{011} and the TM_{111}.

Some modes are also spatially degenerate. Here we may take the TE_{111} as an example. The two profiles of this mode are presented in Figure 2.4. If we want to operate at that mode, it is possible to cancel one of the degeneracies by introducing a thin metallic needle parallel to the E-field of that mode, due to the metallic boundary condition [2].

2.3 Quality factor

There are two parameters that are important to describe a resonator: the resonance frequency and the quality factor. The latter is often referred to as the Q-factor or just Q. The Q-factor is defined as

$$Q = \omega_0 \frac{W}{P_L}, \tag{2.74}$$

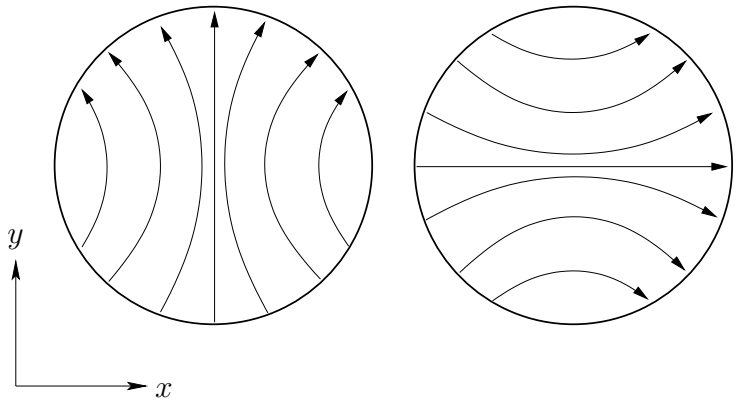

Figure 2.4: The two degenerate profiles of the E-field of the TE_{111} mode.

where ω_0 is the angular resonance frequency, W is the total electromagnetic energy stored in the cavity, and P_L is the average dissipation of energy [2]. The Q-factor is thus a measurement of energy losses in the resonator.

2.3.1 Contributions

If the cavity is filled with a lossless medium, the only contribution to P_L comes from losses in the metallic walls. If the material is lossy, the energy dissipation is the sum of losses in the conducting walls (P_C below) and in the dielectric medium (P_D):

$$Q = \omega_0 \frac{W}{P_L} = \omega_0 \frac{W}{P_C + P_D}. \tag{2.75}$$

It is now clear that the introduction of a lossy medium lowers the Q-factor of the resonator. We can also define two Q-factors, Q_C and Q_D, corresponding to the wall losses and dielectric losses respectively,

$$\frac{1}{Q} = \frac{P_L}{\omega_0 W} = \frac{P_C + P_D}{\omega_0 W} = \frac{1}{Q_C} + \frac{1}{Q_D}. \tag{2.76}$$

So far, we have only considered the resonator itself. The Q-factor is then normally referred to as the *unloaded* Q-factor, which we will call Q_U. In practice, the resonator has to be connected to an external circuit for measurement. The external circuit introduces a new term to the dissipation and the total Q-factor is then referred to as the *loaded* Q-factor, Q_L [19].

$$\frac{1}{Q_L} = \frac{1}{Q_U} + \frac{1}{Q_E} \tag{2.77}$$

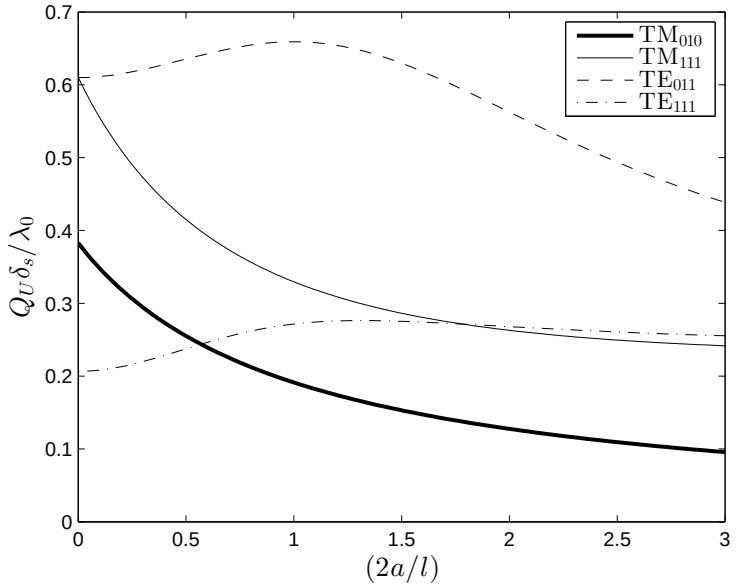

Figure 2.5: Q-factor of four different modes. Adapted from Collin [24].

2.3.2 Characteristics

Since the Q-factor is related to the stored energy, it also follows that different modes give different Q-factors. Collin derives the Q_C for different modes and ends up with the following expressions [24]:

$$\text{TE modes:} \quad Q_C\frac{\delta_s}{\lambda_0} = \frac{\left(1-\left(\frac{n}{u'_{nm}}\right)^2\right)\left(u'^2_{nm}+\left(\frac{p\pi a}{l}\right)^2\right)^{3/2}}{2\pi\left(u'^2_{nm}+\frac{2a}{l}\left(\frac{p\pi a}{l}\right)^2+\left(1-\frac{2a}{l}\right)\left(\frac{np\pi a}{u'_{nm}l}\right)^2\right)} \tag{2.78}$$

$$\text{TM modes:} \quad Q_C\frac{\delta_s}{\lambda_0} = \begin{cases} \dfrac{\left(u^2_{nm}+\left(\frac{p\pi a}{l}\right)^2\right)^{1/2}}{2\pi\left(1+\frac{2a}{l}\right)} & p>0 \\ \dfrac{u_{nm}}{2\pi\left(1+\frac{a}{l}\right)} & p=0 \end{cases}, \tag{2.79}$$

where δ_s is the (material dependent) skin depth and λ_0 is the wavelength. A comparison of the Q-factor for some different modes are presented in Figure 2.5. We observe that, for the TM_{010} mode, a large cavity length is desired to obtain a high Q-factor.

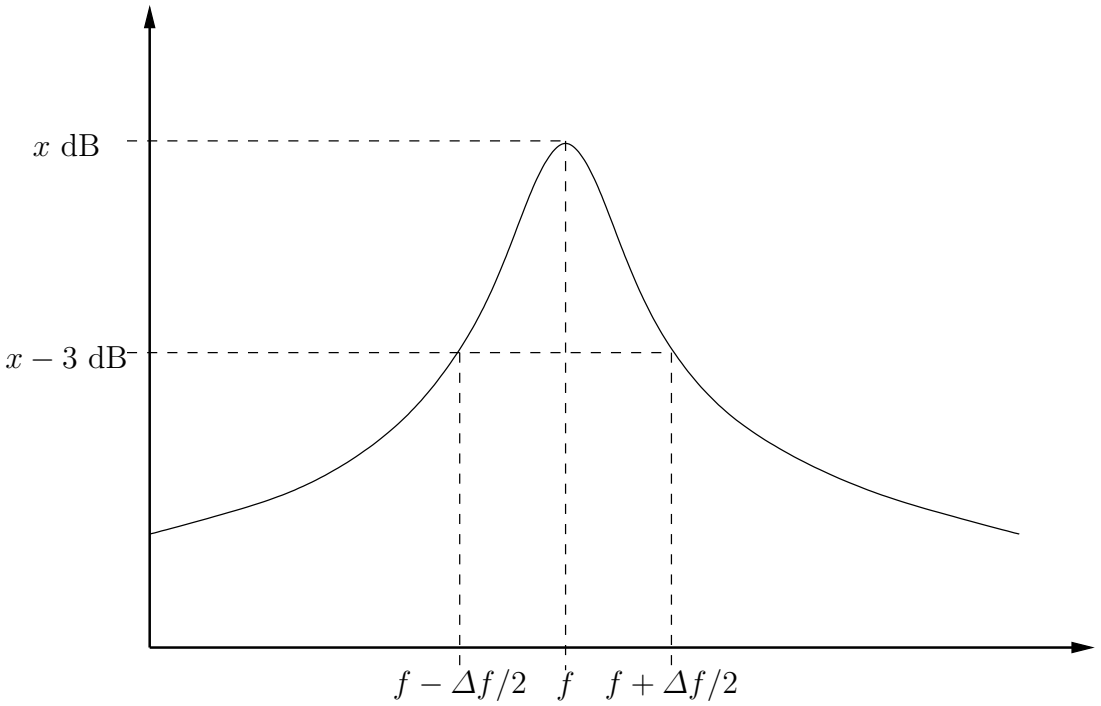

Figure 2.6: Description of how the Q-factor is measured.

2.3.3 Measuring the Q-factor

In order to measure the Q-factor, we need to perform a frequency sweep. As we have discussed earlier, the resonance frequencies appear as peaks in the spectrum. The Q-factor at a certain mode is obtained from the width of the corresponding peak. More precisely, we measure the width where the amplitude is 3 dB lower than at the peak maximum. A graphical explanation can be found in Figure 2.6. The Q-factor is then calculated as

$$Q = \frac{f}{\Delta f} \tag{2.80}$$

where Δf is the bandwidth and f is the resonance frequency [2]. Mathematically, it is also possible to obtain Q from the complex eigenvalue [2]. If we write the eigenvalue as

$$\omega = \omega' + \mathrm{j}\omega'', \tag{2.81}$$

where the real part is related to the resonance frequency f above through

$$\omega' = 2\pi f, \tag{2.82}$$

we can get Q from

$$Q = \frac{\omega'}{2\omega''}. \tag{2.83}$$

2.4 Treatment of the frequency shift

The following derivation is inspired by the work of Chen *et al.* [2]. According to Maxwell's equations, we can write the relation between the electric and magnetic fields as

$$\nabla \times \boldsymbol{E} = -\mathrm{j}\omega\mu\boldsymbol{H} \tag{2.84}$$
$$\nabla \times \boldsymbol{H} = \mathrm{j}\omega\varepsilon\boldsymbol{E}. \tag{2.85}$$

Denoting the fields in the cavity before introducing the sample as $\boldsymbol{E}_1$ and $\boldsymbol{H}_1$; the fields after the sample is introduced as $\boldsymbol{E}_2$ and $\boldsymbol{H}_2$; and the complex resonant angular frequencies of the unperturbed and perturbed cavity respectively as ω_1 and ω_2, we obtain the following:

$$\boldsymbol{H}_2 \cdot \nabla \times \boldsymbol{E}_1^* = \mathrm{j}\omega_1\mu_1\boldsymbol{H}_2 \cdot \boldsymbol{H}_1^* \tag{2.86}$$
$$\boldsymbol{E}_1^* \cdot \nabla \times \boldsymbol{H}_2 = \mathrm{j}\omega_2\varepsilon_2\boldsymbol{E}_1^* \cdot \boldsymbol{E}_2 \tag{2.87}$$
$$\boldsymbol{H}_1^* \cdot \nabla \times \boldsymbol{E}_2 = -\mathrm{j}\omega_2\mu_2\boldsymbol{H}_1^* \cdot \boldsymbol{H}_2 \tag{2.88}$$
$$\boldsymbol{E}_2 \cdot \nabla \times \boldsymbol{H}_1^* = -\mathrm{j}\omega_1\varepsilon_1\boldsymbol{E}_2 \cdot \boldsymbol{E}_1^*. \tag{2.89}$$

The asterisk (*) is here used to denote the complex conjugate. Adding Equations (2.86) and (2.88) together and subtracting (2.87) and (2.89) from this gives us

$$\begin{aligned}\boldsymbol{H}_2 \cdot (\nabla \times \boldsymbol{E}_1^*) - \boldsymbol{E}_1^* \cdot (\nabla \times \boldsymbol{H}_2) + \boldsymbol{H}_1^* \cdot (\nabla \times \boldsymbol{E}_2) - \boldsymbol{E}_2 \cdot (\nabla \times \boldsymbol{H}_1^*) = \\ \mathrm{j}\Big((\omega_1\varepsilon_1 - \omega_2\varepsilon_2)\boldsymbol{E}_2 \cdot \boldsymbol{E}_1^* + (\omega_1\mu_1 - \omega_2\mu_2)\boldsymbol{H}_2 \cdot \boldsymbol{H}_1^*\Big).\end{aligned} \tag{2.90}$$

The first two and the last two terms on the left-hand side may be combined using the following vector identity

$$\nabla \cdot (\boldsymbol{u} \times \boldsymbol{v}) = \boldsymbol{v} \cdot (\nabla \times \boldsymbol{u}) - \boldsymbol{u} \cdot (\nabla \times \boldsymbol{v}). \tag{2.91}$$

Hence, we obtain

$$\begin{aligned}\nabla \cdot (\boldsymbol{E}_1^* \times \boldsymbol{H}_2) + \nabla \cdot (\boldsymbol{E}_2 \times \boldsymbol{H}_1^*) = \\ \mathrm{j}\Big((\omega_1\varepsilon_1 - \omega_2\varepsilon_2)\boldsymbol{E}_2 \cdot \boldsymbol{E}_1^* + (\omega_1\mu_1 - \omega_2\mu_2)\boldsymbol{H}_2 \cdot \boldsymbol{H}_1^*\Big).\end{aligned} \tag{2.92}$$

We integrate this over the whole cavity volume and use Gauss's theorem:

$$\int_V \nabla \cdot (\boldsymbol{H} \times \boldsymbol{E}^*)\,\mathrm{d}V = \oint_S (\boldsymbol{H} \times \boldsymbol{E}^*) \cdot \mathrm{d}\boldsymbol{S}, \tag{2.93}$$

where V denotes a volume and S the corresponding area of that volume. Due to the boundary conditions of a perfect conductor this integral is trivial. Finally, by

denoting $\mu_2 = \mu_1 + \Delta\mu$ and $\varepsilon_2 = \varepsilon_1 + \Delta\varepsilon$, we end up with the following *exact* equation for the frequency shift.

$$\frac{\omega_2 - \omega_1}{\omega_2} = -\frac{\int_{V_0} \mathrm{d}V \left(\Delta\varepsilon \boldsymbol{E}_2 \cdot \boldsymbol{E}_1^* + \Delta\mu \boldsymbol{H}_2 \cdot \boldsymbol{H}_1^*\right)}{\int_{V_0} \mathrm{d}V \left(\varepsilon_1 \boldsymbol{E}_2 \cdot \boldsymbol{E}_1^* + \mu_1 \boldsymbol{H}_2 \cdot \boldsymbol{H}_1^*\right)}. \tag{2.94}$$

The integration region V_0 is the total cavity volume. Since $\Delta\mu$ and $\Delta\varepsilon$ are zero outside the sample, it is sufficient to integrate over the sample volume V_S in the numerator, giving

$$\frac{\omega_2 - \omega_1}{\omega_2} = -\frac{\int_{V_S} \mathrm{d}V \left(\Delta\varepsilon \boldsymbol{E}_2 \cdot \boldsymbol{E}_1^* + \Delta\mu \boldsymbol{H}_2 \cdot \boldsymbol{H}_1^*\right)}{\int_{V_0} \mathrm{d}V \left(\varepsilon_1 \boldsymbol{E}_2 \cdot \boldsymbol{E}_1^* + \mu_1 \boldsymbol{H}_2 \cdot \boldsymbol{H}_1^*\right)}. \tag{2.95}$$

At this point, approximations are usually introduced. This leads to the cavity-perturbation method discussed earlier.

2.4.1 Approximations

Once the field profiles are known, we can compute the right-hand side of Equation (2.95) for given values of ε and μ. These material properties can therefore be calculated iteratively by comparing the computed integrals to the relative shift in complex angular frequency of the resonance.

Let us first expand the left-hand side of Equation (2.95).

$$\begin{aligned}
\frac{\omega_2 - \omega_1}{\omega_2} &= \frac{(\omega_2' - \omega_1') + \mathrm{j}(\omega_2'' - \omega_1'')}{\omega_2' + \mathrm{j}\omega_2''} \\
&= \frac{\omega_2' - \omega_1'}{\omega_2' \left(1 + \mathrm{j}\dfrac{\omega_2''}{\omega_2'}\right)} + \mathrm{j}\frac{\omega_2'' - \omega_1''}{\omega_2' \left(1 + \mathrm{j}\dfrac{\omega_2''}{\omega_2'}\right)} \\
&= \left(\frac{\omega_2' - \omega_1'}{\omega_2'} + \mathrm{j}\frac{\omega_2'' - \omega_1''}{\omega_2'}\right) \cdot \frac{1 - \mathrm{j}\dfrac{\omega_2''}{\omega_2'}}{1 + \left(\dfrac{\omega_2''}{\omega_2'}\right)^2} \\
&= \left(\frac{\omega_2' - \omega_1'}{\omega_2'} + \mathrm{j}\left(\frac{\omega_2''}{\omega_2'} - \frac{\omega_1''}{\omega_2'}\right)\right) \cdot \frac{1 - \mathrm{j}\dfrac{\omega_2''}{\omega_2'}}{1 + \left(\dfrac{\omega_2''}{\omega_2'}\right)^2}
\end{aligned} \tag{2.96}$$

Second, we repeat the definitions introduced in Section 2.3.3:

$$\omega = \omega' + \mathrm{j}\omega'' \tag{2.97}$$

$$\omega' = 2\pi f \tag{2.98}$$

$$Q = \frac{\omega'}{2\omega''}. \tag{2.99}$$

We may then further rewrite Equation (2.96) as

$$\begin{aligned}\frac{\omega_2 - \omega_1}{\omega_2} &= \left(\frac{f_2 - f_1}{f_2} + \mathrm{j}\left(\frac{1}{2Q_2} - \frac{1}{2Q_1}\frac{f_1}{f_2}\right)\right) \cdot \frac{1 - \mathrm{j}\dfrac{1}{2Q_2}}{1 + \left(\dfrac{1}{2Q_2}\right)^2} \\ &= \frac{\dfrac{f_2 - f_1}{f_2} - \dfrac{1}{4Q_1Q_2}\dfrac{f_1}{f_2} + \left(\dfrac{1}{2Q_2}\right)^2 + \mathrm{j}\left(\dfrac{1}{2Q_2} - \dfrac{1}{2Q_1}\right)\dfrac{f_1}{f_2}}{1 + \left(\dfrac{1}{2Q_2}\right)^2}.\end{aligned} \tag{2.100}$$

This can be compared to the approximated value given by Chen *et al.*[2]

$$\frac{\omega_2 - \omega_1}{\omega_2} \approx \frac{f_2 - f_1}{f_2} + \mathrm{j}\left(\frac{1}{2Q_2} - \frac{1}{2Q_1}\right), \tag{2.101}$$

which we obtain by considering Q_1 and Q_2 to be large and $f_1 \approx f_2$.

The right-hand side of Equation (2.95) can also be simplified through approximations. First, we treat the sample as a perturbation (hence the name cavity-perturbation method) that barely affects the fields in the cavity. Thus, we assume $\boldsymbol{E}_2 \approx \boldsymbol{E}_1$ and $\boldsymbol{H}_2 \approx \boldsymbol{H}_1$.

$$\frac{\omega_2 - \omega_1}{\omega_2} \approx -\frac{\int_{V_0} \mathrm{d}V \left(\Delta\varepsilon|\boldsymbol{E}_1|^2 + \Delta\mu|\boldsymbol{H}_1|^2\right)}{\int_{V_0} \mathrm{d}V \left(\varepsilon_1|\boldsymbol{E}_1|^2 + \mu_1|\boldsymbol{H}_1|^2\right)} \tag{2.102}$$

We then simplify the denominator by utilizing that the stored electric and magnetic energies are equal at resonance [24]. In addition, by either considering a non-magnetic sample or placing the sample where the magnetic field is zero, the second term of the numerator may be omitted. Now, the real and imaginary part can be written as

$$\mathrm{Re}\left(\frac{\omega_2 - \omega_1}{\omega_2}\right) \approx (\varepsilon_r' - 1)C \tag{2.103}$$

$$\mathrm{Im}\left(\frac{\omega_2 - \omega_1}{\omega_2}\right) \approx \varepsilon_r'' C \tag{2.104}$$

respectively, where

$$C = -\frac{\int_{V_S} \mathrm{d}V\, \boldsymbol{E}_1^* \cdot \boldsymbol{E}_2}{\int_{V_0} \mathrm{d}V\, |\boldsymbol{E}_1|^2}. \tag{2.105}$$

Normally, this parameter is obtained through calibration. We shall return to this expression in the next chapter to discuss how this calibration is performed.

2.5 Scattering parameters

A cavity resonator or another microwave device may have one or more ports. An incoming signal (for example a voltage wave) at one port will give responses at the other ports. These responses can be represented with so called scattering parameters, or S-parameters [19]. Consider a microwave device with two ports. Denote the *incoming* signal at port i as V_i^{in} and the corresponding *outgoing* signal as V_i^{out}. We may then form a matrix according to

$$\begin{pmatrix} V_1^{\text{out}} \\ V_2^{\text{out}} \end{pmatrix} = \begin{pmatrix} S_{11} & S_{12} \\ S_{21} & S_{22} \end{pmatrix} \begin{pmatrix} V_1^{\text{in}} \\ V_2^{\text{in}} \end{pmatrix}. \tag{2.106}$$

For a signal coming in at port 1, the S_{11}-parameter then describes the reflection, whereas S_{21} describes the transmission to port 2.

2.6 Coupling devices

The fields in the cavity have to be excited somehow. This is done by connecting the cavity to a network analyzer, which is used to measure the reflected and transmitted signal. The analyzer is usually connected via coaxial cables. The extension of the center pin into the cavity may be done in different ways. Either it can be formed as a loop and grounded in the cavity wall (which we will refer to as a coupling loop) or by just be extended into the cavity (which will be referred to as a coupling probe). The probe can also be shaped in different ways. It can be bent, straight or barely extended into the cavity. A graphical description can be found in Figure 2.7. By treating these coupling devices as small currents, the loop takes the role of a magnetic dipole and the probe the role of an electric dipole [24].

Even though a mode is a valid solution to the eigenvalue problem of finding resonances of the cavity, they will not necessarily be excited. The shape and position of the couplers will largely determine which modes are excited and which are not. An example can be found in Figure 2.8 showing the spectra of cavities with radius 15 mm and length 28 mm when the couplers are placed symmetrically on the top of the cavity, close to the periphery. The different spectra correspond to coupling loops, probes bent in the azimuthal direction and straight probes. As

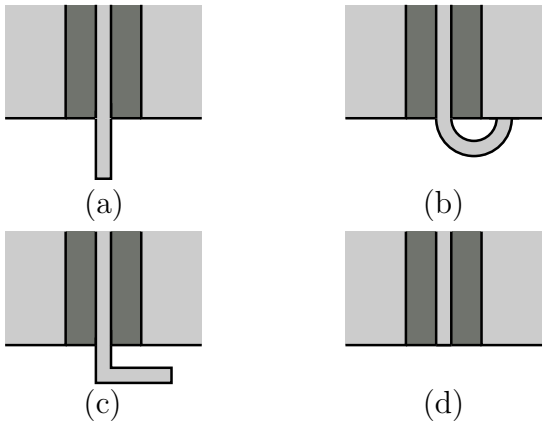

Figure 2.7: Schematic description of different coupling devices. a) probe, b) loop, c) bent probe, d) short probe.

can be seen, the resonance at 8 GHz (which corresponds to the TE_{111} mode) is not excited by the short probe. It appears for the bent probe but not as clearly as for the loop. This way we can to some extent decide which modes should not be excited and may thus come around the problems that degenerate modes can give rise to.

Coupling devices can be constructed in more complex shapes than those discussed here. Examples are the dual-loop and 4-loop developed by Zhang *et al.*, which have shown to be efficient in suppressing unwanted modes [25, 26].

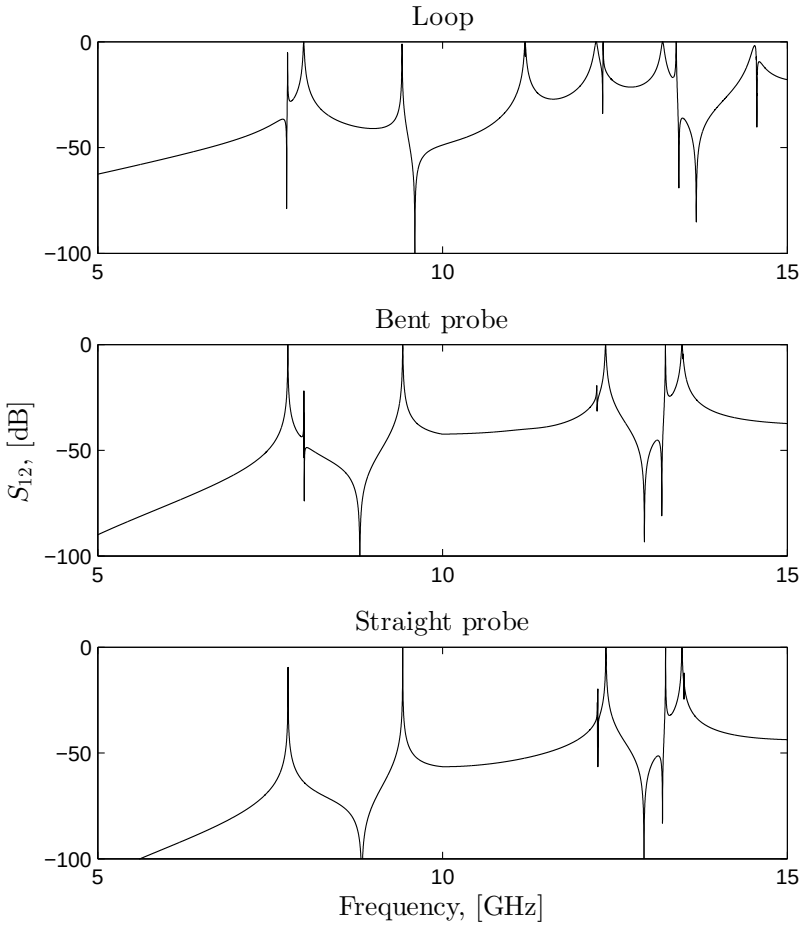

Figure 2.8: Spectra for cylindrical cavity of radius 15 mm and length 28 mm with different types of coupling devices.

Chapter 3

Method

In this chapter, we will study the design of the cavity and explain the measurement procedure. Based on the theoretical treatment presented in Chapter 2, we discuss what dimensions that are appropriate for the cavity. Based on these dimensions and varying different properties, such as the probe position, a cavity resonator is designed.

The second part of the chapter is devoted to the measurement procedure. Here we discuss and describe how a measurement is performed and in what way different parameters can be obtained.

3.1 Designing a cavity

As discussed in Section 1.2.2, a limitation of the resonant-perturbation method is that material parameters can only be measured at discrete frequencies. It is thus not possible to cover the entire spectrum of interest (0.4–40 GHz). However, as we have seen in Section 2.1, this is not a big problem for the permittivity measurement but it can be problematic when measuring the permeability.

There are basically two cavity shapes to choose between: rectangular and cylindrical cavities. Cylindrical ones are often used for the purpose of frequency measurements since they operate at a wide frequency range and have relatively high Q-factors [24]. Therefore, we shall use a cylindrical one.

3.1.1 Cavity dimensions

We have also seen that the operational frequencies of a cavity resonator are dependent on its dimensions. Hence, we should design the cavity with respect to what frequencies we are interested in. A suitable mode to use is the TM_{010} mode since it can be made the dominating mode (which can be seen in the mode chart

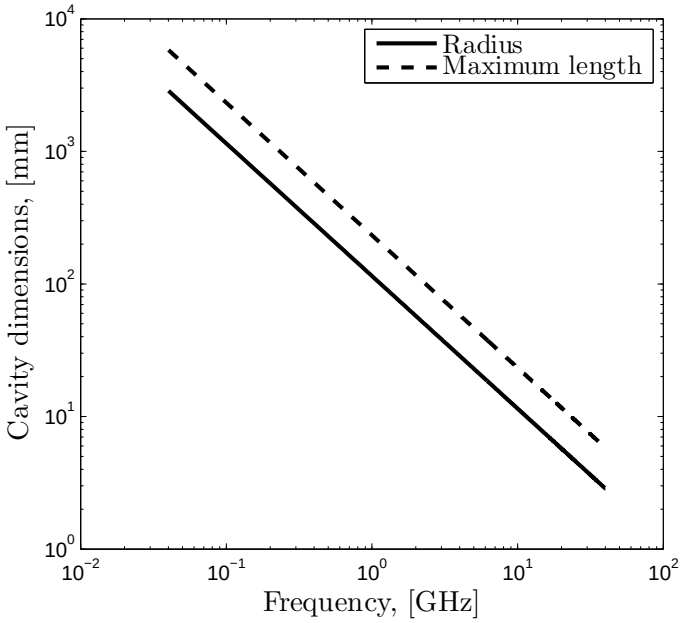

Figure 3.1: Dimensions of a cylindrical cavity necessary to obtain the TM_{010} mode at a given frequency. This mode is independent of the cavity length but in order to be the dominating mode, the cavity length must not exceed the maximum length indicated.

presented earlier in Figure 2.3) and has an azimuthal symmetry. In addition, the amplitudes of the electric and magnetic fields have a maximum and minimum respectively along the axis of rotation. The cutoff frequency of the TM_{010} mode is only dependent on the radius of the cavity as can be seen from Equations (2.60) through (2.65). However, in order for it to be the dominating mode, the ratio between radius and length has to satisfy $a/l > 0.49$. The radius and maximal length of the cavity as function of frequency is presented in Figure 3.1, where the radius a is given by

$$a = \frac{cu_{01}}{2\pi f}. \tag{3.1}$$

As before, c is the speed of light, u_{01} is the first root of $J_0(x)$ and f is the frequency.

However, simulations performed in Ansys HFSS indicated that the sample height has to equal the cavity length in order to yield a satisfying result. Since the materials of interest often are provided in sheets, this puts a new restriction on the cavity length. This restriction also means that the measurement will be sensitive to air gaps occurring when the sample does not reach all the way to the top. In order to avoid this problem, a cavity of adaptive length was designed. A

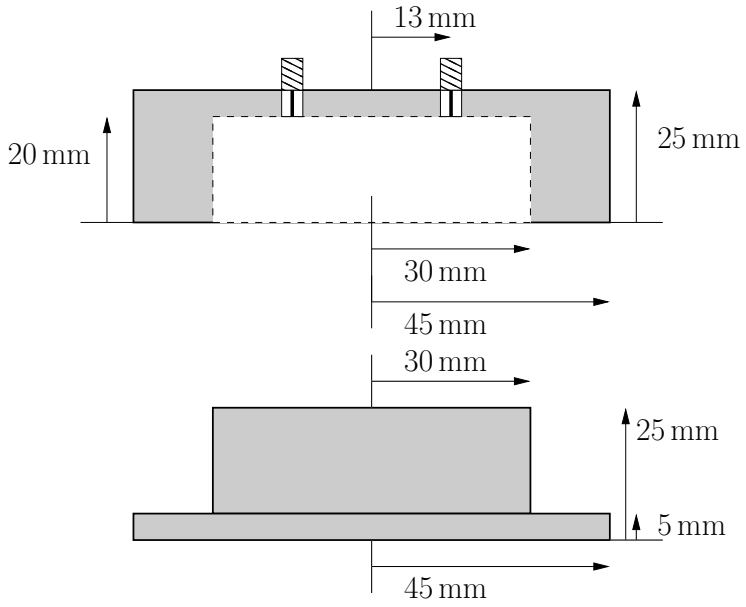

Figure 3.2: Sketch of the cavity including dimensions. The sketch is made to scale and features a cross-section of the two parts as viewed from the side.

graphical description including dimensions is presented in Figure 3.2. The figure presents a cross-section of the cavity resonator, viewed from the side. Instead of using two hollow halves, we use a hollow top and solid bottom part. The top half then takes the role of a mantle and the length of the cavity will equal the sample height.

It is not only the resonant frequencies that are determined by the cavity radius; the amplitude of the S-parameters are also affected. In Figure 3.3, the S_{12}-parameters for different radii are presented. As the radius is increased, the amplitude around the peak decreases. The network analyzer used has a noise level at roughly $-80\,\mathrm{dB}$ and we, therefore, want the signal to lie well above this.

3.1.2 Gaps

For construction reasons, the diameter of the bottom block is slightly smaller than the inner diameter of the top part. An air gap in the radial direction may then be present between the two halves. There may also occur air gaps between the sample and the conducting walls, see Figure 3.4. Air gaps may give a capacitive effect that affects the resonances. The latter of these two examples should be solved by the adaptive height of the designed resonator. If air gaps, either between the two halves or between the sample and conducting wall, turns out to be a problem, previous studies have shown that conducting paste may reduce the problem [27, 28].

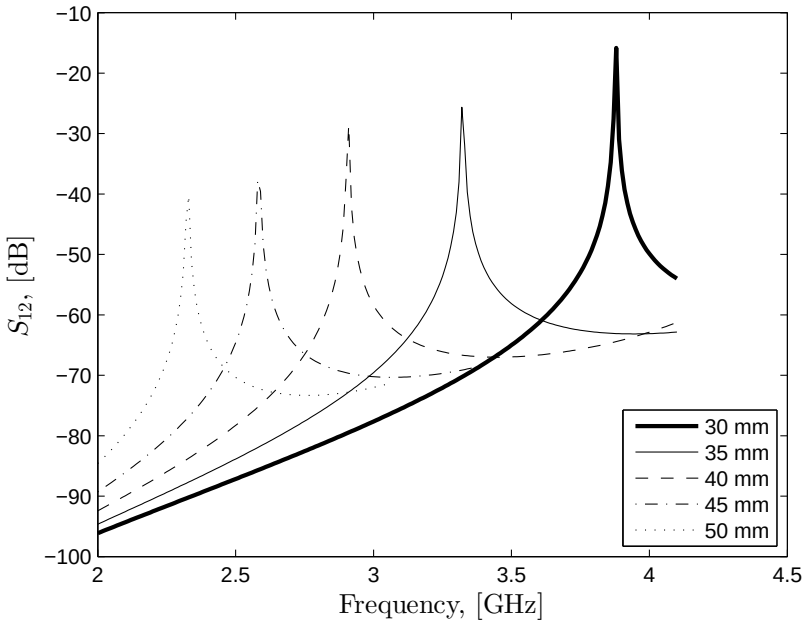

Figure 3.3: The position and amplitude of the TM_{010}-peak for different cavity radii.

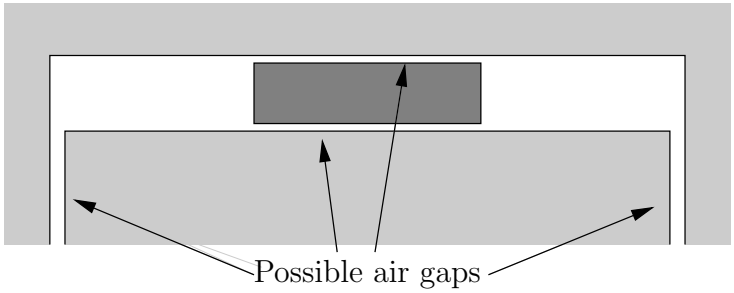

Figure 3.4: A graphical description of the gap between the two resonator parts as well as between the walls and sample.

3.1.3 Coupling devices

In Section 2.6 we discussed different kinds of couplers used to excite and measure the fields. We saw that the scattering parameters and the excitation of different modes are dependent on the shape of the coupler. However, the chosen cavity design does not leave much choice in what coupler to use. Since the cavity length will be quite small, there will not be room to use loops or longer probes. Instead, we are restricted to the probes that barely extend into the cavity. Fortunately, this probe type does excite the modes we are interested in.

3.1.4 Probe positions

Simulations comparing the positions of the probes were also performed. We restrict ourselves to the case where the two probes are placed symmetrically at the top of the cavity and vary their radial position, see Figure 3.2. The results of such a simulation are presented in Figure 3.5. Notice how the amplitude of the S_{12}-parameter in the region 3–5 GHz around the TM_{010}-peak becomes lower as the probes are placed farther away from each other. One should also notice that by placing the probes at around half of the radius, the TM_{020} mode will not be excited since that mode has a node at this position.

3.2 Measurement procedure

In this project, we investigate two different but related ways to utilize the designed cavity resonator. The first one is the cavity-perturbation method and builds on the approximations discussed in Section 2.4. In the second one, the measurement procedure is similar but the results are compared to a matrix of data acquired from simulations. We shall refer to this as the "Curve-set method" for reasons that will be clarified later.

3.2.1 Cavity-perturbation method

For the calibration we require a reference sample of the same shape and size as the sample we are interested in. We also need to know its permittivity and permeability. We then refer to Equations (2.103) and (2.104). We treat the constant C given by Equation (2.105) as being different in the two equations due to our perturbative method. In addition, we may treat these "constants" as being linearly dependent on the ratio between sample and cavity volume [2]. This is of course not necessary if both samples are of exactly the same size but will increase the

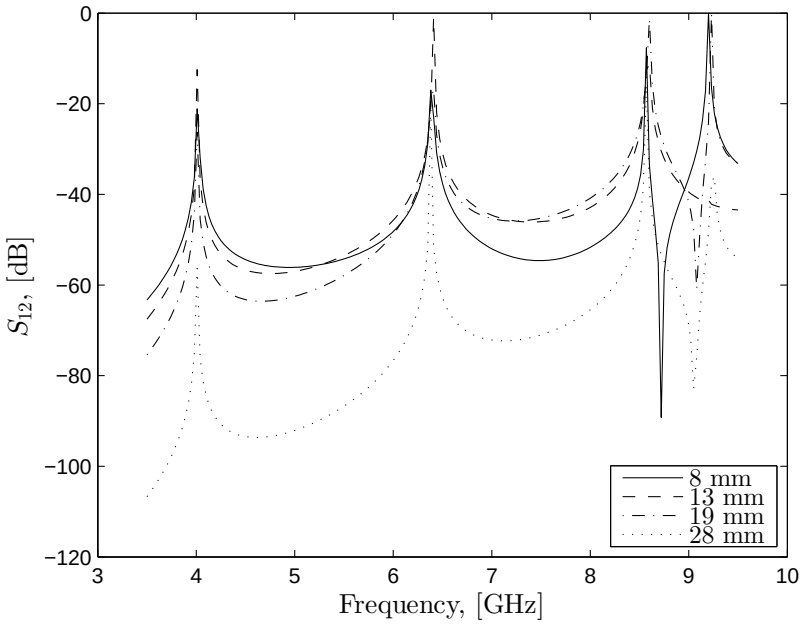

Figure 3.5: The S_{12}-parameter as function of frequency for different probe positions measured in radial distance from the center of the cavity top. The radius of the cavity was 30 mm.

accuracy if one sample is slightly bigger then the other. We may than write

$$\mathrm{Re}\left(\frac{\omega_2-\omega_1}{\omega_2}\right) \approx (\varepsilon_r'-1)A\frac{V_S}{V_C} \tag{3.2}$$

$$\mathrm{Im}\left(\frac{\omega_2-\omega_1}{\omega_2}\right) \approx \varepsilon_r'' B\frac{V_S}{V_C}. \tag{3.3}$$

When performing a measurement, we first measure the empty cavity and then the cavity containing the sample. The left-hand side of Equations (3.2) and (3.3) are calculated using the formulas given by either Equation (2.100) or (2.101). If the permittivity is known, we can calculate the parameters A and B and vice versa.

3.2.1.1 Measurement of permittivity

Using the TM_{010} mode, we place the sample in the middle of the cavity to measure the permittivity, see Figure 3.6. Here, the electric field is strongest and the effect will therefore be largest. In addition the magnetic field is zero in the middle. Therefore, in the case of a magnetic sample, the permeability will ideally not contribute to the shift and broadening of the resonance peak.

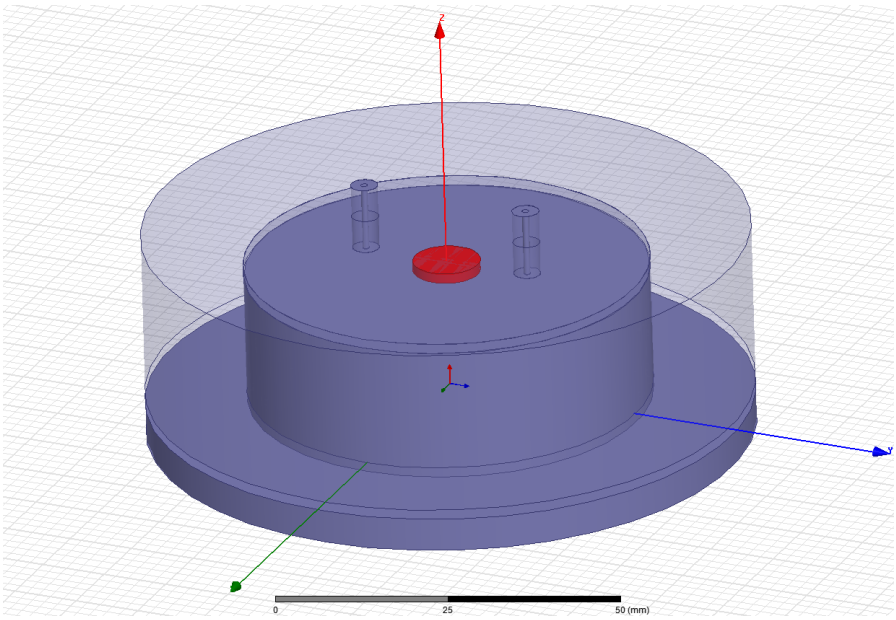

Figure 3.6: The simulated cavity with the sample centered for measurement of the permittivity. The figure is generated in ANSYS HFSS.

To conclude, we measure the permittivity by first measuring the empty cavity. Then, a reference sample is placed in the middle of the cavity and a frequency sweep is performed. We note how the resonance frequency shifts and the Q-factor decreases. It is now possible to solve Equations (3.2)-(3.3) for the parameters A and B. Once we know these, we can perform the actual measurement on the unknown sample and use the obtained values for A and B.

3.2.1.2 Measurement of permeability

We cannot measure the permittivity and permeability simultaneously by the cavity-perturbation method. Instead, we first determine the permittivity by the procedure explained above. Once again, the properties of the TM_{010} mode are appropriate. By placing the sample in the center of the cavity, the magnetic field is small compared to the electric field. Hence, the permeability will affect the shift of the resonant frequency much less than the permittivity.
When the permittivity has been determined, we place the sample where the electric field has a minimum and the magnetic field is large. For the TM_{010} mode this occurs near the cavity edge, see Figure 3.7. An alternative is to use the TM_{110} mode for which the magnetic field has a maximum in the middle whereas the electric field has a minimum. Although the field is not completely symmetric it is still possible that the fields are more evenly disturbed.

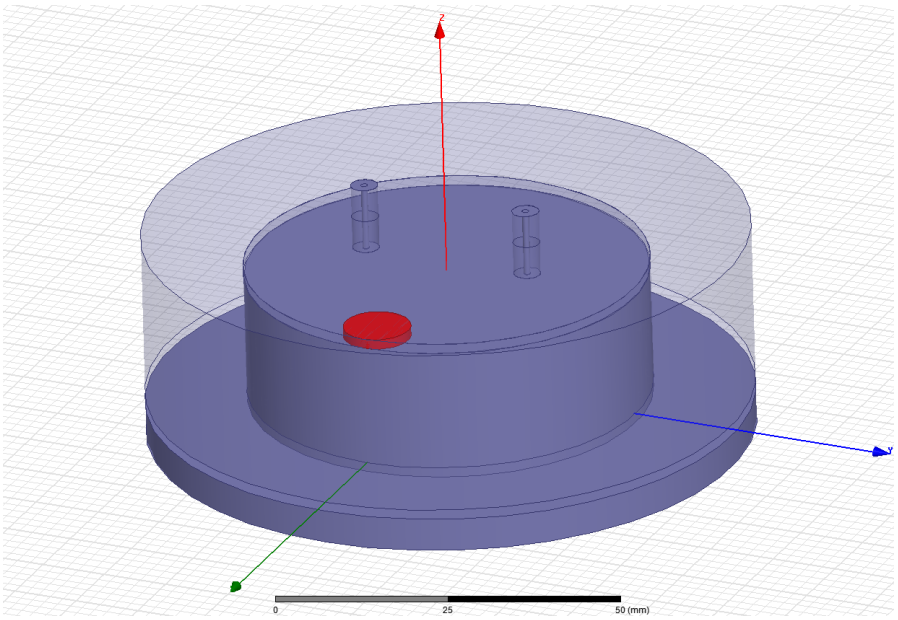

Figure 3.7: The simulated cavity with the sample at the cavity edge for measurement of the permeability. The figure is generated in Ansys HFSS.

The procedure is identical to the one utilized to measure the permittivity; the only difference is the position of the sample and the fact that a magnetic reference sample (i.e. one where the relative permeability is not unity) is needed. Once again we can use Equations (3.2)-(3.3) and simply replace the relative permittivity ε_r with the relative permeability μ_r.

3.2.2 Curve-set method

In the second method, we find inspiration in the perturbative methods discussed so far. Here however, we will not do approximations in order to simplify the analytical expressions. Instead, we perform a series of simulations using Ansys HFSS to obtain a data matrix to which we can compare our measured results. As far as we know, the method has not been studied before. We call this new method the curve-set method since the data can be represented as a set of curves or contour lines.
Now, it should not be necessary to manufacture samples small enough to approximate the fields as unaffected and we should therefore not have to worry about the validity of such an approximation. On the other hand, to be able to measure both permittivity and permeability we cannot let the sample fill the whole cavity either, since we need to perform measurements for two different positions of the sample.

For the simulation, we place a sample of equal size as the one we want to

measure in the middle of the cavity, see Figure 3.6. The real parts of the permittivity and permeability are varied and for each combination of these we calculate the resonant frequency. The sample is then positioned at the cavity edge and the same kind of measurement is performed again, see Figure 3.7. Now we have built up two data matrices containing the resonance frequency as function of ε_r' and μ_r'. For each of the two sample positions, we may plot this data as a set of contour lines. Finally, two measurements of the resonance frequency of the real sample are performed. For each measurement, we find the corresponding curve and the point where the two chosen curves cross should correspond to the actual permittivity and permeability of the sample. Similarly, it should be possible to find the loss tangents by instead studying the Q-factor of the measurements.

An interesting question here is if the frequency shift is independent of the imaginary part of the parameter or not, and if the broadening of the peak is independent of the real part of the parameters. If not, this dependence would sufficiently aggravate this method. In Section 4.2.1.1, we shall see that this is not a problem.

Chapter 4

Results

The purpose of this chapter is to verify the validity of the considered method. This was done through simulations performed with Ansys HFSS. We will in this chapter evaluate the results obtained and compare simulations with measured and theoretical values.

Simulations were performed for two different sample sizes; a small sample of radius 2 mm and a larger of radius 5 mm. Small samples compared to the cavity are necessary for the approximations to be valid. Samples of radii 5 mm were considered to be the smallest size that could easily be fabricated. The smaller value 2 mm is somewhat arbitrarily chosen to see if the results are improved by using smaller samples. Since it is a perturbative method, we expect more accurate solutions when using a smaller sample. Larger samples are however easier to fabricate.

4.1 Design and characterization of the cavity

Since the chosen method cannot be used for arbitrary frequencies in the interval of interest, it was decided to operate around 4 GHz. This corresponds to a cavity of radius 30 mm. As discussed earlier, the cavity height is adaptive. A reasonable sample thickness is 1.5 mm which therefore was used in the simulations. Two coaxial-cable connectors are placed with their centers 13 mm from the cavity center axes. This position was chosen to yield a measurable S_{12} parameter without risking a strong coupling directly between the two connectors. The hope was also to avoid cancellation of the TM_{020}-mode but as we soon shall see this position was probably too close to the node of the E-field.

In Figure 4.1 we present the spectrum in the interval 3–15 GHz of the simulated cavity resonator. Note that for the lower frequencies the resonances are quite distinct and easily separated. However, for higher frequencies the spectrum becomes

Table 4.1: Comparison of theoretical and simulated resonance frequencies for the designed cavity. Frequencies are given in GHz.

Mode	TM_{010}	TM_{110}	TM_{210}	TM_{020}	TM_{310}	TM_{120}
Theoretical	3.82	6.09	8.17	8.78	10.15	11.16
Simulated	3.88	6.19	8.29	—	10.30	11.29

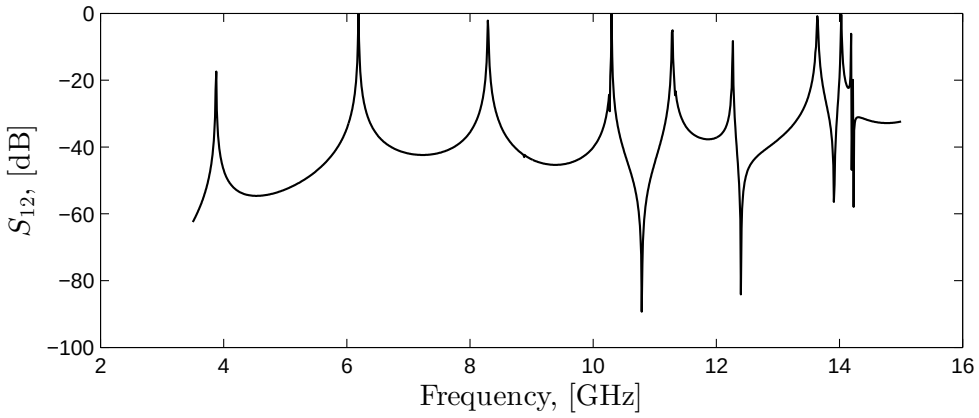

Figure 4.1: Spectrum in the range 3–15 GHz of the cavity designed in this project.

messy and it could be hard to keep track of the different peaks when studying the shifts. The five first peaks correspond well to the theoretical values of the TM_{010}-, TM_{110}-, TM_{210}-, TM_{310}- and TM_{120}-modes. A comparison of theoretical and simulated values are given in Table 4.1. Note that the TM_{020}-mode at 8.8 GHz has been canceled.

4.2 Simulations

Before the resonator was fabricated, simulations were performed to investigate if the properties of the resonator were satisfying. In addition, simulations also allow us to study a greater number of samples of well defined properties and therefore a better characterization of the method can be made.

4.2.1 Cavity-perturbation method

Here we present the results obtained using the cavity-perturbation method described in Section 3.2.1. In this chapter, only a small set of representative simulations are presented. Further analyses varying material parameters can be found in Appendices B through E.

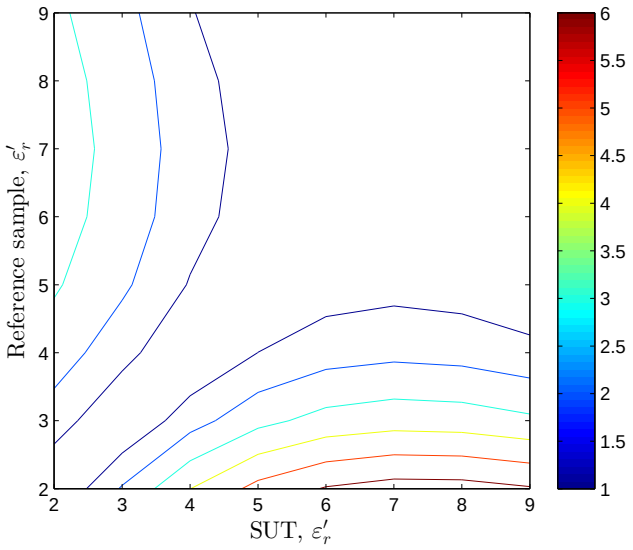

Figure 4.2: Relative error in percent for the permittivity. Sample radius is set to 5 mm.

4.2.1.1 Dielectric materials

First we will focus on non-magnetic materials. The permeability and magnetic loss tangent are therefore set to $\mu_r = 1$ and $\tan\delta_m = 0$.

Lossless dielectrics

We first consider lossless dielectric samples, i.e. both the reference sample and the sample under test have a real-valued permittivity and unit permeability. The relative permittivity was set to integral values in the range 2–9. First, we consider the difference between Equations (2.100) and (2.101). This difference turned out to be of order $10^{-7}$and is thus much smaller than the accuracy of the method. The approximate formula of Equation (2.101) should thus be valid to use.

We continue by studying how accurate the method is and compare the accuracy of two different sample sizes. The obtained values of the permittivities are presented together with the corresponding errors in Tables 4.2 and 4.3. As can be expected, a reference sample and sample under test of similar permittivity yields the best accuracy. In general, the method reproduces the permittivity to integer accuracy. By choosing the reference sample properly, we can obtain the accuracy that we desire, or at least with an absolute error of 0.1–0.2. A smaller sample does not seem to improve the accuracy significantly. In some cases the accuracy even was worse for the smaller sample. The relative error for simulations of 5 mm samples are also presented graphically in Figure 4.2.

Table 4.2: Obtained values for the permittivity of the sample under test of radius 5 mm, using a reference sample of equal radius.

	Relative permittivity of reference sample							
True value	2	Err., %	3	Err., %	4	Err., %	5	Err., %
2	2.0	0.0	2.0	1.5	1.9	2.5	1.9	3.1
3	3.1	2.1	3.0	0.0	3.0	1.4	2.9	2.2
4	4.2	4.0	4.1	1.6	4.0	0.0	4.0	0.9
5	5.3	5.3	5.1	2.7	5.1	1.0	5.0	0.0
6	6.4	6.1	6.2	3.3	6.1	1.6	6.0	0.5
7	7.4	6.4	7.3	3.6	7.1	1.7	7.0	0.7
8	8.5	6.4	8.3	3.5	8.1	1.6	8.0	0.5
9	9.5	6.1	9.3	3.2	9.1	1.3	9.0	0.2

	Relative permittivity of reference sample, continued							
True value	6	Err., %	7	Err., %	8	Err., %	9	Err., %
2	1.9	3.4	1.9	3.5	1.9	3.4	1.9	3.2
3	2.9	2.6	2.9	2.7	2.9	2.6	2.9	2.3
4	3.9	1.4	3.9	1.5	3.9	1.4	4.0	1.1
5	5.0	0.5	5.0	0.6	5.0	0.5	5.0	0.2
6	6.0	0.0	6.0	0.1	6.0	0.0	6.0	0.3
7	7.0	0.1	7.0	0.0	7.0	0.1	7.0	0.5
8	8.0	0.0	8.0	0.1	8.0	0.0	8.0	0.4
9	9.0	0.4	9.0	0.5	9.0	0.4	9.0	0.0

Lossy dielectrics

Before moving on to calculations of losses we conclude that adding an imaginary part to the permittivity barely shifts the resonant peaks, see Figure 4.3. In this figure, we investigate a magnetic material with magnetic losses and see that neither of the two kinds of losses affect the resonance frequency. It is thus safe to say that calculations of the real part of the permittivity will not be affected significantly by adding a loss term. In this paragraph, we therefore fix the real part and study the imaginary part.

Since we are interested in the order of magnitude of $\tan\delta_e$, we study the cases where the loss tangent equals 10^{-5}, 10^{-4}, 10^{-3} and 10^{-2}. Table 4.4 shows the typical behavior, in this case using nonmagnetic materials with $\varepsilon_r' = 3$ for the reference and $\varepsilon_r' = 5$ for the SUT. As can be seen from the table, the results are satisfying when both samples have $\tan\delta_e \geq 10^{-3}$.

Table 4.3: Obtained values for the permittivity of the sample under test of radius 2 mm, using a reference sample of equal radius.

	Relative permittivity of reference sample							
True value	2	Err., %	3	Err., %	4	Err., %	5	Err., %
2	2.0	0.0	2.0	0.8	2.0	1.7	1.9	2.5
3	3.0	1.1	3.0	0.0	3.0	1.2	2.9	2.3
4	4.1	2.6	4.1	1.4	4.0	0.0	3.9	1.3
5	5.2	4.3	5.1	2.9	5.1	1.4	5.0	0.0
6	6.4	5.9	6.3	4.5	6.2	2.9	6.1	1.4
7	7.5	7.7	7.4	6.2	7.3	4.6	7.2	3.0
8	8.7	9.3	8.6	7.8	8.5	6.1	8.4	4.4
9	10.0	11.0	9.8	9.4	9.7	7.6	9.5	5.9

	Relative permittivity of reference sample, continued							
True value	6	Err., %	7	Err., %	8	Err., %	9	Err., %
2	1.9	3.3	1.9	4.1	1.9	4.8	1.9	5.5
3	2.9	3.4	2.9	4.5	2.8	5.4	2.8	6.4
4	3.9	2.5	3.8	3.8	3.8	4.9	3.8	5.9
5	4.9	1.3	4.9	2.7	4.8	3.8	4.8	5.0
6	6.0	0.0	5.9	1.4	5.8	2.6	5.8	3.9
7	7.1	1.5	7.0	0.0	6.9	1.3	6.8	2.6
8	8.2	2.9	8.1	1.3	8.0	0.0	7.9	1.3
9	9.4	4.3	9.2	2.7	9.1	1.4	9.0	0.0

Table 4.4: Obtained values for the dielectric loss tangent of the sample under test of radius 5 mm and $\varepsilon'_r = 5$, using a reference sample with $\varepsilon'_r = 3$ and equal radius.

	Dielectric loss tangent of reference sample			
True value	10^{-5}	10^{-4}	10^{-3}	10^{-2}
10^{-5}	$8.9 \cdot 10^{-6}$	$1.1 \cdot 10^{-4}$	$-3.7 \cdot 10^{-4}$	$-2.7 \cdot 10^{-4}$
10^{-4}	$6.9 \cdot 10^{-6}$	$8.2 \cdot 10^{-5}$	$-2.8 \cdot 10^{-4}$	$-2.0 \cdot 10^{-4}$
10^{-3}	$-2.1 \cdot 10^{-5}$	$-2.6 \cdot 10^{-4}$	$8.9 \cdot 10^{-4}$	$6.3 \cdot 10^{-4}$
10^{-2}	$-3.0 \cdot 10^{-4}$	$-3.6 \cdot 10^{-3}$	$1.3 \cdot 10^{-2}$	$8.9 \cdot 10^{-3}$

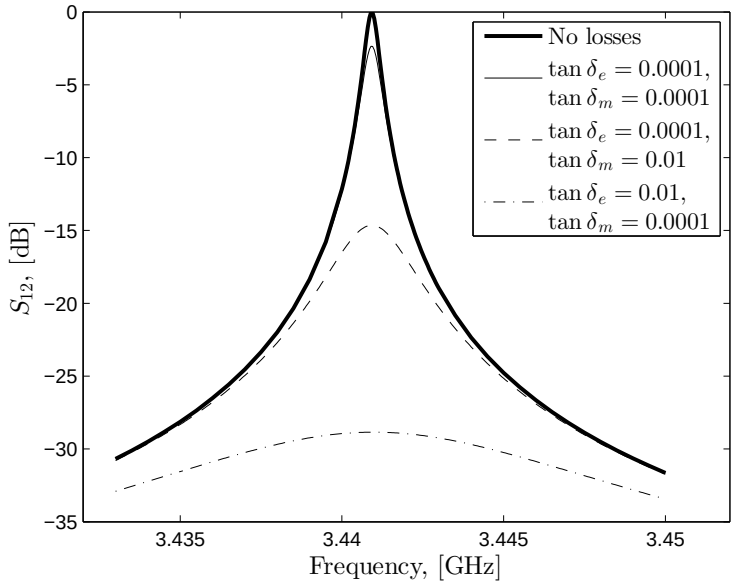

Figure 4.3: The TM_{010}-peak for samples with parameter values $\varepsilon_r' = \mu_r' = 3$ and varying loss tangents. The bandwidth is altered by the loss term but the resonance frequency remain the same.

Table 4.5: Obtained values for the permittivity of the sample under test of radius 5 mm and $\varepsilon_r' = 5$, using a reference sample with $\varepsilon_r' = 3$ and equal radius. Errors are given in percent.

	Relative permeability of reference sample							
Permeability of SUT	1	Err.	3	Err.	5	Err.	7	Err.
1	5.1	2.7	4.5	9.8	4.0	20.8	3.5	30.3
3	6.0	19.4	5.2	4.4	4.6	8.8	4.0	20.2
5	7.0	39.7	6.1	21.6	5.3	5.7	4.6	8.0
7	8.1	63.0	7.1	41.4	6.1	22.4	5.3	6.0

4.2.1.2 Magnetic materials

In general a magnetic material has both a measurable permittivity and permeability. In this section we will first study how sensitive the permittivity measurement is to the introduction of permeability. We then study how the measurement of permeability is affected by the permittivity. Finally, we consider magnetic losses in a way similar to the treatment of dielectric losses.

Table 4.6: Obtained values for the permeability of the sample under test of radius 5 mm and $\varepsilon_r' = 5$, using a reference sample with $\varepsilon_r' = 3$ and equal radius. Errors are given in percent.

	Relative permeability of reference sample							
True value	1	Err.	3	Err.	5	Err.	7	Err.
1	5.5	446.4	2.2	118.0	1.9	87.6	1.7	69.3
3	15.2	405.3	4.7	58.1	3.8	26.0	3.2	6.6
5	25.1	402.4	7.4	47.5	5.7	14.7	4.7	5.1
7	42.6	509.1	12.0	71.5	9.2	31.0	7.5	6.6

Permittivity of lossless magnetic materials

In Table 4.5 we present the results of a permittivity measurement of a magnetic material. In this case, the reference sample had a permittivity of $\varepsilon_r' = 3$ and for the SUT the corresponding value was $\varepsilon_r' = 5$. The table shows what measured value of the permittivity of the SUT that was obtained depending on the permeability of both the reference sample and SUT. The best reproduced values are obtained when the two samples have the same permeability. The general trend is that if the permeability of the reference sample is higher than for the SUT, we obtain a lower permittivity than the true value. Similarly, if the reference sample has a lower permeability, the obtained permittivity is too high.

Permeability of lossless magnetic materials

In Table 4.6 we present the results of a permeability measurement. As in the previous paragraph, the permittivities are kept fixed at $\varepsilon_r' = 5$ for the SUT and $\varepsilon_r' = 3$ for the reference. There are neither dielectric nor magnetic losses. Unfortunately, the reproduced values are far off from the actual value. In fact, the measured value is closer to the permittivity of the SUT, at least when the two samples are of equal permeability.

Lossy magnetic materials

Here we study magnetic materials with magnetic losses. Dielectric losses are set to zero and permittivities are considered to be unity. In Table 4.7 we present the results of such a simulation when the permeabilities are set to $\mu_r' = 3$ for the reference and $\mu_r' = 5$ for the SUT. Exactly as in the case of dielectric losses, we see that there is a limit under which the method can not be used. Above $\tan\delta_m = 10^{-2}$ though, the obtained value has the desired accuracy.

Table 4.7: Obtained values for the magnetic loss tangent of the sample under test of radius 5 mm and $\mu_r' = 5$, using a reference sample with $\mu_r' = 3$ and equal radius. Permittivity is set to unity and there are no dielectric losses.

	Magnetic loss tangent of reference sample				
True value	10^{-5}	10^{-4}	10^{-3}	10^{-2}	10^{-1}
10^{-5}	$7.9 \cdot 10^{-6}$	$7.9 \cdot 10^{-5}$	$-4.7 \cdot 10^{-3}$	$-9.5 \cdot 10^{-4}$	$-8.5 \cdot 10^{-4}$
10^{-4}	$7.9 \cdot 10^{-6}$	$7.9 \cdot 10^{-5}$	$-4.7 \cdot 10^{-3}$	$-9.5 \cdot 10^{-4}$	$-8.5 \cdot 10^{-4}$
10^{-3}	$3.0 \cdot 10^{-6}$	$3.0 \cdot 10^{-5}$	$-1.8 \cdot 10^{-3}$	$-3.6 \cdot 10^{-4}$	$-3.3 \cdot 10^{-4}$
10^{-2}	$-5.0 \cdot 10^{-5}$	$-5.0 \cdot 10^{-4}$	$3.0 \cdot 10^{-2}$	$6.0 \cdot 10^{-3}$	$5.4 \cdot 10^{-3}$
10^{-1}	$-5.6 \cdot 10^{-4}$	$-5.6 \cdot 10^{-3}$	$3.4 \cdot 10^{-1}$	$6.8 \cdot 10^{-2}$	$6.0 \cdot 10^{-2}$

Table 4.8: Properties of some general materials used in the verification of the method. The properties used are those listed in Ansys HFSS version 15.

ID	Material	ε_r'	$\tan \delta_e$	μ_r'	$\tan \delta_m$
A	PTFE (Teflon)	2.1	0.001	1	0
B	Taconic TLE$^{\text{TM}}$	2.95	0.0028	1	0
C	GE GETEK ML200/RG200$^{\text{TM}}$	3.9	0.012	1	0
D	Polyamide	4.3	0.004	1	0
E	RogersTMM6$^{\text{TM}}$	6	0.0023	1	0
F	—	2	0.001	5	0.01
G	—	5	0.001	2	0.01
H	—	2	0.01	5	0.01
I	—	2	0.001	5	0.1

4.2.1.3 General materials

We have now seen how different electric and magnetic properties affect the outcome of the measurement procedure. Now, we shall study the results of general materials that can have both a relative permittivity and relative permeability larger than one and both dielectric and magnetic losses. The used materials are presented in Table 4.8. A sample size of 5 mm was used. For the nonmagnetic materials A–E, the obtained permittivities and dielectric loss tangents with errors are presented in Table 4.9 and 4.10. For the magnetic materials F–I, the corresponding values are found in Table 4.11 and 4.12. Similarly, the obtained permeabilities and magnetic loss tangents are presented in Table 4.13 and 4.14.

Table 4.9: Obtained values for the permittivity of the sample under test of radius 5 mm, using a reference sample of equal radius. Errors are given in percent.

	Reference sample									
SUT	A	Err.	B	Err.	C	Err.	D	Err.	E	Err.
A	2.1	0.0	2.1	1.3	2.1	2.3	2.0	2.7	2.0	3.4
B	3.0	1.7	3.0	0.0	2.9	1.3	2.9	1.7	2.9	2.6
C	4.0	3.5	4.0	1.5	3.9	0.0	3.9	0.5	3.8	1.5
D	4.5	4.1	4.4	2.1	4.3	0.5	4.3	0.0	4.3	1.1
E	6.3	5.7	6.2	3.5	6.1	1.7	6.1	1.2	6.0	0.0

Table 4.10: Obtained values for the dielectric loss tangent of the sample under test of radius 5 mm, using a reference sample of equal radius.

	Reference sample				
SUT	A	B	C	D	E
A	$1.0 \cdot 10^{-3}$	$8.0 \cdot 10^{-4}$	$7.6 \cdot 10^{-4}$	$8.2 \cdot 10^{-4}$	$1.0 \cdot 10^{-3}$
B	$3.5 \cdot 10^{-3}$	$2.8 \cdot 10^{-3}$	$2.7 \cdot 10^{-3}$	$2.9 \cdot 10^{-3}$	$3.6 \cdot 10^{-3}$
C	$1.6 \cdot 10^{-2}$	$1.3 \cdot 10^{-2}$	$1.2 \cdot 10^{-2}$	$1.3 \cdot 10^{-2}$	$1.6 \cdot 10^{-2}$
D	$4.8 \cdot 10^{-3}$	$3.9 \cdot 10^{-3}$	$3.7 \cdot 10^{-3}$	$4.0 \cdot 10^{-3}$	$5.1 \cdot 10^{-3}$
E	$2.2 \cdot 10^{-3}$	$1.8 \cdot 10^{-3}$	$1.7 \cdot 10^{-3}$	$1.8 \cdot 10^{-3}$	$2.3 \cdot 10^{-3}$

Table 4.11: Obtained values for the permittivity of the sample under test of radius 5 mm, using a reference sample of equal radius.

	Reference sample							
SUT	F	Err., %	G	Err., %	H	Err., %	I	Err., %
F	2.0	0.0	2.2	8.5	2.0	0.0	2.0	0.1
G	4.4	11.6	5.0	0.0	4.4	11.6	4.4	11.6
H	2.0	0.0	2.2	8.5	2.0	0.0	2.0	0.1
I	2.0	0.1	2.2	8.4	2.0	0.1	2.0	0.0

Table 4.12: Obtained values for the dielectric loss tangent of the sample under test of radius 5 mm, using a reference sample of equal radius.

	Reference sample			
SUT	F	G	H	I
F	$1.0 \cdot 10^{-3}$	$1.6 \cdot 10^{-3}$	$2.3 \cdot 10^{-3}$	$1.3 \cdot 10^{-4}$
G	$6.7 \cdot 10^{-4}$	$1.0 \cdot 10^{-3}$	$1.5 \cdot 10^{-3}$	$8.8 \cdot 10^{-5}$
H	$4.4 \cdot 10^{-3}$	$6.8 \cdot 10^{-3}$	$1.0 \cdot 10^{-2}$	$5.7 \cdot 10^{-4}$
I	$7.7 \cdot 10^{-3}$	$1.2 \cdot 10^{-2}$	$1.7 \cdot 10^{-2}$	$1.0 \cdot 10^{-3}$

Table 4.13: Obtained values for the permeability of the sample under test of radius 5 mm, using a reference sample of equal radius.

	Reference sample							
SUT	F	Err., %	G	Err., %	H	Err., %	I	Err., %
F	2.0	0.0	3.9	65.5	2.0	0.0	2.0	0.0
G	2.4	226	5.0	0.0	2.4	226	2.4	226
H	2.0	0.0	3.9	65.5	2.0	0.0	2.0	0.0
I	2.0	0.0	3.9	65.5	2.0	0.0	2.0	0.0

Table 4.14: Obtained values for the magnetic loss tangent of the sample under test of radius 5 mm, using a reference sample of equal radius.

	Reference sample			
SUT	F	G	H	I
F	$1.0 \cdot 10^{-2}$	$4.2 \cdot 10^{-3}$	$4.5 \cdot 10^{-3}$	$1.1 \cdot 10^{-2}$
G	$2.1 \cdot 10^{-2}$	$1.0 \cdot 10^{-2}$	$9.6 \cdot 10^{-3}$	$2.3 \cdot 10^{-2}$
H	$2.2 \cdot 10^{-2}$	$9.3 \cdot 10^{-3}$	$1.0 \cdot 10^{-2}$	$2.5 \cdot 10^{-2}$
I	$9.1 \cdot 10^{-2}$	$3.8 \cdot 10^{-2}$	$4.1 \cdot 10^{-2}$	$1.0 \cdot 10^{-1}$

4.2.1.4 Tolerance tests

We have now seen that satisfying results can be obtained for permittivity and losses using the cavity-perturbation method. However, in the simulations the dimensions of the sample are defined with high precision. In reality, we may encounter small deviations from these values. The SUT may be slightly thicker or thinner than the reference sample. The same can occur for the radius. In addition, the sample may be somewhat displaced from the center or cavity edge. We shall in this section study how sensitive the measurements are to such deviations. We here restrict ourselves to samples of radius 5 mm. For samples of radius 2 mm, the reader is referred to Appendix F.

For permittivity tests, the dielectric loss tangent was set to 0.001 and the permittivity was tested for $\varepsilon_r' = 3$ and $\varepsilon_r' = 5$. For permeability tests, the magnetic loss tangent was set to 0.01 and the permeability was tested for $\mu_r' = 3$ and $\mu_r' = 5$.

We first turn our attention to the height of the sample. This is in some sense the most crucial error source since the materials of interest often are provided in sheets and it might be difficult to choose a specified thickness. The tolerance test of the sample heights are presented in Table 4.15 through 4.16 for permittivity and dielectric loss tangent respectively. The corresponding tests for the permeability and magnetic loss tangent are presented in Table 4.17 and 4.18. As can be seen from the data, the permittivity measurement seems to be quite sensitive to the

Table 4.15: Tolerance test of relative permittivity for deviating height. Sample radii are 5 mm. Errors are given in percent.

		Height h and permittivity ε_r' of reference sample							
		$h = 1.5\,\text{mm}$				$h = 1.6\,\text{mm}$			
SUT values		$\varepsilon_r' = 3$	Err.	$\varepsilon_r' = 5$	Err.	$\varepsilon_r' = 3$	Err.	$\varepsilon_r' = 5$	Err.
$h =$ 1.5 mm	$\varepsilon_r' = 3$	3.0	0.0	2.9	2.2	3.4	13.1	3.6	18.5
	$\varepsilon_r' = 5$	5.1	2.7	5.0	0.0	5.9	19.0	6.3	25.7
$h =$ 1.6 mm	$\varepsilon_r' = 3$	2.7	11.0	2.6	12.8	3.0	0.0	3.1	4.5
	$\varepsilon_r' = 5$	4.1	17.4	4.0	19.4	4.7	5.1	5.0	0.0

Table 4.16: Tolerance test of dielectric loss tangent for deviating height. Sample radii are 5 mm.

		Height h and permittivity ε_r' of reference sample			
		$h = 1.5\,\text{mm}$		$h = 1.6\,\text{mm}$	
SUT values		$\varepsilon_r' = 3$	$\varepsilon_r' = 5$	$\varepsilon_r' = 3$	$\varepsilon_r' = 5$
$h = 1.5\,\text{mm}$	$\varepsilon_r' = 3$	$1.0 \cdot 10^{-3}$	$6.0 \cdot 10^{-4}$	$1.4 \cdot 10^{-3}$	$1.1 \cdot 10^{-3}$
	$\varepsilon_r' = 5$	$1.7 \cdot 10^{-3}$	$1.0 \cdot 10^{-3}$	$2.2 \cdot 10^{-3}$	$1.7 \cdot 10^{-3}$
$h = 1.6\,\text{mm}$	$\varepsilon_r' = 3$	$7.3 \cdot 10^{-4}$	$4.3 \cdot 10^{-4}$	$1.0 \cdot 10^{-3}$	$7.8 \cdot 10^{-4}$
	$\varepsilon_r' = 5$	$9.6 \cdot 10^{-4}$	$5.8 \cdot 10^{-4}$	$1.3 \cdot 10^{-3}$	$1.0 \cdot 10^{-3}$

sample height. However, the dielectric loss tangent is in general reproduced to the desired accuracy. Permeability measurements do not show the same sensitivity but the errors were unreasonably large already. The magnetic losses were reproduced to the correct order of magnitude when the reference sample was thicker but not thinner.

We then move on to the sample radius. The results are presented in Tables 4.19, 4.20, 4.21 and 4.22. Using the volume dependent calibration constants almost eliminates the error due to the radius. Even though the answer still may be off, a slightly bigger sample still yields the same accuracy. In other words, as long as we can measure the radius accurately, it does not matter if one sample is slightly bigger.

Finally, we study how a deviation of the sample placement affects the outcome. The results of these simulations are presented in Tables 4.23, 4.24, 4.25 and 4.26. Here, we see that displacing the sample by a millimeter does not affect the results significantly. This is of course satisfying since it may be difficult to place the sample exactly in the middle.

Table 4.17: Tolerance test of relative permeability for deviating height. Sample radii are 5 mm. Errors are given in percent.

		Height h and permeability μ_r' of reference sample							
		$h = 1.5\,\text{mm}$				$h = 1.6\,\text{mm}$			
SUT values		$\mu_r' = 3$	Err.	$\mu_r' = 5$	Err.	$\mu_r' = 3$	Err.	$\mu_r' = 5$	Err.
$h =$ 1.5 mm	$\mu_r' = 3$	3.0	0.0	4.0	34.8	3.1	2.1	4.1	37.1
	$\mu_r' = 5$	3.6	27.4	5.0	0.0	3.7	25.8	5.1	1.8
$h =$ 1.6 mm	$\mu_r' = 3$	2.9	2.1	3.9	31.7	3.0	0.0	4.0	33.9
	$\mu_r' = 5$	3.6	28.6	4.9	1.8	3.7	26.9	5.0	0.0

Table 4.18: Tolerance test of magnetic loss tangent for deviating height. Sample radii are 5 mm.

		Height h and permeability μ_r' of reference sample			
		$h = 1.5\,\text{mm}$		$h = 1.6\,\text{mm}$	
SUT values		$\mu_r' = 3$	$\mu_r' = 5$	$\mu_r' = 3$	$\mu_r' = 5$
$h = 1.5\,\text{mm}$	$\mu_r' = 3$	$1.0 \cdot 10^{-2}$	$1.3 \cdot 10^{-2}$	$3.4 \cdot 10^{-2}$	$3.1 \cdot 10^{-2}$
	$\mu_r' = 5$	$7.9 \cdot 10^{-3}$	$1.0 \cdot 10^{-2}$	$2.7 \cdot 10^{-2}$	$2.4 \cdot 10^{-2}$
$h = 1.6\,\text{mm}$	$\mu_r' = 3$	$3.0 \cdot 10^{-3}$	$3.8 \cdot 10^{-3}$	$1.0 \cdot 10^{-2}$	$9.2 \cdot 10^{-3}$
	$\mu_r' = 5$	$3.3 \cdot 10^{-3}$	$4.2 \cdot 10^{-3}$	$1.1 \cdot 10^{-2}$	$1.0 \cdot 10^{-2}$

Table 4.19: Tolerance test of relative permittivity for deviating radius. Errors are given in percent.

		Radius r and permittivity ε_r' of reference sample							
		$r = 5.0\,\text{mm}$				$r = 5.1\,\text{mm}$			
SUT values		$\varepsilon_r' = 3$	Err.	$\varepsilon_r' = 5$	Err.	$\varepsilon_r' = 3$	Err.	$\varepsilon_r' = 5$	Err.
$r =$ 5.0 mm	$\varepsilon_r' = 3$	3.0	0.0	2.9	2.2	3.0	0.1	2.9	1.9
	$\varepsilon_r' = 5$	5.1	2.7	5.0	0.0	5.1	2.9	5.0	0.3
$r =$ 5.1 mm	$\varepsilon_r' = 3$	3.0	0.1	2.9	2.3	3.0	0.0	2.9	2.0
	$\varepsilon_r' = 5$	5.1	2.4	5.0	0.3	5.1	2.5	5.0	0.0

Table 4.20: Tolerance test of dielectric loss tangent for deviating radius.

		Radius r and permittivity ε'_r of reference sample			
		$r = 5.0\,\text{mm}$		$r = 5.1\,\text{mm}$	
SUT values		$\varepsilon'_r = 3$	$\varepsilon'_r = 5$	$\varepsilon'_r = 3$	$\varepsilon'_r = 5$
$r = 5.0\,\text{mm}$	$\varepsilon'_r = 3$	$1.0 \cdot 10^{-3}$	$6.0 \cdot 10^{-4}$	$8.8 \cdot 10^{-4}$	$5.7 \cdot 10^{-4}$
	$\varepsilon'_r = 5$	$1.7 \cdot 10^{-3}$	$1.0 \cdot 10^{-3}$	$1.5 \cdot 10^{-3}$	$9.6 \cdot 10^{-4}$
$r = 5.1\,\text{mm}$	$\varepsilon'_r = 3$	$1.1 \cdot 10^{-3}$	$6.8 \cdot 10^{-4}$	$1.0 \cdot 10^{-3}$	$6.5 \cdot 10^{-4}$
	$\varepsilon'_r = 5$	$1.7 \cdot 10^{-3}$	$1.0 \cdot 10^{-3}$	$1.5 \cdot 10^{-3}$	$1.0 \cdot 10^{-3}$

Table 4.21: Tolerance test of relative permeability for deviating radius. Errors are given in percent.

		Radius r and permeability μ'_r of reference sample							
		$r = 5.0\,\text{mm}$				$r = 5.1\,\text{mm}$			
SUT values		$\mu'_r = 3$	Err.	$\mu'_r = 5$	Err.	$\mu'_r = 3$	Err.	$\mu'_r = 5$	Err.
$r =$ 5.0 mm	$\mu'_r = 3$	3.0	0.0	4.0	34.8	3.0	0.0	4.1	35.2
	$\mu'_r = 5$	3.6	27.4	5.0	0.0	3.6	27.4	5.0	0.3
$r =$ 5.1 mm	$\mu'_r = 3$	3.0	0.0	4.0	34.8	3.0	0.0	4.1	35.1
	$\mu'_r = 5$	3.6	27.6	5.0	0.3	3.6	27.6	5.0	0.0

Table 4.22: Tolerance test of magnetic loss tangent for deviating radius.

		Radius r and permeability μ'_r of reference sample			
		$r = 5.0\,\text{mm}$		$r = 5.1\,\text{mm}$	
SUT values		$\mu'_r = 3$	$\mu'_r = 5$	$\mu'_r = 3$	$\mu'_r = 5$
$r = 5.0\,\text{mm}$	$\mu'_r = 3$	$1.0 \cdot 10^{-2}$	$1.3 \cdot 10^{-2}$	$8.8 \cdot 10^{-3}$	$1.3 \cdot 10^{-2}$
	$\mu'_r = 5$	$7.9 \cdot 10^{-3}$	$1.0 \cdot 10^{-2}$	$6.9 \cdot 10^{-3}$	$1.0 \cdot 10^{-2}$
$r = 5.1\,\text{mm}$	$\mu'_r = 3$	$1.1 \cdot 10^{-2}$	$1.5 \cdot 10^{-2}$	$1.0 \cdot 10^{-2}$	$1.5 \cdot 10^{-2}$
	$\mu'_r = 5$	$7.9 \cdot 10^{-3}$	$1.0 \cdot 10^{-2}$	$6.9 \cdot 10^{-3}$	$1.0 \cdot 10^{-2}$

Table 4.23: Tolerance test of relative permittivity for deviating placement. Sample radii are 5 mm. Errors are given in percent.

		Displacement from edge x and permeability μ'_r of reference sample							
		$x = 0$ mm				$x = 1$ mm			
SUT values		$\varepsilon'_r = 3$	Err.	$\varepsilon'_r = 5$	Err.	$\varepsilon'_r = 3$	Err.	$\varepsilon'_r = 5$	Err.
$x =$ 0 mm	$\varepsilon'_r = 3$	3.0	0.0	2.9	2.2	3.0	0.2	2.9	2.1
	$\varepsilon'_r = 5$	5.1	2.7	5.0	0.0	5.1	2.9	5.0	0.2
$x =$ 1 mm	$\varepsilon'_r = 3$	3.0	0.2	2.9	2.3	3.0	0.0	2.9	2.2
	$\varepsilon'_r = 5$	5.1	2.5	5.0	0.2	5.1	2.7	5.0	0.0

Table 4.24: Tolerance test of dielectric loss tangent for deviating placement. Sample radii are 5 mm.

		Displacement from edge x and permeability μ'_r of reference sample			
		$x = 0$ mm		$x = 1$ mm	
SUT values		$\varepsilon'_r = 3$	$\varepsilon'_r = 5$	$\varepsilon'_r = 3$	$\varepsilon'_r = 5$
$x =$ 0 mm	$\varepsilon'_r = 3$	$1.0 \cdot 10^{-3}$	$6.0 \cdot 10^{-4}$	$1.0 \cdot 10^{-3}$	$6.0 \cdot 10^{-4}$
	$\varepsilon'_r = 5$	$1.7 \cdot 10^{-3}$	$1.0 \cdot 10^{-3}$	$1.7 \cdot 10^{-3}$	$1.0 \cdot 10^{-3}$
$x =$ 1 mm	$\varepsilon'_r = 3$	$1.0 \cdot 10^{-3}$	$6.0 \cdot 10^{-4}$	$1.0 \cdot 10^{-3}$	$6.0 \cdot 10^{-4}$
	$\varepsilon'_r = 5$	$1.7 \cdot 10^{-3}$	$1.0 \cdot 10^{-3}$	$1.7 \cdot 10^{-3}$	$1.0 \cdot 10^{-3}$

Table 4.25: Tolerance test of relative permeability for deviating placement. Sample radii are 5 mm. Errors are given in percent.

		Displacement from edge x and permeability μ'_r of reference sample							
		$x = 0$ mm				$x = 1$ mm			
SUT values		$\mu'_r = 3$	Err.	$\mu'_r = 5$	Err.	$\mu'_r = 3$	Err.	$\mu'_r = 5$	Err.
$x =$ 0 mm	$\mu'_r = 3$	3.0	0.0	4.0	34.8	2.9	2.5	3.9	30.5
	$\mu'_r = 5$	3.6	27.4	5.0	0.0	3.5	29.4	4.8	3.4
$x =$ 1 mm	$\mu'_r = 3$	3.1	2.6	4.2	38.8	3.0	0.0	4.0	34.3
	$\mu'_r = 5$	3.7	25.1	5.2	3.6	3.6	27.2	5.0	0.0

Table 4.26: Tolerance test of magnetic loss tangent for deviating placement. Sample radii are 5 mm.

		Displacement from edge x and permeability μ_r' of reference sample			
		$x = 0$ mm		$x = 1$ mm	
SUT values		$\mu_r' = 3$	$\mu_r' = 5$	$\mu_r' = 3$	$\mu_r' = 5$
$x =$ 0 mm	$\mu_r' = 3$	$1.0 \cdot 10^{-2}$	$1.3 \cdot 10^{-2}$	$9.2 \cdot 10^{-3}$	$1.3 \cdot 10^{-2}$
	$\mu_r' = 5$	$7.9 \cdot 10^{-3}$	$1.0 \cdot 10^{-2}$	$7.3 \cdot 10^{-3}$	$9.9 \cdot 10^{-3}$
$x =$ 1 mm	$\mu_r' = 3$	$1.1 \cdot 10^{-2}$	$1.4 \cdot 10^{-2}$	$1.0 \cdot 10^{-2}$	$1.4 \cdot 10^{-2}$
	$\mu_r' = 5$	$8.0 \cdot 10^{-3}$	$1.0 \cdot 10^{-2}$	$7.4 \cdot 10^{-3}$	$1.0 \cdot 10^{-2}$

4.2.2 Curve-set method

A series of simulations where the relative permittivity and permeability were varied was performed using the eigenvalue solver in Ansys HFSS. The same cavity resonator was used as in the cavity-perturbation method, see Figure 3.2. The sample radius was set to 5 mm and the materials are lossless. The resulting frequency of the TM_{010} mode as function of the permittivity and permeability is presented in Figure 4.4. Here, dashed lines correspond to a centered sample and full lines to a sample at the cavity edge. As we see, it is possible to find points where the curves corresponding to different positions cross and these points correspond to the actual properties of the sample.

As stated previously, the resonances barely shift when we add an imaginary part to the material properties. Hence, the results presented in Figure 4.4 above still hold for lossy materials. However, the Q-factor is dependent of the resonance frequency and we would thus need one Q-factor graph for each pair of ε and μ. The easiest way might thus be to first determine the real parts. When these are known, they can be used in simulations together with varying imaginary parts. Comparing the measurement to this second data set should give us the imaginary parts of the parameters. In Figure 4.5 we present the Q-factor as function of the dielectric and magnetic loss tangent when the sample has radius 5 mm and $\varepsilon_r' = 3$ and $\mu_r' = 3$.

In this method, we are not relying on approximations of field profiles, nor is the sample size a crucial factor. It all comes down to if simulations and experimental measurements yield similar answers.

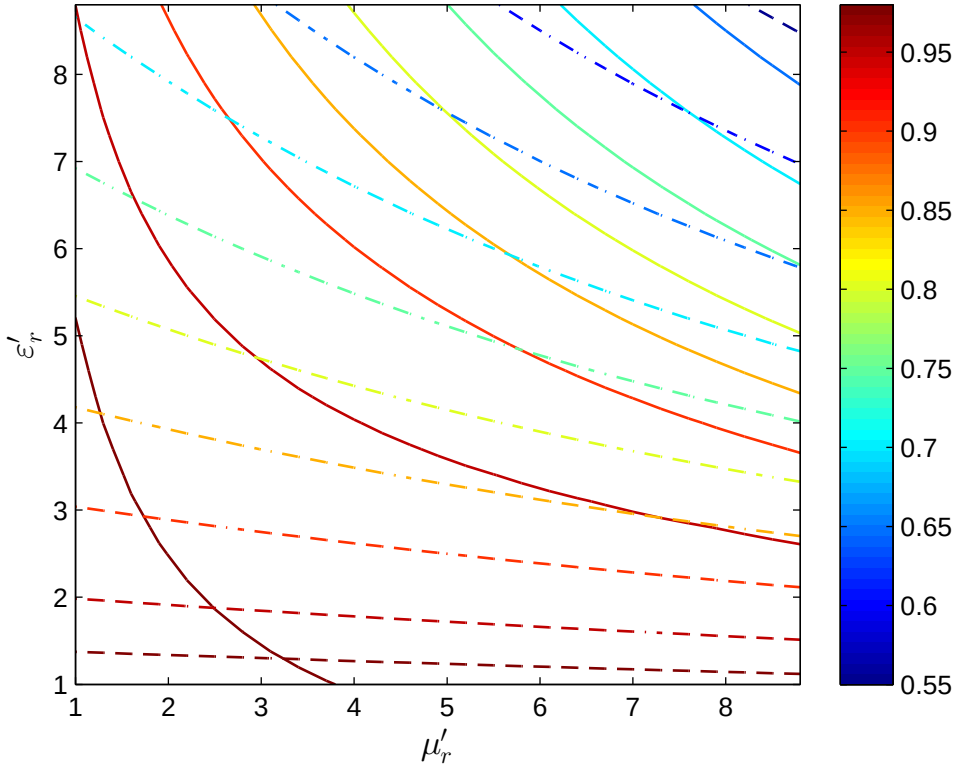

Figure 4.4: A set of curves describing the resonance frequency of the TM_{010} mode as function of the (real part of the) permittivity and permeability. Values are normalized to the resonance of an empty cavity (3.88 GHz). Dashed lines refer to measurements with the sample centered and full lines to when the sample is placed at the cavity edge. The contours indicate the relative frequency of the TM_{010} mode.

4.3 Experimental measurements

A few test measurements have been conducted on the designed cavity. In Figure 4.6, the measured and simulated spectra are presented. The corresponding resonance frequencies are given together with theoretical values in Table 4.27. A measurement on a PTFE (teflon) sample of radius 5 mm is presented in Figure 4.7. The three curves presented correspond to an empty cavity, a loaded cavity with the sample at the edge, and a loaded cavity with a centered sample. One should here note that placing the sample at the cavity edge shifts the frequency by almost nothing, since PTFE is not magnetic.

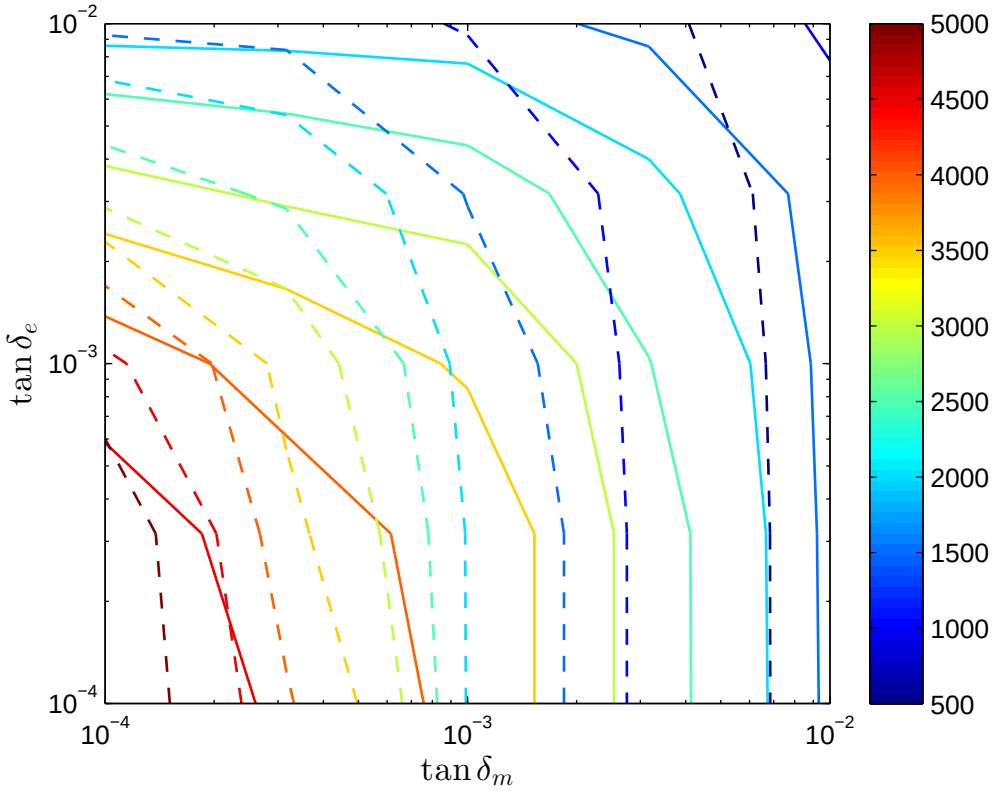

Figure 4.5: A crowd of curves describing the Q-factor as function of the dielectric and magnetic loss tangents. For this particular figure, the real part of the permittivity and permeability are set to 3. Dashed lines refer to measurements with the sample centered and full lines when the sample is placed at the cavity edge. (Note that as this figure was generated, leakage was accidentally neglected. The actual Q-factor should therefore be lower. This figure mainly works as a proof of concept, that we get crossing contours.)

Table 4.27: Comparison of theoretical, simulated, and measured resonance frequencies for the designed cavity. Frequencies are given in GHz.

Mode	Theoretical	Simulated	Experimental
TM_{010}	3.82	3.88	3.79
TM_{110}	6.09	6.19	6.02
TM_{210}	8.18	8.29	7.94

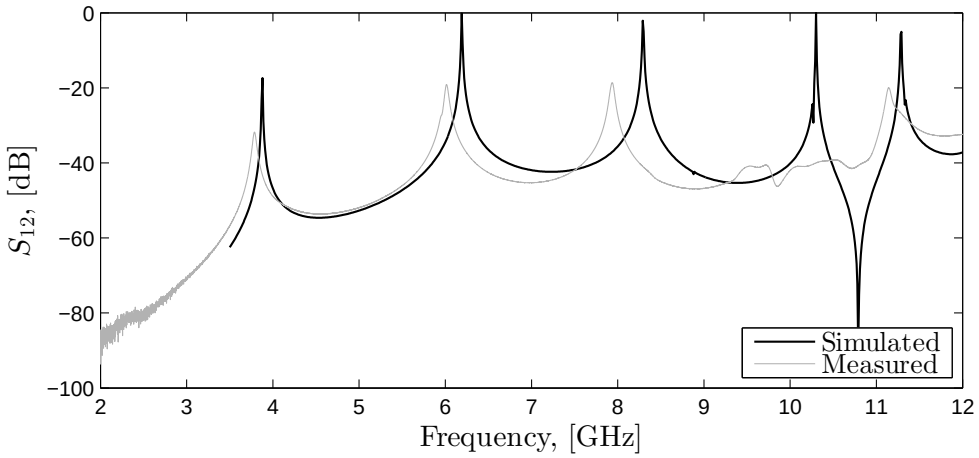

Figure 4.6: Comparison of measured and simulated cavity, with radius 15 mm and length 28 mm.

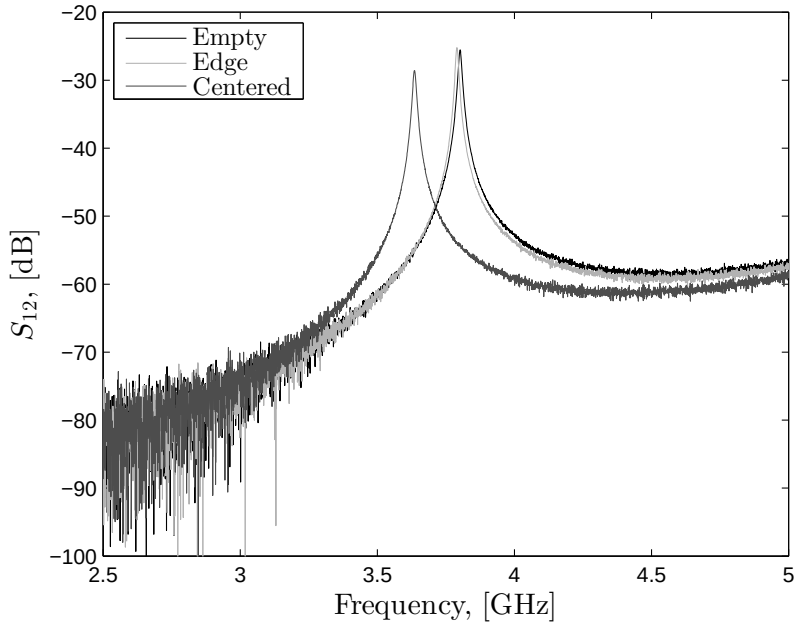

Figure 4.7: Experimental measurement of an empty cavity, a cavity with a sample loaded at the edge, and a cavity with a centered sample.

Table 4.28: Results obtained via the curve-set method.

Material	Documented ε'_r	Measured	Documented μ'_r	Measured
POM	3.7	2.7	1.0	1.0
PTFE	2.1	1.9	1.0	1.0
Unknown magnetic	—	8.3	—	2.5

4.3.1 Cavity-perturbation method

Two samples were used to test the method. The first sample was PTFE, which has a permittivity $\varepsilon'_r = 2.1$ and a dielectric loss of $\tan\delta_e = 0.001$. The second material was marked as POM (delrin), which has a permittivity $\varepsilon'_r = 3.7$ but no documented value of the dielectric loss could be found.

Using POM as the reference sample resulted in a measured value of $\varepsilon'_r = 2.3$ for the PTFE. Using PTFE as reference yielded a value of $\varepsilon'_r = 3.2$ for POM. Neither result was perfect but the obtained result for PTFE is at least fairly close to the correct value.

The obtained value for the dielectric loss of POM was $\tan\delta_e = 0.004$. Since we do not have any documented value, we cannot say if it is correct but it is at least reasonable.

4.3.2 Curve-set method

For the curve-set method, we investigate the same samples as before and an unknown magnetic material. The results are presented in Table 4.28. Once again, the result for PTFE is in the vicinity of the right one. POM is now even more off than before but there is a possibility that the material investigated was not POM. Unfortunately, the value obtained from the cavity-perturbation method is in the middle between the documented value and the one obtained from the curve-set method. Thus, it cannot be used to confirm this hypothesis.

For the magnetic material, there is no documentation to compare with. However, we can confirm that it is a magnetic material.

Chapter 5

Concluding remarks

In this final chapter we will summarize and discuss the project and the results. In addition, we give an outline for further development and suggestions on how to improve the method.

5.1 Summary

This project aimed to design an experimental setup used for the measurement of the complex permittivity and permeability. The desired accuracy was to determine ε_r' and μ_r' up to the first decimal place and to determine the order of magnitude of $\tan\delta_e$ and $\tan\delta_m$. The frequency range of interest was 400 MHz–40 GHz.

The focus of this project has been on the cavity-perturbation method. This method utilizes the resonance frequencies of a metallic cavity to determine the permittivity and permeability of an introduced sample. By introducing a sample into the cavity, the resonance frequencies are shifted. In the case of lossy materials, the resonance peaks are also broadened. By studying these changes of the spectrum, it is possible to determine the material parameters of the sample.

A circular cavity of radius 30 mm and adaptive height was designed to operate around 4 GHz using the TM_{010} mode. Using Ansys HFSS, simulations were performed to evaluate the cavity. In these simulations, samples of height 1.5 mm and of radii 2 mm and 5 mm were used. The latter of these would be easiest to fabricate. The simulations indicated that the cavity resonator can be used to determine the permittivity of nonmagnetic materials of samples with radius 5 mm to almost the desired accuracy. They also showed satisfying results in the determination of losses and to some extent measurement of permittivity for magnetic materials. It however proved difficult to measure the permeability.

In addition to the cavity-perturbation method, we have developed the "curve-set method". This method utilizes the procedure of the cavity-perturbation method

partly by demanding two measurements; one with the sample centered and one with the sample at the cavity edge. The measured frequencies are compared to the curves in Figure 4.4, which has been generated by simulating a set of permittivity and permeability pairs. The point where the two curves cross each other should correspond to the true material parameters of the sample.

5.2 Applicability

We shall here discuss the validity of the two methods and when they are applicable. These conclusions are based on the results of both simulations and experiments.

5.2.1 Cavity-perturbation theory

According to the simulations, the method turned out to reproduce the permittivity more or less accurately. Using a reference sample of (almost) equal permittivity as the SUT indeed gave an accurate result and an "iterative" method could in theory be used to determine the permittivity accurately. Our simulations also show that the method can be used to measure the loss tangents with the desired accuracy, as long as we are above a certain lower limit, 10^{-3} for the dielectric loss and 10^{-2} for the magnetic loss.

Measurements show that the resonances indeed are shifted by introducing a sample inside the cavity but the measured values of the relative permittivity are not as accurate as in the simulations. Although, we should still get quite accurate results for materials of similar properties and the iterative method could still be possible to use.

On the other hand, the method did not succeed to reproduce the correct values of the permeability. The most likely reason is that the sample is too large. It is thus not possible to place it where only the electric field is zero. In addition, the fields will be distorted more than a perturbation allows for. In the case of permittivity, this problem is not that apparent. In this case, the sample is centered in the cavity which of course distorts the field more uniformly. One should also note that as long as we restrict ourselves to non-magnetic materials, there is no need to place the sample where the magnetic field is zero.

In retrospect, it is possible that another method would have been a better choice. The limitation that we are restricted to shape the samples as discs, due to the fabrication process, limits us to quite large samples. Simultaneously, we cannot make the cavity radius bigger since that lowers the amplitude of the S_{12}-parameter to an unmeasurable level (according to simulations). In addition, it is not practical with a larger setup. Still, the method appears to be a good choice if one is only interested in nonmagnetic materials.

5.2.2 Curve-set method

It is important to emphasize that the curve-set method is not a perturbative method and we are thus not limited to small samples compared to the cavity. As long as the simulations reproduce the actual values, this should be an accurate method to measure the real parts of both permittivity and permeability. However, the loss tangents are not as easy to obtain. It seems like we need a set of loss dependent curves (such as the one presented in Figure 4.5) for each pair of ε_r' and μ_r'. One way would be to first determine the real parts and then perform a simulation with those values while varying the losses. On the other hand, the cavity-perturbation method showed good results in measuring the losses and the two methods can therefore be used to complement each other.

5.3 Encountered problems

During this project some problems were encountered. Some of these are worth to mention and discuss in order to justify choices made and discuss limitations to the method.

Ansys HFSS has a few different solution types. In this project, we have used the "Driven terminal" and "Eigenmode" solution types. The first was used to perform the frequency sweeps and study the frequency dependence of the S_{12}-parameter. The second one was used to study the eigenfrequencies. The complex-valued eigenfrequencies can be related to the resonance peaks in the spectra. However, these values are, of course, not perfectly matching. This occurs since there are more than one resonance present in the system. In particular, this discrepancy appears when calculating the Q-factor. This can either be calculated via the bandwidth through Equation (2.80) or via the complex eigenvalue through Equation (2.83). As can be seen in Figure 5.1, this yields different values of Q, particularly for low-loss materials. One should here note that leakage has not been concerned and the difference between the two methods should come from the influence of the probes. As the loss tangent increases, the difference between the two methods seems to disappear asymptotically. In this project, we have used the bandwidth to determine Q since this should include losses from leakage and the influence of the probes. The eigenvalue solver treats the system as closed by imposing metallic boundary conditions. However, for the real part the eigenvalue solver was used to create Figure 4.4, since this saved a lot of time and the difference in this case was much smaller. For a more exact solution, one should use the driven terminal solution type here as well.

Previous studies of the cavity-perturbation method have shown that a calibration is not always necessary. By using samples that are small compared to the cav-

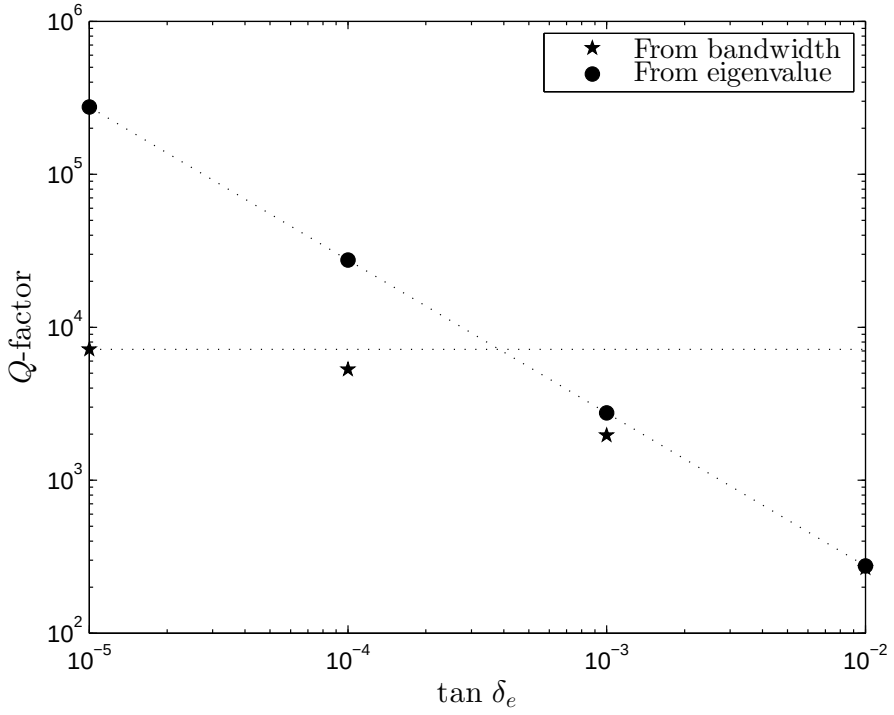

Figure 5.1: Comparison of Q-factor as calculated from the bandwidth and from the complex eigenvalues.

ity, the field profile may approximately be considered unaffected and the constant C in Equation (2.105) can be calculated analytically. Parkash *et al.* [29] consider a cylindrical cavity operating at the TM_{010} mode, just as in this project. For a sample that reaches from the bottom to the top of the cavity they present the following equations:

$$\varepsilon_r' = 1 + 0.539 \cdot \frac{V_S}{V_C} \frac{\omega_2 - \omega_1}{\omega_2} \tag{5.1}$$

$$\varepsilon_r'' = 0.539 \cdot \frac{V_S}{V_C} \left(\frac{1}{Q_2} - \frac{1}{Q_1} \right). \tag{5.2}$$

For our setup, it is however not possible to use this since it is not possible to fabricate sufficiently small samples.

Parkash *et al.*[29] further extend their work to account for samples that do not reach through the whole cavity, a work that later was extended by Lin and Afsar [30]. This is done by introducing a depolarization factor that enters Equations (2.103) and (2.104). The sample is then treated as an oblate or a prolate spheroid, depending on if it is a disc or a rod. Unfortunately, such an approximation is only

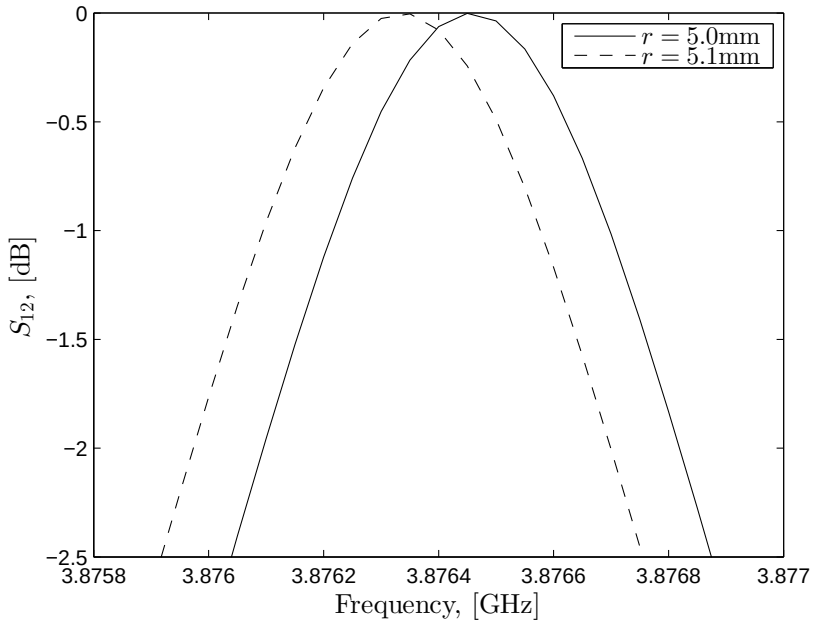

Figure 5.2: The TM_{010} for two samples of $\varepsilon_r' = \mu_r' = 1$ and $\tan\delta_e = \tan\delta_m = 0$ but different radii.

valid if the sample height is either much smaller or much larger than its radius and is thus not applicable for this setup.

In this setup, we found it necessary for the sample to reach from the bottom to the top of the cavity. Since we have implemented a perturbation method, it is possible that this is not necessary if the sample is much smaller than the cavity. However, in our case the volumes differ by a factor of 36 (for the sample of radius 5 mm), which may distort the field too much if the sample thickness does not equal the cavity height. With the curve-set method, this is no longer a problem, as long as the simulation represents the studied system.

One should also note that we have discussed the problems that air gaps can give rise to. Nonetheless, a mode where the electric field is directed normally to the sample surface was chosen. It is however our hope that the adaptive cavity length will solve this potential problem.

Finally, an empty cavity corresponds to setting $\varepsilon_r' = \mu_r' = 1$ and $\tan\delta_e = \tan\delta_m = 0$. Doing this, the spectrum is still slightly dependent of the position and radius of the sample, see Figure 5.2. This discrepancy probably comes from the different meshes.

5.4 Conclusion

Introduction of a dielectric sample into a metallic cavity will affect the resonance frequencies of the cavity. This shift and broadening of the peaks can be used to calculate material parameters such as permittivity, permeability and loss tangents. Using the cavity-perturbation method, the cavity resonator designed in this project can be used to determine the permittivity and losses to a reasonable accuracy according to simulations, although experimental measurements shows larger errors. Permeabilities should in theory be possible to measure, but apparently much smaller samples are needed in order to avoid effects from the permittivity simultaneously.

On the other hand, the curve-set method developed in this project should be possible to use regardless of the sample size as long as the simulated sample has the same size and shape as the real one. For a further evaluation of the method, more experiments should be conducted. It is also important that experimental measurements and simulations are similar for the method to be accurate. It is possible that the overall precision can be improved by performing frequency sweeps, so that possible leakage and effects from the couplings are taken into account.

5.5 Further development

More experimental measurements should be conducted in order to verify the techniques. It is possible that the simulation model can be improved to further resemble the experimental results, which would improve the curve-set method. There is also a possibility that the cavity-perturbation method can be improved by applying a layer of conductive paste, or perhaps even water, to minimize leakage and improve the results of the cavity-perturbation method.

As we have seen, the cavity-perturbation method does not reproduce the loss tangent for samples of low losses. In fact, introduction of low-loss samples even seem to increase the Q-factor, resulting in the negative values in e.g. Table 4.4. This has been investigated experimentally by Chen *et al.* who introduce the concept of *expected* Q [31]. Here, a set of reference samples of varying sizes are used. By extrapolating the calibration constant as function of the sample size, Chen *et al.* managed to extend the investigation of dielectric losses down to loss tangents of order 10^{-4}.

Bibliography

[1] M. Sebastian. *Dielectric Materials for Wireless Communication*. Elsevier, Amsterdam, 1st edition, 2008.

[2] L. Chen, C. P. Neo, C. K. Ong, V. V. Varadan, and V. K. Varadan. *Microwave Electronics : Measurement and Materials Characterization*. Wiley, Chichester, 1st edition, 2004.

[3] B. W. Hakki and P. D. Coleman. A Dielectric Resonator Method of Measuring Inductive Capacities in the Millimeter Range. *IRE Trans. Microwave Theory Tech.*, 8:402–410, 1960.

[4] W. E. Courtney. Analysis and Evaluation of a Method of Measuring Complex Permittivity and Permeability of Microwave Insulators. *IEEE T Microw Theory*, 18:476–485, 1970.

[5] J. Krupka. Frequency Domain Complex Permittivity Measurements at Microwave Frequencies. *Meas Sci Technol*, 17:R55–R70, 2006.

[6] C. A. Jones. Permittivity and Permeability Measurements Using Stripline Resonator Cavities - a Comparison. *IEEE T Instrum Meas*, 48:843–848, 1999.

[7] C. M. Weil, C. A. Jones, Y. Kantur, and J. H. Grosvenor. On RF Material Characterization in the Stripline Cavity. *IEEE T Microw Theory*, 48:266–275, 2000.

[8] D. A. Rudy, J. P. Mendelsohn, and P. J. Muniz. Measurement of RF Dielectric Properties With Series Resonant Microstrip elements. *Microwave J*, 41:22–39, 1998.

[9] N. K. Das, S. Voda, and D. M. Pozar. Two Methods for the Measurement of Substrate Dielectric Constant. *IEEE T Microw Theory*, 35:636–642, 1987.

[10] J. E. Allnutt and J. A. Staniforth. A Mach-Zehnder Interferometer for the Measurement of the Complex Permittivity of Lossy Dielectrics at Submillimetre Wavelengths. *J Phys E Sci Instrum*, 4:730–732, 1971.

[11] V. I. Borisov and A. V. Karpenko. Using of the Michelson Microwave Interferometer for the Measurement of Permittivity of Thin-Layer Materials. *Russ J Nondestruct+*, 37:597–599, 2001.

[12] W. Culshaw and M. V. Anderson. Measurement of Permittivity and Dielectric Loss With a Millimetre-wave Fabry-Perôt interferometer. *Proc IEE B*, 109:820–826, 1962.

[13] W. Culshaw. The Michelson Interferometer at Millimetre Wavelengths. *P Phys Soc B*, 63:939–954, 1950.

[14] N. Suzuki. A 40-120-GHz Michelson Interferometer-Type Band-Splitting Filter. *IEEE T Microw Theory*, 22:565–566, 1974.

[15] V. V. Varadan, R. D. Hollinger, D. K. Ghodgaonkar, and V. K. Varadan. Free-Space, Broadband Measurements of High-Temperature, Complex Dielectric Properties at Microwave Frequencies. *IEEE T Instrum Meas*, 40:842–846, 1991.

[16] D. K. Ghodgaonkar, V. V. Varadan, and V. K. Varadan. Free-Space Measurement of Complex Permittivity and Complex Permeability of Magnetic Materials at Microwave Frequencies. *IEEE T Instrum Meas*, 39:387–394, 1990.

[17] D. K. Ghodgaonkar, V. V. Varadan, and V. K. Varadan. A Free-Space Method for Measurement of Dielectric Constants and Loss Tangents at Microwave Frequencies. *IEEE T Instrum Meas*, 38:789–793, 1989.

[18] B. T. Rosner and D. W. van der Weide. High-Frequency Near-Field Microscopy. *Rev Sci Instrum*, 73:2505–2525, 2002.

[19] D. Pozar. *Microwave Engineering*. Wiley, Hoboken, 4th edition, 2012.

[20] J. D. Jackson. *Classical Electrodynamics*. Wiley, New York, 3rd edition, 1999.

[21] S. Ramo, J. R. Whinnery, and T. van Duzer. *Fields and Waves in Communication Electronics*. Wiley, New York, 3rd edition, 1994.

[22] G. B. Arfken and F. E. Weber, H. J. ad Harris. *Mathematical Methods for Physicists*. Academic, Oxford, 7th edition, 2013.

[23] A. J. B. Fuller. *Ferrites at Microwave Frequencies*, volume 23 of *IEE Electromagnetic Waves*. Peregrinus, London, 1987.

[24] R. E. Collin. *Foundations for Microwave Engineering*. IEEE Press, New York, 2nd edition, 2001.

[25] H. Zhang, B. Q. Zeng, L. Ao, and Z. Zhang. A Novel Dual-Loop Coupler for One-Port Cylindrical Cavity Permittivity Measurement. *Prog Electromagn Res*, 127:537–552, 2012.

[26] H. Zhang, B. Zeng, L. Ao, et al. Novel 4 Loops Coupler in Microwave Cavity Measurement of Permittivity. In *Wireless Symposium (IWS), 2013 IEEE International*, pages 1–3, 2013.

[27] R. Luebbers. Effects of Waveguide Wall Grooves Used to Hold Samples for Measurement of Permittivity and Permeability. *IEEE T Microw Theory*, 41:1959–1964, 1993.

[28] S. B. Wilson. Modal Analysis of the 'Gap Effect' in Waveguide Dielectric Measurements. *IEEE T Microw Theory*, 36:752–756, 1988.

[29] A. Parkash, J. K. Vaid, and A. Mansingh. Measurement of Dielectric Parameters at Microwave Frequencies by Cavity-Perturbation Technique. *IEEE T Microw Theory*, 27:791–795, 1979.

[30] M. Lin and M. N. Afsar. A New Cavity Perturbation Technique for Accurate Measurement of Dielectric Parameters. In *Microwave Symposium Digest, 2006. IEEE MTT-S International*, pages 1630–1633, 2006.

[31] L. Chen, C. K. Ong, and B. T. G. Tan. Amendment of Cavity Perturbation Method for Permittivity Measurement of Extremely Low-Loss Dielectrics. *IEEE T Instrum Meas*, 48:1031–1037, 1999.

Appendix A

Matlab scripts

The following MATLAB script can be used to calculate the material parameters of interest. Input values are vectors containing frequencies and S_{12}-parameters for an empty cavity, cavity with resonance sample and cavity with test sample. For future needs, the MATLAB and HFSS files can also be found in SEVS as a zip-file with document number: D-A-MIS-1154742-RSE.

A.1 Cavity-perturbation method

CavityPerturbation.m is the main script for the cavity-perturbation method. the subroutines and their purposes are:

- Calibrate.m: Calculates the calibration parameters.
- UseCalibration.m: Uses these parameters to calculate the permittivity and dielectric loss tangent.
- FindQ.m: Finds the Q-factor and resonance frequency for a certain peak.

A.1.1 CavityPerturbation.m

```
function [epsR,delta]=CavityPerturbation(freqRefEmpty,...
    SRefEmpty,freqRef,SRef,freqTestEmpty,STestEmpty,...
    freqTest,STest,epsRefR,epsRefI,refRad,testRad)
%CavityPerturbation is used to obtain the permittivity and
%dielectric loss tangent through the cavity-perturbation
%method.
%   Input:
```

```
%   freqRefEmpty - Frequency sweep for empty cavity
%                  (length equal to ref sample height)
%   SRefEmpty - S-parameters for empty cavity
%                  (length equal to ref sample height)
%   freqTestEmpty - Frequency sweep for empty cavity
%                  (length equal to test sample height)
%   STestEmpty - S-parameters for empty cavity
%                  (length equal to test sample height)
%   freqRef - Frequency sweep for reference sample
%   SRef - S-parameters for reference sample
%   freqTest - Frequency sweep for test sample
%   STest - S-parameters for test sample
%   refRad - Radius of reference sample
%   testRad - Radius of test sample
%   Output:
%   epsR - real part of permittivity for test sample
%   delta - dielectric loss tangent for test sample
[QRefEmpty,fRefEmpty]=FindQ(freqRefEmpty,SRefEmpty);
[QTestEmpty,fTestEmpty]=FindQ(freqTestEmpty,STestEmpty);
[Q1,f1]=FindQ(freqRef,SRef);
[Q2,f2]=FindQ(freqTest,STest);

radRatio = testRad/refRad;

[A,B] = ...
    Calibrate(fRefEmpty,f1,QRefEmpty,Q1,epsRefR,epsRefI);
A = A/radRatio^2;
B = B/radRatio^2;
[epsR,epsI] = ...
    UseCalibration(fTestEmpty,f2,QTestEmpty,Q2,A,B);
delta = epsI/epsR;
end
```

A.1.2 Calibrate.m

```
function [A,B] = Calibrate(f1,f2,Q1,Q2,epsR,epsI)
%Calibrate returns the calibration parameters A and B.
%   f1 = frequency of empty cavity
%   f2 = frequency with reference sample
%   Q1 = Q-factor for empty cavity
%   Q2 = Q-factor with reference sample
%   epsR = real part of permittivity for reference sample
```

```
%   epsI = imaginary part of permittivity for reference
%       sample
%   Returns:
%   A = calibration parameter for real part
%   B = calibration parameter for imaginary part
df = f2-f1;

A = df/(f2*(epsR - 1));
B = (1/Q2 - 1/Q1)/(2*epsI);
end
```

A.1.3 UseCalibration.m

```
function [epsR,epsI] = UseCalibration(f1,f2,Q1,Q2,A,B)
%UseCalibration returns the real and imaginary parts of
%the permittivity for the test sample.
%   f1 = frequency of empty cavity
%   f2 = frequency with sample
%   Q1 = Q-factor for empty cavity
%   Q2 = Q-factor with sample
%   A = calibration parameter for real part
%   B = calibration parameter for imaginary part
%   Returns:
%   epsR = real part of permittivity
%   epsI = imaginary part of permittivity

df = f2-f1;

epsR = df/(f2*A) + 1;
epsI = (1/Q2 - 1/Q1)/(2*B);

end
```

A.1.4 FindQ.m

```
function [Q,fmax] = FindQ(f,e)
%FindQ takes a frequency vector f and amplitude vector e
%as input and returns the Q factor together with the
%resonance frequency.

[maxe,res]=max(e);
[~,u]=min(abs(e(res+1:end)-(maxe-3)));
```

```
[~,l]=min(abs(e(1:res)-(maxe-3)));
Q = f(res)/(f(res+u)-f(l));
fmax=f(res);
end
```

A.2 Curve-set method

The script below plots the curve-sets used to obtain the permittivity and permeability. The file curveSetData.m contains vectors of different permittivities and permeabilities as well as matrices containing the resonance frequencies for different $\varepsilon_r'\mu_r'$-pairs.

A.2.1 CurveSet.m

```
%Plots the frequency of the first eigenmode as function of
%epsilon and mu. Also, the section "Find curve" finds the
%epsilon-mu pair corresponging to the measured resonances.
clear
close all
load('curveSetData.mat');% Contains simulation data
normFreq=3.878;% Resonance frequency for empty cavity, GHz

figure(1)
contour(muVec,epsVec,displaced/normFreq,...
    'linewidth',1,'LevelList',...
    [0.55 0.6 0.65 0.7 0.75 0.8 0.85 0.9 0.95 0.98])
hold on
contour(muVec,epsVec,centered/normFreq,':',...
    'linewidth',1,'LevelList',...
    [0.55 0.6 0.65 0.7 0.75 0.8 0.85 0.9 0.95 0.98])
hold off
colorbar
xlabel('$\mu_r''$','interpreter','latex','fontsize',13)
ylabel('$\varepsilon_r''$','interpreter','latex',...
    'fontsize',13)

%% Find curve
resEmpty = input('Enter frequency of empty cavity:\n');
resDisp =...
    input('Enter frequency of displaced measurement:\n');
epsResDisp = zeros(1,length(muVec));
```

```
for i=1:length(muVec)
    [~,epsTmp] = ...
      min(abs(displaced(:,i)/normFreq-resDisp./resEmpty));
    epsResDisp(i) = epsVec(epsTmp);
end

resCenter = ...
    input('Enter frequency of centered measurement:\n');
epsResCenter = zeros(1,length(muVec));
for i=1:length(muVec)
    [~,epsTmp] = ...
     min(abs(centered(:,i)/normFreq-resCenter./resEmpty));
    epsResCenter(i) = epsVec(epsTmp);
end

% Exclude saturated values
eMaxC = max(epsResCenter);
eMinC = min(epsResCenter);
eMaxD = max(epsResDisp);
eMinD = min(epsResDisp);
epsResCenterCut = [];
epsResDispCut= [];
muVecCutC = [];
muVecCutD = [];
epsResFinalCut1 = [];
epsResFinalCut2 = [];
for i=1:length(muVec)
    if ~(((epsResCenter(i)==eMaxC)&&...
            (epsResCenter(i+1)==eMaxC))||...
            ((epsResCenter(i)==eMinC)&&...
            (epsResCenter(i-1)==eMinC)))
        epsResCenterCut(end+1) = epsResCenter(i);
        muVecCutC(end+1) = muVec(i);
        epsResFinalCut1(end+1) = epsResCenter(i);
    end
    if ~(((epsResDisp(i)==eMaxD)&&...
            (epsResDisp(i+1)==eMaxD))...
            ||((epsResDisp(i)==eMinD)&&...
            (epsResDisp(i-1)==eMinD)))
        epsResDispCut(end+1) = epsResDisp(i);
        muVecCutD(end+1) = muVec(i);
        epsResFinalCut2(end+1) = epsResCenter(i);
    end
```

```
end

%Fit
figure(2)
plot(muVecCutD,epsResDispCut)
disp('To fit the data, use Tools -> Basic fitting.')
fitOrderDisp = ...
    input(['Enter the best polynomial order',...
    ' for displaced sample:\n']);
close
figure(2)
plot(muVecCutC,epsResCenterCut)
fitOrderCenter = input(['Enter the best polynomial'...
    'order for centered sample:\n']);
pDisp = polyfit(muVecCutD,epsResDispCut,fitOrderDisp);
pCenter=polyfit(muVecCutC,epsResCenterCut,fitOrderCenter);
if length(muVecCutC)<length(muVecCutD)
    muVecCut = muVecCutC;
    epsResFinalCut = epsResFinalCut1;
else
    muVecCut = muVecCutD;
    epsResFinalCut = epsResFinalCut2;
end
fitDisp = polyval(pDisp,muVecCut);
fitCenter = polyval(pCenter,muVecCut);

figure(2)
plot(muVec,epsResDisp)
hold on
plot(muVec,epsResCenter,'r')
plot(muVecCut,fitDisp,'b:')
plot(muVecCut,fitCenter,'r:')
hold off
xlabel('$\mu$','interpreter','latex')
ylabel('$\epsilon$','interpreter','latex')
legend('Displaced','Centered')

% Find mu and epsilon
[~,indexFound] = min(abs(fitDisp-fitCenter));
muFound = muVecCut(indexFound)
epsFound = epsResFinalCut(indexFound)
```

Appendix B

Results on dielectric losses

Here we present a more complete set of results for the simulations performed to obtain the dielectric loss tangent.

Table B.1: Obtained values for the dielectric loss tangent of the sample under test of radius 5 mm and $\varepsilon'_r = 1$, using a reference sample with $\varepsilon'_r = 3$ and equal radius.

	Dielectric loss tangent of reference sample			
True value	10^{-5}	10^{-4}	10^{-3}	10^{-2}
10^{-5}	$-0.0 \cdot 10^{0}$	$-0.0 \cdot 10^{0}$	$0.0 \cdot 10^{0}$	$0.0 \cdot 10^{0}$
10^{-4}	$-4.4 \cdot 10^{-6}$	$-5.3 \cdot 10^{-5}$	$1.8 \cdot 10^{-4}$	$1.3 \cdot 10^{-4}$
10^{-3}	$-3.1 \cdot 10^{-5}$	$-3.7 \cdot 10^{-4}$	$1.3 \cdot 10^{-3}$	$9.1 \cdot 10^{-4}$
10^{-2}	$-3.4 \cdot 10^{-4}$	$-4.0 \cdot 10^{-3}$	$1.4 \cdot 10^{-2}$	$1.0 \cdot 10^{-2}$

Table B.2: Obtained values for the dielectric loss tangent of the sample under test of radius 5 mm and $\varepsilon'_r = 1$, using a reference sample with $\varepsilon'_r = 5$ and equal radius.

	Dielectric loss tangent of reference sample			
True value	10^{-5}	10^{-4}	10^{-3}	10^{-2}
10^{-5}	$-0.0 \cdot 10^{0}$	$-0.0 \cdot 10^{0}$	$0.0 \cdot 10^{0}$	$0.0 \cdot 10^{0}$
10^{-4}	$-4.8 \cdot 10^{-6}$	$-6.3 \cdot 10^{-5}$	$2.0 \cdot 10^{-4}$	$1.4 \cdot 10^{-4}$
10^{-3}	$-3.4 \cdot 10^{-5}$	$-4.4 \cdot 10^{-4}$	$1.4 \cdot 10^{-3}$	$9.9 \cdot 10^{-4}$
10^{-2}	$-3.7 \cdot 10^{-4}$	$-4.8 \cdot 10^{-3}$	$1.5 \cdot 10^{-2}$	$1.1 \cdot 10^{-2}$

Table B.3: Obtained values for the dielectric loss tangent of the sample under test of radius 5 mm and $\varepsilon'_r = 1$, using a reference sample with $\varepsilon'_r = 7$ and equal radius.

	Dielectric loss tangent of reference sample			
True value	10^{-5}	10^{-4}	10^{-3}	10^{-2}
10^{-5}	$-0.0 \cdot 10^{0}$	$-0.0 \cdot 10^{0}$	$0.0 \cdot 10^{0}$	$0.0 \cdot 10^{0}$
10^{-4}	$-5.7 \cdot 10^{-6}$	$-7.3 \cdot 10^{-5}$	$2.3 \cdot 10^{-4}$	$1.6 \cdot 10^{-4}$
10^{-3}	$-4.0 \cdot 10^{-5}$	$-5.1 \cdot 10^{-4}$	$1.6 \cdot 10^{-3}$	$1.1 \cdot 10^{-3}$
10^{-2}	$-4.4 \cdot 10^{-4}$	$-5.6 \cdot 10^{-3}$	$1.8 \cdot 10^{-2}$	$1.2 \cdot 10^{-2}$

Table B.4: Obtained values for the dielectric loss tangent of the sample under test of radius 5 mm and $\varepsilon'_r = 3$, using a reference sample with $\varepsilon'_r = 3$ and equal radius.

	Dielectric loss tangent of reference sample			
True value	10^{-5}	10^{-4}	10^{-3}	10^{-2}
10^{-5}	$1.0 \cdot 10^{-5}$	$1.2 \cdot 10^{-4}$	$-4.1 \cdot 10^{-4}$	$-3.0 \cdot 10^{-4}$
10^{-4}	$8.4 \cdot 10^{-6}$	$1.0 \cdot 10^{-4}$	$-3.5 \cdot 10^{-4}$	$-2.5 \cdot 10^{-4}$
10^{-3}	$-2.4 \cdot 10^{-5}$	$-2.9 \cdot 10^{-4}$	$1.0 \cdot 10^{-3}$	$7.1 \cdot 10^{-4}$
10^{-2}	$-3.4 \cdot 10^{-4}$	$-4.0 \cdot 10^{-3}$	$1.4 \cdot 10^{-2}$	$1.0 \cdot 10^{-2}$

Table B.5: Obtained values for the dielectric loss tangent of the sample under test of radius 5 mm and $\varepsilon'_r = 3$, using a reference sample with $\varepsilon'_r = 5$ and equal radius.

	Dielectric loss tangent of reference sample			
True value	10^{-5}	10^{-4}	10^{-3}	10^{-2}
10^{-5}	$1.1 \cdot 10^{-5}$	$1.5 \cdot 10^{-4}$	$-4.6 \cdot 10^{-4}$	$-3.3 \cdot 10^{-4}$
10^{-4}	$9.3 \cdot 10^{-6}$	$1.2 \cdot 10^{-4}$	$-3.9 \cdot 10^{-4}$	$-2.8 \cdot 10^{-4}$
10^{-3}	$-2.7 \cdot 10^{-5}$	$-3.5 \cdot 10^{-4}$	$1.1 \cdot 10^{-3}$	$7.9 \cdot 10^{-4}$
10^{-2}	$-3.8 \cdot 10^{-4}$	$-4.9 \cdot 10^{-3}$	$1.6 \cdot 10^{-2}$	$1.1 \cdot 10^{-2}$

Table B.6: Obtained values for the dielectric loss tangent of the sample under test of radius 5 mm and $\varepsilon'_r = 3$, using a reference sample with $\varepsilon'_r = 7$ and equal radius.

	Dielectric loss tangent of reference sample			
True value	10^{-5}	10^{-4}	10^{-3}	10^{-2}
10^{-5}	$1.3 \cdot 10^{-5}$	$1.7 \cdot 10^{-4}$	$-5.4 \cdot 10^{-4}$	$-3.7 \cdot 10^{-4}$
10^{-4}	$1.1 \cdot 10^{-5}$	$1.4 \cdot 10^{-4}$	$-4.5 \cdot 10^{-4}$	$-3.1 \cdot 10^{-4}$
10^{-3}	$-3.2 \cdot 10^{-5}$	$-4.1 \cdot 10^{-4}$	$1.3 \cdot 10^{-3}$	$9.0 \cdot 10^{-4}$
10^{-2}	$-4.5 \cdot 10^{-4}$	$-5.7 \cdot 10^{-3}$	$1.8 \cdot 10^{-2}$	$1.3 \cdot 10^{-2}$

Table B.7: Obtained values for the dielectric loss tangent of the sample under test of radius 5 mm and $\varepsilon'_r = 5$, using a reference sample with $\varepsilon'_r = 3$ and equal radius.

	Dielectric loss tangent of reference sample			
True value	10^{-5}	10^{-4}	10^{-3}	10^{-2}
10^{-5}	$8.9 \cdot 10^{-6}$	$1.1 \cdot 10^{-4}$	$-3.7 \cdot 10^{-4}$	$-2.7 \cdot 10^{-4}$
10^{-4}	$6.9 \cdot 10^{-6}$	$8.2 \cdot 10^{-5}$	$-2.8 \cdot 10^{-4}$	$-2.0 \cdot 10^{-4}$
10^{-3}	$-2.1 \cdot 10^{-5}$	$-2.6 \cdot 10^{-4}$	$8.9 \cdot 10^{-4}$	$6.3 \cdot 10^{-4}$
10^{-2}	$-3.0 \cdot 10^{-4}$	$-3.6 \cdot 10^{-3}$	$1.3 \cdot 10^{-2}$	$8.9 \cdot 10^{-3}$

Table B.8: Obtained values for the dielectric loss tangent of the sample under test of radius 5 mm and $\varepsilon'_r = 5$, using a reference sample with $\varepsilon'_r = 5$ and equal radius.

	Dielectric loss tangent of reference sample			
True value	10^{-5}	10^{-4}	10^{-3}	10^{-2}
10^{-5}	$1.0 \cdot 10^{-5}$	$1.3 \cdot 10^{-4}$	$-4.2 \cdot 10^{-4}$	$-3.0 \cdot 10^{-4}$
10^{-4}	$7.7 \cdot 10^{-6}$	$1.0 \cdot 10^{-4}$	$-3.2 \cdot 10^{-4}$	$-2.3 \cdot 10^{-4}$
10^{-3}	$-2.4 \cdot 10^{-5}$	$-3.1 \cdot 10^{-4}$	$1.0 \cdot 10^{-3}$	$7.1 \cdot 10^{-4}$
10^{-2}	$-3.4 \cdot 10^{-4}$	$-4.4 \cdot 10^{-3}$	$1.4 \cdot 10^{-2}$	$1.0 \cdot 10^{-2}$

Table B.9: Obtained values for the dielectric loss tangent of the sample under test of radius 5 mm and $\varepsilon'_r = 5$, using a reference sample with $\varepsilon'_r = 7$ and equal radius.

	Dielectric loss tangent of reference sample			
True value	10^{-5}	10^{-4}	10^{-3}	10^{-2}
10^{-5}	$1.2 \cdot 10^{-5}$	$1.5 \cdot 10^{-4}$	$-4.8 \cdot 10^{-4}$	$-3.3 \cdot 10^{-4}$
10^{-4}	$9.1 \cdot 10^{-6}$	$1.2 \cdot 10^{-4}$	$-3.7 \cdot 10^{-4}$	$-2.6 \cdot 10^{-4}$
10^{-3}	$-2.9 \cdot 10^{-5}$	$-3.6 \cdot 10^{-4}$	$1.2 \cdot 10^{-3}$	$8.0 \cdot 10^{-4}$
10^{-2}	$-4.0 \cdot 10^{-4}$	$-5.1 \cdot 10^{-3}$	$1.6 \cdot 10^{-2}$	$1.1 \cdot 10^{-2}$

Table B.10: Obtained values for the dielectric loss tangent of the sample under test of radius 5 mm and $\varepsilon'_r = 7$, using a reference sample with $\varepsilon'_r = 3$ and equal radius.

	Dielectric loss tangent of reference sample			
True value	10^{-5}	10^{-4}	10^{-3}	10^{-2}
10^{-5}	$7.5 \cdot 10^{-6}$	$8.9 \cdot 10^{-5}$	$-3.1 \cdot 10^{-4}$	$-2.2 \cdot 10^{-4}$
10^{-4}	$5.9 \cdot 10^{-6}$	$7.0 \cdot 10^{-5}$	$-2.4 \cdot 10^{-4}$	$-1.7 \cdot 10^{-4}$
10^{-3}	$-1.8 \cdot 10^{-5}$	$-2.2 \cdot 10^{-4}$	$7.7 \cdot 10^{-4}$	$5.5 \cdot 10^{-4}$
10^{-2}	$-2.7 \cdot 10^{-4}$	$-3.2 \cdot 10^{-3}$	$1.1 \cdot 10^{-2}$	$7.9 \cdot 10^{-3}$

Table B.11: Obtained values for the dielectric loss tangent of the sample under test of radius 5 mm and $\varepsilon'_r = 7$, using a reference sample with $\varepsilon'_r = 5$ and equal radius.

	Dielectric loss tangent of reference sample			
True value	10^{-5}	10^{-4}	10^{-3}	10^{-2}
10^{-5}	$8.4 \cdot 10^{-6}$	$1.1 \cdot 10^{-4}$	$-3.5 \cdot 10^{-4}$	$-2.5 \cdot 10^{-4}$
10^{-4}	$6.6 \cdot 10^{-6}$	$8.6 \cdot 10^{-5}$	$-2.7 \cdot 10^{-4}$	$-1.9 \cdot 10^{-4}$
10^{-3}	$-2.1 \cdot 10^{-5}$	$-2.7 \cdot 10^{-4}$	$8.6 \cdot 10^{-4}$	$6.1 \cdot 10^{-4}$
10^{-2}	$-3.0 \cdot 10^{-4}$	$-3.9 \cdot 10^{-3}$	$1.2 \cdot 10^{-2}$	$8.8 \cdot 10^{-3}$

Table B.12: Obtained values for the dielectric loss tangent of the sample under test of radius 5 mm and $\varepsilon'_r = 7$, using a reference sample with $\varepsilon'_r = 7$ and equal radius.

	Dielectric loss tangent of reference sample			
True value	10^{-5}	10^{-4}	10^{-3}	10^{-2}
10^{-5}	$1.0 \cdot 10^{-5}$	$1.3 \cdot 10^{-4}$	$-4.0 \cdot 10^{-4}$	$-2.8 \cdot 10^{-4}$
10^{-4}	$7.8 \cdot 10^{-6}$	$1.0 \cdot 10^{-4}$	$-3.2 \cdot 10^{-4}$	$-2.2 \cdot 10^{-4}$
10^{-3}	$-2.5 \cdot 10^{-5}$	$-3.2 \cdot 10^{-4}$	$1.0 \cdot 10^{-3}$	$6.9 \cdot 10^{-4}$
10^{-2}	$-3.6 \cdot 10^{-4}$	$-4.6 \cdot 10^{-3}$	$1.4 \cdot 10^{-2}$	$1.0 \cdot 10^{-2}$

Table B.13: Obtained values for the dielectric loss tangent of the sample under test of radius 2 mm and $\varepsilon'_r = 1$, using a reference sample with $\varepsilon'_r = 3$ and equal radius.

	Dielectric loss tangent of reference sample			
True value	10^{-5}	10^{-4}	10^{-3}	10^{-2}
10^{-5}	$-0.0 \cdot 10^{0}$	$-0.0 \cdot 10^{0}$	$0.0 \cdot 10^{0}$	$0.0 \cdot 10^{0}$
10^{-4}	$-0.0 \cdot 10^{0}$	$-0.0 \cdot 10^{0}$	$0.0 \cdot 10^{0}$	$0.0 \cdot 10^{0}$
10^{-3}	$-4.3 \cdot 10^{-5}$	$-4.3 \cdot 10^{-4}$	$8.9 \cdot 10^{-4}$	$7.7 \cdot 10^{-4}$
10^{-2}	$-5.6 \cdot 10^{-4}$	$-5.6 \cdot 10^{-3}$	$1.2 \cdot 10^{-2}$	$1.0 \cdot 10^{-2}$

Table B.14: Obtained values for the dielectric loss tangent of the sample under test of radius 2 mm and $\varepsilon'_r = 1$, using a reference sample with $\varepsilon'_r = 5$ and equal radius.

	Dielectric loss tangent of reference sample			
True value	10^{-5}	10^{-4}	10^{-3}	10^{-2}
10^{-5}	$-0.0 \cdot 10^{0}$	$-0.0 \cdot 10^{0}$	$0.0 \cdot 10^{0}$	$0.0 \cdot 10^{0}$
10^{-4}	$-0.0 \cdot 10^{0}$	$-0.0 \cdot 10^{0}$	$0.0 \cdot 10^{0}$	$0.0 \cdot 10^{0}$
10^{-3}	$-2.1 \cdot 10^{-5}$	$-2.1 \cdot 10^{-4}$	$1.3 \cdot 10^{-3}$	$7.4 \cdot 10^{-4}$
10^{-2}	$-2.7 \cdot 10^{-4}$	$-2.7 \cdot 10^{-3}$	$1.7 \cdot 10^{-2}$	$9.6 \cdot 10^{-3}$

Table B.15: Obtained values for the dielectric loss tangent of the sample under test of radius 2 mm and $\varepsilon'_r = 1$, using a reference sample with $\varepsilon'_r = 7$ and equal radius.

	Dielectric loss tangent of reference sample			
True value	10^{-5}	10^{-4}	10^{-3}	10^{-2}
10^{-5}	$-0.0 \cdot 10^{0}$	$-0.0 \cdot 10^{0}$	$0.0 \cdot 10^{0}$	$0.0 \cdot 10^{0}$
10^{-4}	$-0.0 \cdot 10^{0}$	$-0.0 \cdot 10^{0}$	$0.0 \cdot 10^{0}$	$0.0 \cdot 10^{0}$
10^{-3}	$-1.7 \cdot 10^{-5}$	$-3.3 \cdot 10^{-4}$	$1.1 \cdot 10^{-3}$	$7.1 \cdot 10^{-4}$
10^{-2}	$-2.2 \cdot 10^{-4}$	$-4.3 \cdot 10^{-3}$	$1.4 \cdot 10^{-2}$	$9.2 \cdot 10^{-3}$

Table B.16: Obtained values for the dielectric loss tangent of the sample under test of radius 2 mm and $\varepsilon'_r = 3$, using a reference sample with $\varepsilon'_r = 3$ and equal radius.

	Dielectric loss tangent of reference sample			
True value	10^{-5}	10^{-4}	10^{-3}	10^{-2}
10^{-5}	$1.0 \cdot 10^{-5}$	$1.0 \cdot 10^{-4}$	$-2.0 \cdot 10^{-4}$	$-1.8 \cdot 10^{-4}$
10^{-4}	$1.0 \cdot 10^{-5}$	$1.0 \cdot 10^{-4}$	$-2.0 \cdot 10^{-4}$	$-1.8 \cdot 10^{-4}$
10^{-3}	$-4.9 \cdot 10^{-5}$	$-4.9 \cdot 10^{-4}$	$1.0 \cdot 10^{-3}$	$8.7 \cdot 10^{-4}$
10^{-2}	$-5.6 \cdot 10^{-4}$	$-5.6 \cdot 10^{-3}$	$1.2 \cdot 10^{-2}$	$1.0 \cdot 10^{-2}$

Table B.17: Obtained values for the dielectric loss tangent of the sample under test of radius 2 mm and $\varepsilon'_r = 3$, using a reference sample with $\varepsilon'_r = 5$ and equal radius.

	Dielectric loss tangent of reference sample			
True value	10^{-5}	10^{-4}	10^{-3}	10^{-2}
10^{-5}	$4.9 \cdot 10^{-6}$	$4.9 \cdot 10^{-5}$	$-3.1 \cdot 10^{-4}$	$-1.7 \cdot 10^{-4}$
10^{-4}	$4.9 \cdot 10^{-6}$	$4.9 \cdot 10^{-5}$	$-3.1 \cdot 10^{-4}$	$-1.7 \cdot 10^{-4}$
10^{-3}	$-2.4 \cdot 10^{-5}$	$-2.4 \cdot 10^{-4}$	$1.5 \cdot 10^{-3}$	$8.5 \cdot 10^{-4}$
10^{-2}	$-2.7 \cdot 10^{-4}$	$-2.7 \cdot 10^{-3}$	$1.8 \cdot 10^{-2}$	$9.8 \cdot 10^{-3}$

Table B.18: Obtained values for the dielectric loss tangent of the sample under test of radius 2 mm and $\varepsilon'_r = 3$, using a reference sample with $\varepsilon'_r = 7$ and equal radius.

	Dielectric loss tangent of reference sample			
True value	10^{-5}	10^{-4}	10^{-3}	10^{-2}
10^{-5}	$4.0 \cdot 10^{-6}$	$8.0 \cdot 10^{-5}$	$-2.7 \cdot 10^{-4}$	$-1.7 \cdot 10^{-4}$
10^{-4}	$4.0 \cdot 10^{-6}$	$8.0 \cdot 10^{-5}$	$-2.7 \cdot 10^{-4}$	$-1.7 \cdot 10^{-4}$
10^{-3}	$-2.0 \cdot 10^{-5}$	$-3.9 \cdot 10^{-4}$	$1.3 \cdot 10^{-3}$	$8.3 \cdot 10^{-4}$
10^{-2}	$-2.3 \cdot 10^{-4}$	$-4.5 \cdot 10^{-3}$	$1.5 \cdot 10^{-2}$	$9.6 \cdot 10^{-3}$

Table B.19: Obtained values for the dielectric loss tangent of the sample under test of radius 2 mm and $\varepsilon'_r = 5$, using a reference sample with $\varepsilon'_r = 3$ and equal radius.

	Dielectric loss tangent of reference sample			
True value	10^{-5}	10^{-4}	10^{-3}	10^{-2}
10^{-5}	$2.1 \cdot 10^{-5}$	$2.1 \cdot 10^{-4}$	$-4.2 \cdot 10^{-4}$	$-3.6 \cdot 10^{-4}$
10^{-4}	$2.1 \cdot 10^{-5}$	$2.1 \cdot 10^{-4}$	$-4.2 \cdot 10^{-4}$	$-3.6 \cdot 10^{-4}$
10^{-3}	$-3.2 \cdot 10^{-5}$	$-3.2 \cdot 10^{-4}$	$6.5 \cdot 10^{-4}$	$5.7 \cdot 10^{-4}$
10^{-2}	$-5.7 \cdot 10^{-4}$	$-5.7 \cdot 10^{-3}$	$1.2 \cdot 10^{-2}$	$1.0 \cdot 10^{-2}$

Table B.20: Obtained values for the dielectric loss tangent of the sample under test of radius 2 mm and $\varepsilon'_r = 5$, using a reference sample with $\varepsilon'_r = 5$ and equal radius.

	Dielectric loss tangent of reference sample			
True value	10^{-5}	10^{-4}	10^{-3}	10^{-2}
10^{-5}	$1.0 \cdot 10^{-5}$	$1.0 \cdot 10^{-4}$	$-6.4 \cdot 10^{-4}$	$-3.6 \cdot 10^{-4}$
10^{-4}	$1.0 \cdot 10^{-5}$	$1.0 \cdot 10^{-4}$	$-6.4 \cdot 10^{-4}$	$-3.6 \cdot 10^{-4}$
10^{-3}	$-1.6 \cdot 10^{-5}$	$-1.6 \cdot 10^{-4}$	$1.0 \cdot 10^{-3}$	$5.6 \cdot 10^{-4}$
10^{-2}	$-2.8 \cdot 10^{-4}$	$-2.8 \cdot 10^{-3}$	$1.8 \cdot 10^{-2}$	$1.0 \cdot 10^{-2}$

Table B.21: Obtained values for the dielectric loss tangent of the sample under test of radius 2 mm and $\varepsilon'_r = 5$, using a reference sample with $\varepsilon'_r = 7$ and equal radius.

	Dielectric loss tangent of reference sample			
True value	10^{-5}	10^{-4}	10^{-3}	10^{-2}
10^{-5}	$8.3 \cdot 10^{-6}$	$1.7 \cdot 10^{-4}$	$-5.5 \cdot 10^{-4}$	$-3.5 \cdot 10^{-4}$
10^{-4}	$8.3 \cdot 10^{-6}$	$1.7 \cdot 10^{-4}$	$-5.5 \cdot 10^{-4}$	$-3.5 \cdot 10^{-4}$
10^{-3}	$-1.3 \cdot 10^{-5}$	$-2.6 \cdot 10^{-4}$	$8.6 \cdot 10^{-4}$	$5.5 \cdot 10^{-4}$
10^{-2}	$-2.3 \cdot 10^{-4}$	$-4.6 \cdot 10^{-3}$	$1.5 \cdot 10^{-2}$	$9.9 \cdot 10^{-3}$

Table B.22: Obtained values for the dielectric loss tangent of the sample under test of radius 2 mm and $\varepsilon'_r = 7$, using a reference sample with $\varepsilon'_r = 3$ and equal radius.

	Dielectric loss tangent of reference sample			
True value	10^{-5}	10^{-4}	10^{-3}	10^{-2}
10^{-5}	$2.5 \cdot 10^{-5}$	$2.5 \cdot 10^{-4}$	$-5.1 \cdot 10^{-4}$	$-4.4 \cdot 10^{-4}$
10^{-4}	$1.2 \cdot 10^{-5}$	$1.2 \cdot 10^{-4}$	$-2.5 \cdot 10^{-4}$	$-2.2 \cdot 10^{-4}$
10^{-3}	$-3.7 \cdot 10^{-5}$	$-3.7 \cdot 10^{-4}$	$7.6 \cdot 10^{-4}$	$6.5 \cdot 10^{-4}$
10^{-2}	$-5.8 \cdot 10^{-4}$	$-5.8 \cdot 10^{-3}$	$1.2 \cdot 10^{-2}$	$1.0 \cdot 10^{-2}$

Table B.23: Obtained values for the dielectric loss tangent of the sample under test of radius 2 mm and $\varepsilon'_r = 7$, using a reference sample with $\varepsilon'_r = 5$ and equal radius.

	Dielectric loss tangent of reference sample			
True value	10^{-5}	10^{-4}	10^{-3}	10^{-2}
10^{-5}	$1.2 \cdot 10^{-5}$	$1.2 \cdot 10^{-4}$	$-7.8 \cdot 10^{-4}$	$-4.3 \cdot 10^{-4}$
10^{-4}	$6.0 \cdot 10^{-6}$	$6.0 \cdot 10^{-5}$	$-3.9 \cdot 10^{-4}$	$-2.2 \cdot 10^{-4}$
10^{-3}	$-1.8 \cdot 10^{-5}$	$-1.8 \cdot 10^{-4}$	$1.2 \cdot 10^{-3}$	$6.5 \cdot 10^{-4}$
10^{-2}	$-2.8 \cdot 10^{-4}$	$-2.8 \cdot 10^{-3}$	$1.8 \cdot 10^{-2}$	$1.0 \cdot 10^{-2}$

Table B.24: Obtained values for the dielectric loss tangent of the sample under test of radius 2 mm and $\varepsilon'_r = 7$, using a reference sample with $\varepsilon'_r = 7$ and equal radius.

	Dielectric loss tangent of reference sample			
True value	10^{-5}	10^{-4}	10^{-3}	10^{-2}
10^{-5}	$1.0 \cdot 10^{-5}$	$2.0 \cdot 10^{-4}$	$-6.7 \cdot 10^{-4}$	$-4.3 \cdot 10^{-4}$
10^{-4}	$5.0 \cdot 10^{-6}$	$1.0 \cdot 10^{-4}$	$-3.3 \cdot 10^{-4}$	$-2.1 \cdot 10^{-4}$
10^{-3}	$-1.5 \cdot 10^{-5}$	$-3.0 \cdot 10^{-4}$	$1.0 \cdot 10^{-3}$	$6.4 \cdot 10^{-4}$
10^{-2}	$-2.3 \cdot 10^{-4}$	$-4.7 \cdot 10^{-3}$	$1.6 \cdot 10^{-2}$	$1.0 \cdot 10^{-2}$

Appendix C

Results on permittivity of magnetic materials

Here we present a more complete set of results for the simulations performed to obtain the permittivity of magnetic materials.

Table C.1: Obtained values for the permittivity of the sample under test of radius 5 mm and $\varepsilon'_r = 1$, using a reference sample with $\varepsilon'_r = 3$ and equal radius. Errors are given in percent.

	Relative permeability of reference sample							
Permeability of SUT	1	Err.	3	Err.	5	Err.	7	Err.
1	1.0	0.0	1.0	0.0	1.0	0.0	1.0	0.0
3	1.0	3.9	1.0	3.3	1.0	2.8	1.0	2.4
5	1.1	8.3	1.1	7.1	1.1	6.0	1.1	5.0
7	1.1	13.2	1.1	11.2	1.1	9.5	1.1	8.0

Table C.2: Obtained values for the permittivity of the sample under test of radius 5 mm and $\varepsilon'_r = 1$, using a reference sample with $\varepsilon'_r = 5$ and equal radius. Errors are given in percent.

	Relative permeability of reference sample							
Permeability of SUT	1	Err.	3	Err.	5	Err.	7	Err.
1	1.0	0.0	1.0	0.0	1.0	0.0	1.0	0.0
3	1.0	3.8	1.0	3.2	1.0	2.6	1.0	2.2
5	1.1	8.1	1.1	6.7	1.1	5.6	1.0	4.7
7	1.1	12.8	1.1	10.7	1.1	8.9	1.1	7.4

Table C.3: Obtained values for the permittivity of the sample under test of radius 5 mm and $\varepsilon'_r = 3$, using a reference sample with $\varepsilon'_r = 3$ and equal radius. Errors are given in percent.

	Relative permeability of reference sample							
Permeability of SUT	1	Err.	3	Err.	5	Err.	7	Err.
1	3.0	0.0	2.7	10.1	2.4	18.9	2.2	26.6
3	3.4	11.8	3.0	0.0	2.7	10.4	2.4	19.5
5	3.8	26.4	3.4	12.4	3.0	0.0	2.7	10.7
7	4.3	44.2	3.8	27.5	3.4	12.7	3.0	0.0

Table C.4: Obtained values for the permittivity of the sample under test of radius 5 mm and $\varepsilon'_r = 3$, using a reference sample with $\varepsilon'_r = 5$ and equal radius. Errors are given in percent.

	Relative permeability of reference sample							
Permeability of SUT	1	Err.	3	Err.	5	Err.	7	Err.
1	2.9	2.2	2.6	13.0	2.3	22.1	2.1	29.4
3	3.3	9.3	2.9	3.5	2.6	14.2	2.3	22.7
5	3.7	23.4	3.2	8.2	2.9	4.4	2.6	14.6
7	4.2	40.6	3.7	22.5	3.2	7.4	2.9	4.6

Table C.5: Obtained values for the permittivity of the sample under test of radius 5 mm and $\varepsilon'_r = 5$, using a reference sample with $\varepsilon'_r = 3$ and equal radius. Errors are given in percent.

	Relative permeability of reference sample							
Permeability of SUT	1	Err.	3	Err.	5	Err.	7	Err.
1	5.1	2.7	4.5	9.8	4.0	20.8	3.5	30.3
3	6.0	19.4	5.2	4.4	4.6	8.8	4.0	20.2
5	7.0	39.7	6.1	21.6	5.3	5.7	4.6	8.0
7	8.1	63.0	7.1	41.4	6.1	22.4	5.3	6.0

Table C.6: Obtained values for the permittivity of the sample under test of radius 5 mm and $\varepsilon'_r = 5$, using a reference sample with $\varepsilon'_r = 5$ and equal radius. Errors are given in percent.

	Relative permeability of reference sample							
Permeability of SUT	1	Err.	3	Err.	5	Err.	7	Err.
1	5.0	0.0	4.3	13.5	3.8	24.7	3.3	33.7
3	5.8	16.2	5.0	0.0	4.3	13.5	3.8	24.4
5	6.8	35.8	5.8	16.3	5.0	0.0	4.3	13.0
7	7.9	58.3	6.8	35.0	5.8	15.6	5.0	0.0

Table C.7: Obtained values for the permittivity of the sample under test of radius 2 mm and $\varepsilon'_r = 1$, using a reference sample with $\varepsilon'_r = 3$ and equal radius. Errors are given in percent.

	Relative permeability of reference sample							
Permeability of SUT	1	Err.	3	Err.	5	Err.	7	Err.
1	1.0	0.0	1.0	0.0	1.0	0.0	1.0	0.0
3	1.0	0.9	1.0	0.9	1.0	0.9	1.0	0.8
5	1.0	1.5	1.0	1.5	1.0	1.4	1.0	1.4
7	1.0	2.1	1.0	2.0	1.0	2.0	1.0	1.9

Table C.8: Obtained values for the permittivity of the sample under test of radius 2 mm and $\varepsilon'_r = 1$, using a reference sample with $\varepsilon'_r = 5$ and equal radius. Errors are given in percent.

	Relative permeability of reference sample							
Permeability of SUT	1	Err.	3	Err.	5	Err.	7	Err.
1	1.0	0.0	1.0	0.0	1.0	0.0	1.0	0.0
3	1.0	0.9	1.0	0.8	1.0	0.8	1.0	0.8
5	1.0	1.5	1.0	1.4	1.0	1.3	1.0	1.3
7	1.0	2.0	1.0	2.0	1.0	1.9	1.0	1.8

Table C.9: Obtained values for the permittivity of the sample under test of radius 2 mm and $\varepsilon'_r = 3$, using a reference sample with $\varepsilon'_r = 3$ and equal radius. Errors are given in percent.

	Relative permeability of reference sample							
Permeability of SUT	1	Err.	3	Err.	5	Err.	7	Err.
1	3.0	0.0	2.9	1.9	2.9	3.9	2.8	5.7
3	3.1	2.0	3.0	0.0	2.9	2.0	2.9	3.9
5	3.1	4.1	3.1	2.1	3.0	0.0	2.9	2.0
7	3.2	6.3	3.1	4.2	3.1	2.1	3.0	0.0

Table C.10: Obtained values for the permittivity of the sample under test of radius 2 mm and $\varepsilon'_r = 3$, using a reference sample with $\varepsilon'_r = 5$ and equal radius. Errors are given in percent.

	Relative permeability of reference sample							
Permeability of SUT	1	Err.	3	Err.	5	Err.	7	Err.
1	2.9	2.3	2.9	5.0	2.8	7.5	2.7	10.1
3	3.0	0.4	2.9	3.1	2.8	5.7	2.7	8.4
5	3.0	1.6	3.0	1.2	2.9	3.9	2.8	6.6
7	3.1	3.7	3.0	0.9	2.9	1.9	2.9	4.8

Table C.11: Obtained values for the permittivity of the sample under test of radius 2 mm and $\varepsilon'_r = 5$, using a reference sample with $\varepsilon'_r = 3$ and equal radius. Errors are given in percent.

	Relative permeability of reference sample							
Permeability of SUT	1	Err.	3	Err.	5	Err.	7	Err.
1	5.1	2.9	5.0	0.5	4.9	1.9	4.8	4.2
3	5.3	6.4	5.2	4.0	5.1	1.4	4.9	1.0
5	5.5	10.1	5.4	7.5	5.2	4.9	5.1	2.4
7	5.7	14.3	5.6	11.6	5.4	8.8	5.3	6.2

Table C.12: Obtained values for the permittivity of the sample under test of radius 2 mm and $\varepsilon'_r = 5$, using a reference sample with $\varepsilon'_r = 5$ and equal radius. Errors are given in percent.

	Relative permeability of reference sample							
Permeability of SUT	1	Err.	3	Err.	5	Err.	7	Err.
1	5.0	0.0	4.8	3.3	4.7	6.4	4.5	9.7
3	5.2	3.4	5.0	0.0	4.8	3.3	4.7	6.7
5	5.3	7.0	5.2	3.4	5.0	0.0	4.8	3.5
7	5.5	11.0	5.4	7.3	5.2	3.7	5.0	0.0

Appendix D

Results on permeability of magnetic materials

Here we present a more complete set of results for the simulations performed to obtain the permeability.

Table D.1: Obtained values for the permeability of the sample under test of radius 5 mm and $\varepsilon'_r = 3$, using a reference sample with $\varepsilon'_r = 3$ and equal radius. Errors are given in percent.

	Relative permeability of reference sample							
True value	1	Err.	3	Err.	5	Err.	7	Err.
1	3.0	200.0	1.5	52.9	1.4	39.3	1.3	31.1
3	8.6	185.5	3.0	0.0	2.5	17.2	2.2	27.5
5	11.2	123.8	3.7	26.1	3.0	40.0	2.6	48.4
7	13.9	98.3	4.4	37.1	3.5	49.6	3.0	57.1

Table D.2: Obtained values for the permeability of the sample under test of radius 5 mm and $\varepsilon'_r = 5$, using a reference sample with $\varepsilon'_r = 3$ and equal radius. Errors are given in percent.

	Relative permeability of reference sample							
True value	1	Err.	3	Err.	5	Err.	7	Err.
1	5.5	446.4	2.2	118.0	1.9	87.6	1.7	69.3
3	15.2	405.3	4.7	58.1	3.8	26.0	3.2	6.6
5	25.1	402.4	7.4	47.5	5.7	14.7	4.7	5.1
7	42.6	509.1	12.0	71.5	9.2	31.0	7.5	6.6

Table D.3: Obtained values for the permeability of the sample under test of radius 5 mm and $\varepsilon'_r = 3$, using a reference sample with $\varepsilon'_r = 5$ and equal radius. Errors are given in percent.

	Relative permeability of reference sample							
True value	1	Err.	3	Err.	5	Err.	7	Err.
1	2.8	179.2	1.6	56.5	1.3	33.2	1.2	19.2
3	7.8	159.3	3.1	4.6	2.3	24.8	1.7	42.4
5	10.1	102.6	3.9	22.4	2.7	46.2	2.0	60.4
7	12.5	79.2	4.6	33.7	3.1	55.2	2.2	68.0

Table D.4: Obtained values for the permeability of the sample under test of radius 5 mm and $\varepsilon'_r = 5$, using a reference sample with $\varepsilon'_r = 5$ and equal radius. Errors are given in percent.

	Relative permeability of reference sample							
True value	1	Err.	3	Err.	5	Err.	7	Err.
1	5.0	400.0	2.3	126.1	1.7	74.0	1.4	42.9
3	13.7	356.2	5.0	66.7	3.3	11.6	2.4	21.3
5	22.6	352.2	7.8	56.3	5.0	0.0	3.3	33.7
7	38.3	447.2	12.8	82.3	7.9	12.9	5.0	28.6

Table D.5: Obtained values for the permeability of the sample under test of radius 2 mm and $\varepsilon'_r = 3$, using a reference sample with $\varepsilon'_r = 3$ and equal radius. Errors are given in percent.

	Relative permeability of reference sample							
True value	1	Err.	3	Err.	5	Err.	7	Err.
1	3.0	200.0	1.5	52.9	1.4	39.3	1.3	31.1
3	8.6	185.5	3.0	0.0	2.5	17.2	2.2	27.5
5	11.2	123.8	3.7	26.1	3.0	40.0	2.6	48.4
7	13.9	98.3	4.4	37.1	3.5	49.6	3.0	57.1

Table D.6: Obtained values for the permeability of the sample under test of radius 2 mm and $\varepsilon'_r = 5$, using a reference sample with $\varepsilon'_r = 3$ and equal radius. Errors are given in percent.

	Relative permeability of reference sample							
True value	1	Err.	3	Err.	5	Err.	7	Err.
1	3.6	256.4	1.5	49.4	1.4	40.1	1.4	36.5
3	12.3	310.3	3.2	6.0	2.8	7.8	2.6	13.0
5	14.9	197.8	3.7	26.5	3.2	36.6	3.0	40.4
7	16.2	131.9	3.9	43.8	3.4	51.7	3.2	54.7

Table D.7: Obtained values for the permeability of the sample under test of radius 2 mm and $\varepsilon'_r = 3$, using a reference sample with $\varepsilon'_r = 5$ and equal radius. Errors are given in percent.

	Relative permeability of reference sample							
True value	1	Err.	3	Err.	5	Err.	7	Err.
1	4.1	312.0	1.7	70.7	1.6	57.6	1.5	52.5
3	17.2	473.1	4.7	55.7	4.0	33.0	3.7	24.2
5	21.0	319.4	5.5	10.6	4.7	6.2	4.4	12.7
7	22.9	227.2	6.0	14.8	5.0	27.9	4.7	33.0

Table D.8: Obtained values for the permeability of the sample under test of radius 2 mm and $\varepsilon'_r = 5$, using a reference sample with $\varepsilon'_r = 5$ and equal radius. Errors are given in percent.

	Relative permeability of reference sample							
True value	1	Err.	3	Err.	5	Err.	7	Err.
1	5.0	400.0	1.9	90.7	1.7	73.9	1.7	67.4
3	18.6	521.3	5.0	66.7	4.3	41.9	4.0	32.3
5	22.7	353.2	5.9	18.2	5.0	0.0	4.6	7.1
7	24.8	253.6	6.4	8.8	5.4	23.0	5.0	28.6

Appendix E

Losses of magnetic materials

Here we present a more complete set of results for the simulations performed to obtain the magnetic loss tangent.

Table E.1: Obtained values for the magnetic loss tangent of the sample under test of radius 5 mm and $\mu_r' = 1$, using a reference sample with $\mu_r' = 3$ and equal radius. Permittivity is set to unity and there are no dielectric losses.

	Magnetic loss tangent of reference sample				
True value	10^{-5}	10^{-4}	10^{-3}	10^{-2}	10^{-1}
10^{-5}	$-0.0 \cdot 10^{0}$	$-0.0 \cdot 10^{0}$	$0.0 \cdot 10^{0}$	$0.0 \cdot 10^{0}$	$0.0 \cdot 10^{0}$
10^{-4}	$-0.0 \cdot 10^{0}$	$-0.0 \cdot 10^{0}$	$0.0 \cdot 10^{0}$	$0.0 \cdot 10^{0}$	$0.0 \cdot 10^{0}$
10^{-3}	$-3.4 \cdot 10^{-5}$	$-3.4 \cdot 10^{-4}$	$2.1 \cdot 10^{-2}$	$4.1 \cdot 10^{-3}$	$3.7 \cdot 10^{-3}$
10^{-2}	$-4.5 \cdot 10^{-4}$	$-4.5 \cdot 10^{-3}$	$2.7 \cdot 10^{-1}$	$5.4 \cdot 10^{-2}$	$4.8 \cdot 10^{-2}$
10^{-1}	$-4.3 \cdot 10^{-3}$	$-4.3 \cdot 10^{-2}$	$2.6 \cdot 10^{0}$	$5.2 \cdot 10^{-1}$	$4.6 \cdot 10^{-1}$

Table E.2: Obtained values for the magnetic loss tangent of the sample under test of radius 5 mm and $\mu_r' = 1$, using a reference sample with $\mu_r' = 5$ and equal radius. Permittivity is set to unity and there are no dielectric losses.

	Magnetic loss tangent of reference sample				
True value	10^{-5}	10^{-4}	10^{-3}	10^{-2}	10^{-1}
10^{-5}	$-0.0 \cdot 10^{0}$	$-0.0 \cdot 10^{0}$	$-0.0 \cdot 10^{0}$	$0.0 \cdot 10^{0}$	$0.0 \cdot 10^{0}$
10^{-4}	$-0.0 \cdot 10^{0}$	$-0.0 \cdot 10^{0}$	$-0.0 \cdot 10^{0}$	$0.0 \cdot 10^{0}$	$0.0 \cdot 10^{0}$
10^{-3}	$-6.0 \cdot 10^{-5}$	$-6.0 \cdot 10^{-4}$	$-1.6 \cdot 10^{-2}$	$9.4 \cdot 10^{-3}$	$8.4 \cdot 10^{-3}$
10^{-2}	$-7.8 \cdot 10^{-4}$	$-7.8 \cdot 10^{-3}$	$-2.0 \cdot 10^{-1}$	$1.2 \cdot 10^{-1}$	$1.1 \cdot 10^{-1}$
10^{-1}	$-7.5 \cdot 10^{-3}$	$-7.5 \cdot 10^{-2}$	$-1.9 \cdot 10^{0}$	$1.2 \cdot 10^{0}$	$1.0 \cdot 10^{0}$

Table E.3: Obtained values for the magnetic loss tangent of the sample under test of radius 5 mm and $\mu_r' = 1$, using a reference sample with $\mu_r' = 7$ and equal radius. Permittivity is set to unity and there are no dielectric losses.

	Magnetic loss tangent of reference sample				
True value	10^{-5}	10^{-4}	10^{-3}	10^{-2}	10^{-1}
10^{-5}	$-0.0 \cdot 10^{0}$	$-0.0 \cdot 10^{0}$	$-0.0 \cdot 10^{0}$	$0.0 \cdot 10^{0}$	$0.0 \cdot 10^{0}$
10^{-4}	$-0.0 \cdot 10^{0}$	$-0.0 \cdot 10^{0}$	$-0.0 \cdot 10^{0}$	$0.0 \cdot 10^{0}$	$0.0 \cdot 10^{0}$
10^{-3}	$-5.3 \cdot 10^{-5}$	$-5.3 \cdot 10^{-4}$	$-2.4 \cdot 10^{-2}$	$1.8 \cdot 10^{-2}$	$1.4 \cdot 10^{-2}$
10^{-2}	$-6.9 \cdot 10^{-4}$	$-6.9 \cdot 10^{-3}$	$-3.1 \cdot 10^{-1}$	$2.4 \cdot 10^{-1}$	$1.8 \cdot 10^{-1}$
10^{-1}	$-6.6 \cdot 10^{-3}$	$-6.6 \cdot 10^{-2}$	$-2.9 \cdot 10^{0}$	$2.3 \cdot 10^{0}$	$1.8 \cdot 10^{0}$

Table E.4: Obtained values for the magnetic loss tangent of the sample under test of radius 5 mm and $\mu_r' = 3$, using a reference sample with $\mu_r' = 3$ and equal radius. Permittivity is set to unity and there are no dielectric losses.

	Magnetic loss tangent of reference sample				
True value	10^{-5}	10^{-4}	10^{-3}	10^{-2}	10^{-1}
10^{-5}	$1.0 \cdot 10^{-5}$	$1.0 \cdot 10^{-4}$	$-6.0 \cdot 10^{-3}$	$-1.2 \cdot 10^{-3}$	$-1.1 \cdot 10^{-3}$
10^{-4}	$1.0 \cdot 10^{-5}$	$1.0 \cdot 10^{-4}$	$-6.0 \cdot 10^{-3}$	$-1.2 \cdot 10^{-3}$	$-1.1 \cdot 10^{-3}$
10^{-3}	$-1.7 \cdot 10^{-6}$	$-1.7 \cdot 10^{-5}$	$1.0 \cdot 10^{-3}$	$2.0 \cdot 10^{-4}$	$1.8 \cdot 10^{-4}$
10^{-2}	$-8.3 \cdot 10^{-5}$	$-8.3 \cdot 10^{-4}$	$5.0 \cdot 10^{-2}$	$1.0 \cdot 10^{-2}$	$8.9 \cdot 10^{-3}$
10^{-1}	$-9.3 \cdot 10^{-4}$	$-9.3 \cdot 10^{-3}$	$5.6 \cdot 10^{-1}$	$1.1 \cdot 10^{-1}$	$1.0 \cdot 10^{-1}$

Table E.5: Obtained values for the magnetic loss tangent of the sample under test of radius 5 mm and $\mu_r' = 3$, using a reference sample with $\mu_r' = 5$ and equal radius. Permittivity is set to unity and there are no dielectric losses.

	Magnetic loss tangent of reference sample				
True value	10^{-5}	10^{-4}	10^{-3}	10^{-2}	10^{-1}
10^{-5}	$1.3 \cdot 10^{-5}$	$1.3 \cdot 10^{-4}$	$3.4 \cdot 10^{-3}$	$-2.0 \cdot 10^{-3}$	$-1.8 \cdot 10^{-3}$
10^{-4}	$1.3 \cdot 10^{-5}$	$1.3 \cdot 10^{-4}$	$3.4 \cdot 10^{-3}$	$-2.0 \cdot 10^{-3}$	$-1.8 \cdot 10^{-3}$
10^{-3}	$-2.2 \cdot 10^{-6}$	$-2.2 \cdot 10^{-5}$	$-5.6 \cdot 10^{-4}$	$3.4 \cdot 10^{-4}$	$3.0 \cdot 10^{-4}$
10^{-2}	$-1.1 \cdot 10^{-4}$	$-1.1 \cdot 10^{-3}$	$-2.8 \cdot 10^{-2}$	$1.7 \cdot 10^{-2}$	$1.5 \cdot 10^{-2}$
10^{-1}	$-1.2 \cdot 10^{-3}$	$-1.2 \cdot 10^{-2}$	$-3.1 \cdot 10^{-1}$	$1.9 \cdot 10^{-1}$	$1.7 \cdot 10^{-1}$

Table E.6: Obtained values for the magnetic loss tangent of the sample under test of radius 5 mm and $\mu_r' = 3$, using a reference sample with $\mu_r' = 7$ and equal radius. Permittivity is set to unity and there are no dielectric losses.

	Magnetic loss tangent of reference sample				
True value	10^{-5}	10^{-4}	10^{-3}	10^{-2}	10^{-1}
10^{-5}	$9.1 \cdot 10^{-6}$	$9.1 \cdot 10^{-5}$	$4.0 \cdot 10^{-3}$	$-3.2 \cdot 10^{-3}$	$-2.4 \cdot 10^{-3}$
10^{-4}	$9.1 \cdot 10^{-6}$	$9.1 \cdot 10^{-5}$	$4.0 \cdot 10^{-3}$	$-3.2 \cdot 10^{-3}$	$-2.4 \cdot 10^{-3}$
10^{-3}	$-1.5 \cdot 10^{-6}$	$-1.5 \cdot 10^{-5}$	$-6.7 \cdot 10^{-4}$	$5.3 \cdot 10^{-4}$	$4.1 \cdot 10^{-4}$
10^{-2}	$-7.6 \cdot 10^{-5}$	$-7.6 \cdot 10^{-4}$	$-3.4 \cdot 10^{-2}$	$2.6 \cdot 10^{-2}$	$2.0 \cdot 10^{-2}$
10^{-1}	$-8.5 \cdot 10^{-4}$	$-8.5 \cdot 10^{-3}$	$-3.8 \cdot 10^{-1}$	$2.9 \cdot 10^{-1}$	$2.3 \cdot 10^{-1}$

Table E.7: Obtained values for the magnetic loss tangent of the sample under test of radius 5 mm and $\mu_r' = 5$, using a reference sample with $\mu_r' = 3$ and equal radius. Permittivity is set to unity and there are no dielectric losses.

	Magnetic loss tangent of reference sample				
True value	10^{-5}	10^{-4}	10^{-3}	10^{-2}	10^{-1}
10^{-5}	$7.9 \cdot 10^{-6}$	$7.9 \cdot 10^{-5}$	$-4.7 \cdot 10^{-3}$	$-9.5 \cdot 10^{-4}$	$-8.5 \cdot 10^{-4}$
10^{-4}	$7.9 \cdot 10^{-6}$	$7.9 \cdot 10^{-5}$	$-4.7 \cdot 10^{-3}$	$-9.5 \cdot 10^{-4}$	$-8.5 \cdot 10^{-4}$
10^{-3}	$3.0 \cdot 10^{-6}$	$3.0 \cdot 10^{-5}$	$-1.8 \cdot 10^{-3}$	$-3.6 \cdot 10^{-4}$	$-3.3 \cdot 10^{-4}$
10^{-2}	$-5.0 \cdot 10^{-5}$	$-5.0 \cdot 10^{-4}$	$3.0 \cdot 10^{-2}$	$6.0 \cdot 10^{-3}$	$5.4 \cdot 10^{-3}$
10^{-1}	$-5.6 \cdot 10^{-4}$	$-5.6 \cdot 10^{-3}$	$3.4 \cdot 10^{-1}$	$6.8 \cdot 10^{-2}$	$6.0 \cdot 10^{-2}$

Table E.8: Obtained values for the magnetic loss tangent of the sample under test of radius 5 mm and $\mu_r' = 5$, using a reference sample with $\mu_r' = 5$ and equal radius. Permittivity is set to unity and there are no dielectric losses.

	Magnetic loss tangent of reference sample				
True value	10^{-5}	10^{-4}	10^{-3}	10^{-2}	10^{-1}
10^{-5}	$1.0 \cdot 10^{-5}$	$1.0 \cdot 10^{-4}$	$2.6 \cdot 10^{-3}$	$-1.6 \cdot 10^{-3}$	$-1.4 \cdot 10^{-3}$
10^{-4}	$1.0 \cdot 10^{-5}$	$1.0 \cdot 10^{-4}$	$2.6 \cdot 10^{-3}$	$-1.6 \cdot 10^{-3}$	$-1.4 \cdot 10^{-3}$
10^{-3}	$3.8 \cdot 10^{-6}$	$3.8 \cdot 10^{-5}$	$1.0 \cdot 10^{-3}$	$-6.0 \cdot 10^{-4}$	$-5.4 \cdot 10^{-4}$
10^{-2}	$-6.4 \cdot 10^{-5}$	$-6.4 \cdot 10^{-4}$	$-1.7 \cdot 10^{-2}$	$1.0 \cdot 10^{-2}$	$8.9 \cdot 10^{-3}$
10^{-1}	$-7.1 \cdot 10^{-4}$	$-7.1 \cdot 10^{-3}$	$-1.9 \cdot 10^{-1}$	$1.1 \cdot 10^{-1}$	$1.0 \cdot 10^{-1}$

Table E.9: Obtained values for the magnetic loss tangent of the sample under test of radius 5 mm and $\mu_r' = 5$, using a reference sample with $\mu_r' = 7$ and equal radius. Permittivity is set to unity and there are no dielectric losses.

	Magnetic loss tangent of reference sample				
True value	10^{-5}	10^{-4}	10^{-3}	10^{-2}	10^{-1}
10^{-5}	$6.9 \cdot 10^{-6}$	$6.9 \cdot 10^{-5}$	$3.1 \cdot 10^{-3}$	$-2.4 \cdot 10^{-3}$	$-1.9 \cdot 10^{-3}$
10^{-4}	$6.9 \cdot 10^{-6}$	$6.9 \cdot 10^{-5}$	$3.1 \cdot 10^{-3}$	$-2.4 \cdot 10^{-3}$	$-1.9 \cdot 10^{-3}$
10^{-3}	$2.7 \cdot 10^{-6}$	$2.7 \cdot 10^{-5}$	$1.2 \cdot 10^{-3}$	$-9.3 \cdot 10^{-4}$	$-7.1 \cdot 10^{-4}$
10^{-2}	$-4.4 \cdot 10^{-5}$	$-4.4 \cdot 10^{-4}$	$-2.0 \cdot 10^{-2}$	$1.5 \cdot 10^{-2}$	$1.2 \cdot 10^{-2}$
10^{-1}	$-4.9 \cdot 10^{-4}$	$-4.9 \cdot 10^{-3}$	$-2.2 \cdot 10^{-1}$	$1.7 \cdot 10^{-1}$	$1.3 \cdot 10^{-1}$

Table E.10: Obtained values for the magnetic loss tangent of the sample under test of radius 5 mm and $\mu_r' = 7$, using a reference sample with $\mu_r' = 3$ and equal radius. Permittivity is set to unity and there are no dielectric losses.

	Magnetic loss tangent of reference sample				
True value	10^{-5}	10^{-4}	10^{-3}	10^{-2}	10^{-1}
10^{-5}	$1.2 \cdot 10^{-5}$	$1.2 \cdot 10^{-4}$	$-6.9 \cdot 10^{-3}$	$-1.4 \cdot 10^{-3}$	$-1.2 \cdot 10^{-3}$
10^{-4}	$1.2 \cdot 10^{-5}$	$1.2 \cdot 10^{-4}$	$-6.9 \cdot 10^{-3}$	$-1.4 \cdot 10^{-3}$	$-1.2 \cdot 10^{-3}$
10^{-3}	$2.6 \cdot 10^{-6}$	$2.6 \cdot 10^{-5}$	$-1.6 \cdot 10^{-3}$	$-3.1 \cdot 10^{-4}$	$-2.8 \cdot 10^{-4}$
10^{-2}	$-3.3 \cdot 10^{-5}$	$-3.3 \cdot 10^{-4}$	$2.0 \cdot 10^{-2}$	$4.0 \cdot 10^{-3}$	$3.6 \cdot 10^{-3}$
10^{-1}	$-4.3 \cdot 10^{-4}$	$-4.3 \cdot 10^{-3}$	$2.6 \cdot 10^{-1}$	$5.2 \cdot 10^{-2}$	$4.6 \cdot 10^{-2}$

Table E.11: Obtained values for the magnetic loss tangent of the sample under test of radius 5 mm and $\mu_r' = 7$, using a reference sample with $\mu_r' = 5$ and equal radius. Permittivity is set to unity and there are no dielectric losses.

	Magnetic loss tangent of reference sample				
True value	10^{-5}	10^{-4}	10^{-3}	10^{-2}	10^{-1}
10^{-5}	$1.5 \cdot 10^{-5}$	$1.5 \cdot 10^{-4}$	$3.8 \cdot 10^{-3}$	$-2.3 \cdot 10^{-3}$	$-2.0 \cdot 10^{-3}$
10^{-4}	$1.5 \cdot 10^{-5}$	$1.5 \cdot 10^{-4}$	$3.8 \cdot 10^{-3}$	$-2.3 \cdot 10^{-3}$	$-2.0 \cdot 10^{-3}$
10^{-3}	$3.3 \cdot 10^{-6}$	$3.3 \cdot 10^{-5}$	$8.5 \cdot 10^{-4}$	$-5.1 \cdot 10^{-4}$	$-4.6 \cdot 10^{-4}$
10^{-2}	$-4.2 \cdot 10^{-5}$	$-4.2 \cdot 10^{-4}$	$-1.1 \cdot 10^{-2}$	$6.5 \cdot 10^{-3}$	$5.8 \cdot 10^{-3}$
10^{-1}	$-5.4 \cdot 10^{-4}$	$-5.4 \cdot 10^{-3}$	$-1.4 \cdot 10^{-1}$	$8.5 \cdot 10^{-2}$	$7.6 \cdot 10^{-2}$

Table E.12: Obtained values for the magnetic loss tangent of the sample under test of radius 5 mm and $\mu_r' = 7$, using a reference sample with $\mu_r' = 7$ and equal radius. Permittivity is set to unity and there are no dielectric losses.

	Magnetic loss tangent of reference sample				
True value	10^{-5}	10^{-4}	10^{-3}	10^{-2}	10^{-1}
10^{-5}	$1.0 \cdot 10^{-5}$	$1.0 \cdot 10^{-4}$	$4.4 \cdot 10^{-3}$	$-3.5 \cdot 10^{-3}$	$-2.7 \cdot 10^{-3}$
10^{-4}	$1.0 \cdot 10^{-5}$	$1.0 \cdot 10^{-4}$	$4.4 \cdot 10^{-3}$	$-3.5 \cdot 10^{-3}$	$-2.7 \cdot 10^{-3}$
10^{-3}	$2.3 \cdot 10^{-6}$	$2.3 \cdot 10^{-5}$	$1.0 \cdot 10^{-3}$	$-7.8 \cdot 10^{-4}$	$-6.0 \cdot 10^{-4}$
10^{-2}	$-2.9 \cdot 10^{-5}$	$-2.9 \cdot 10^{-4}$	$-1.3 \cdot 10^{-2}$	$1.0 \cdot 10^{-2}$	$7.7 \cdot 10^{-3}$
10^{-1}	$-3.7 \cdot 10^{-4}$	$-3.7 \cdot 10^{-3}$	$-1.7 \cdot 10^{-1}$	$1.3 \cdot 10^{-1}$	$1.0 \cdot 10^{-1}$

Table E.13: Obtained values for the magnetic loss tangent of the sample under test of radius 2 mm and $\mu_r' = 1$, using a reference sample with $\mu_r' = 3$ and equal radius. Permittivity is set to unity and there are no dielectric losses.

	Magnetic loss tangent of reference sample				
True value	10^{-5}	10^{-4}	10^{-3}	10^{-2}	10^{-1}
10^{-5}	$-0.0 \cdot 10^{0}$	$-0.0 \cdot 10^{0}$	$-0.0 \cdot 10^{0}$	$0.0 \cdot 10^{0}$	$0.0 \cdot 10^{0}$
10^{-4}	$-0.0 \cdot 10^{0}$	$-0.0 \cdot 10^{0}$	$-0.0 \cdot 10^{0}$	$0.0 \cdot 10^{0}$	$0.0 \cdot 10^{0}$
10^{-3}	$-0.0 \cdot 10^{0}$	$-0.0 \cdot 10^{0}$	$-0.0 \cdot 10^{0}$	$0.0 \cdot 10^{0}$	$0.0 \cdot 10^{0}$
10^{-2}	$-1.2 \cdot 10^{-4}$	$-1.2 \cdot 10^{-3}$	$-1.2 \cdot 10^{-2}$	$1.2 \cdot 10^{-1}$	$5.7 \cdot 10^{-2}$
10^{-1}	$-1.1 \cdot 10^{-3}$	$-1.1 \cdot 10^{-2}$	$-1.1 \cdot 10^{-1}$	$10.0 \cdot 10^{-1}$	$4.9 \cdot 10^{-1}$

Table E.14: Obtained values for the magnetic loss tangent of the sample under test of radius 2 mm and $\mu_r' = 1$, using a reference sample with $\mu_r' = 5$ and equal radius. Permittivity is set to unity and there are no dielectric losses.

	Magnetic loss tangent of reference sample				
True value	10^{-5}	10^{-4}	10^{-3}	10^{-2}	10^{-1}
10^{-5}	$-0.0 \cdot 10^{0}$	$-0.0 \cdot 10^{0}$	$0.0 \cdot 10^{0}$	$0.0 \cdot 10^{0}$	$0.0 \cdot 10^{0}$
10^{-4}	$-0.0 \cdot 10^{0}$	$-0.0 \cdot 10^{0}$	$0.0 \cdot 10^{0}$	$0.0 \cdot 10^{0}$	$0.0 \cdot 10^{0}$
10^{-3}	$-0.0 \cdot 10^{0}$	$-0.0 \cdot 10^{0}$	$0.0 \cdot 10^{0}$	$0.0 \cdot 10^{0}$	$0.0 \cdot 10^{0}$
10^{-2}	$-2.1 \cdot 10^{-4}$	$-2.1 \cdot 10^{-3}$	$4.0 \cdot 10^{-1}$	$1.9 \cdot 10^{-1}$	$1.4 \cdot 10^{-1}$
10^{-1}	$-1.8 \cdot 10^{-3}$	$-1.8 \cdot 10^{-2}$	$3.4 \cdot 10^{0}$	$1.6 \cdot 10^{0}$	$1.2 \cdot 10^{0}$

Table E.15: Obtained values for the magnetic loss tangent of the sample under test of radius 2 mm and $\mu_r' = 1$, using a reference sample with $\mu_r' = 7$ and equal radius. Permittivity is set to unity and there are no dielectric losses.

	Magnetic loss tangent of reference sample				
True value	10^{-5}	10^{-4}	10^{-3}	10^{-2}	10^{-1}
10^{-5}	$-0.0 \cdot 10^{0}$	$-0.0 \cdot 10^{0}$	$-0.0 \cdot 10^{0}$	$0.0 \cdot 10^{0}$	$0.0 \cdot 10^{0}$
10^{-4}	$-0.0 \cdot 10^{0}$	$-0.0 \cdot 10^{0}$	$-0.0 \cdot 10^{0}$	$0.0 \cdot 10^{0}$	$0.0 \cdot 10^{0}$
10^{-3}	$-0.0 \cdot 10^{0}$	$-0.0 \cdot 10^{0}$	$-0.0 \cdot 10^{0}$	$0.0 \cdot 10^{0}$	$0.0 \cdot 10^{0}$
10^{-2}	$-3.0 \cdot 10^{-4}$	$-3.0 \cdot 10^{-3}$	$-3.0 \cdot 10^{-2}$	$2.6 \cdot 10^{-1}$	$2.5 \cdot 10^{-1}$
10^{-1}	$-2.5 \cdot 10^{-3}$	$-2.5 \cdot 10^{-2}$	$-2.5 \cdot 10^{-1}$	$2.3 \cdot 10^{0}$	$2.2 \cdot 10^{0}$

Table E.16: Obtained values for the magnetic loss tangent of the sample under test of radius 2 mm and $\mu_r' = 3$, using a reference sample with $\mu_r' = 3$ and equal radius. Permittivity is set to unity and there are no dielectric losses.

	Magnetic loss tangent of reference sample				
True value	10^{-5}	10^{-4}	10^{-3}	10^{-2}	10^{-1}
10^{-5}	$1.0 \cdot 10^{-5}$	$1.0 \cdot 10^{-4}$	$1.0 \cdot 10^{-3}$	$-9.3 \cdot 10^{-3}$	$-4.6 \cdot 10^{-3}$
10^{-4}	$1.0 \cdot 10^{-5}$	$1.0 \cdot 10^{-4}$	$1.0 \cdot 10^{-3}$	$-9.3 \cdot 10^{-3}$	$-4.6 \cdot 10^{-3}$
10^{-3}	$1.0 \cdot 10^{-5}$	$1.0 \cdot 10^{-4}$	$1.0 \cdot 10^{-3}$	$-9.3 \cdot 10^{-3}$	$-4.6 \cdot 10^{-3}$
10^{-2}	$-1.1 \cdot 10^{-5}$	$-1.1 \cdot 10^{-4}$	$-1.1 \cdot 10^{-3}$	$1.0 \cdot 10^{-2}$	$5.0 \cdot 10^{-3}$
10^{-1}	$-2.2 \cdot 10^{-4}$	$-2.2 \cdot 10^{-3}$	$-2.2 \cdot 10^{-2}$	$2.0 \cdot 10^{-1}$	$1.0 \cdot 10^{-1}$

Table E.17: Obtained values for the magnetic loss tangent of the sample under test of radius 2 mm and $\mu_r' = 3$, using a reference sample with $\mu_r' = 5$ and equal radius. Permittivity is set to unity and there are no dielectric losses.

	Magnetic loss tangent of reference sample				
True value	10^{-5}	10^{-4}	10^{-3}	10^{-2}	10^{-1}
10^{-5}	$1.2 \cdot 10^{-5}$	$1.2 \cdot 10^{-4}$	$-2.4 \cdot 10^{-2}$	$-1.1 \cdot 10^{-2}$	$-8.4 \cdot 10^{-3}$
10^{-4}	$1.2 \cdot 10^{-5}$	$1.2 \cdot 10^{-4}$	$-2.4 \cdot 10^{-2}$	$-1.1 \cdot 10^{-2}$	$-8.4 \cdot 10^{-3}$
10^{-3}	$1.2 \cdot 10^{-5}$	$1.2 \cdot 10^{-4}$	$-2.4 \cdot 10^{-2}$	$-1.1 \cdot 10^{-2}$	$-8.4 \cdot 10^{-3}$
10^{-2}	$-1.3 \cdot 10^{-5}$	$-1.3 \cdot 10^{-4}$	$2.5 \cdot 10^{-2}$	$1.2 \cdot 10^{-2}$	$9.0 \cdot 10^{-3}$
10^{-1}	$-2.7 \cdot 10^{-4}$	$-2.7 \cdot 10^{-3}$	$5.1 \cdot 10^{-1}$	$2.4 \cdot 10^{-1}$	$1.8 \cdot 10^{-1}$

Table E.18: Obtained values for the magnetic loss tangent of the sample under test of radius 2 mm and $\mu_r' = 3$, using a reference sample with $\mu_r' = 7$ and equal radius. Permittivity is set to unity and there are no dielectric losses.

	Magnetic loss tangent of reference sample				
True value	10^{-5}	10^{-4}	10^{-3}	10^{-2}	10^{-1}
10^{-5}	$1.4 \cdot 10^{-5}$	$1.4 \cdot 10^{-4}$	$1.4 \cdot 10^{-3}$	$-1.2 \cdot 10^{-2}$	$-1.2 \cdot 10^{-2}$
10^{-4}	$1.4 \cdot 10^{-5}$	$1.4 \cdot 10^{-4}$	$1.4 \cdot 10^{-3}$	$-1.2 \cdot 10^{-2}$	$-1.2 \cdot 10^{-2}$
10^{-3}	$1.4 \cdot 10^{-5}$	$1.4 \cdot 10^{-4}$	$1.4 \cdot 10^{-3}$	$-1.2 \cdot 10^{-2}$	$-1.2 \cdot 10^{-2}$
10^{-2}	$-1.5 \cdot 10^{-5}$	$-1.5 \cdot 10^{-4}$	$-1.5 \cdot 10^{-3}$	$1.3 \cdot 10^{-2}$	$1.3 \cdot 10^{-2}$
10^{-1}	$-3.0 \cdot 10^{-4}$	$-3.0 \cdot 10^{-3}$	$-3.0 \cdot 10^{-2}$	$2.7 \cdot 10^{-1}$	$2.5 \cdot 10^{-1}$

Table E.19: Obtained values for the magnetic loss tangent of the sample under test of radius 2 mm and $\mu_r' = 5$, using a reference sample with $\mu_r' = 3$ and equal radius. Permittivity is set to unity and there are no dielectric losses.

	Magnetic loss tangent of reference sample				
True value	10^{-5}	10^{-4}	10^{-3}	10^{-2}	10^{-1}
10^{-5}	$8.3 \cdot 10^{-6}$	$8.3 \cdot 10^{-5}$	$8.3 \cdot 10^{-4}$	$-7.7 \cdot 10^{-3}$	$-3.8 \cdot 10^{-3}$
10^{-4}	$8.3 \cdot 10^{-6}$	$8.3 \cdot 10^{-5}$	$8.3 \cdot 10^{-4}$	$-7.7 \cdot 10^{-3}$	$-3.8 \cdot 10^{-3}$
10^{-3}	$-4.3 \cdot 10^{-7}$	$-4.3 \cdot 10^{-6}$	$-4.3 \cdot 10^{-5}$	$4.0 \cdot 10^{-4}$	$2.0 \cdot 10^{-4}$
10^{-2}	$-9.1 \cdot 10^{-6}$	$-9.1 \cdot 10^{-5}$	$-9.1 \cdot 10^{-4}$	$8.5 \cdot 10^{-3}$	$4.2 \cdot 10^{-3}$
10^{-1}	$-1.2 \cdot 10^{-4}$	$-1.2 \cdot 10^{-3}$	$-1.2 \cdot 10^{-2}$	$1.1 \cdot 10^{-1}$	$5.6 \cdot 10^{-2}$

Table E.20: Obtained values for the magnetic loss tangent of the sample under test of radius 2 mm and $\mu_r' = 5$, using a reference sample with $\mu_r' = 5$ and equal radius. Permittivity is set to unity and there are no dielectric losses.

	Magnetic loss tangent of reference sample				
True value	10^{-5}	10^{-4}	10^{-3}	10^{-2}	10^{-1}
10^{-5}	$1.0 \cdot 10^{-5}$	$1.0 \cdot 10^{-4}$	$-1.9 \cdot 10^{-2}$	$-9.1 \cdot 10^{-3}$	$-6.8 \cdot 10^{-3}$
10^{-4}	$1.0 \cdot 10^{-5}$	$1.0 \cdot 10^{-4}$	$-1.9 \cdot 10^{-2}$	$-9.1 \cdot 10^{-3}$	$-6.8 \cdot 10^{-3}$
10^{-3}	$-5.2 \cdot 10^{-7}$	$-5.2 \cdot 10^{-6}$	$1.0 \cdot 10^{-3}$	$4.7 \cdot 10^{-4}$	$3.5 \cdot 10^{-4}$
10^{-2}	$-1.1 \cdot 10^{-5}$	$-1.1 \cdot 10^{-4}$	$2.1 \cdot 10^{-2}$	$1.0 \cdot 10^{-2}$	$7.5 \cdot 10^{-3}$
10^{-1}	$-1.5 \cdot 10^{-4}$	$-1.5 \cdot 10^{-3}$	$2.8 \cdot 10^{-1}$	$1.3 \cdot 10^{-1}$	$1.0 \cdot 10^{-1}$

Table E.21: Obtained values for the magnetic loss tangent of the sample under test of radius 2 mm and $\mu_r' = 5$, using a reference sample with $\mu_r' = 7$ and equal radius. Permittivity is set to unity and there are no dielectric losses.

	Magnetic loss tangent of reference sample				
True value	10^{-5}	10^{-4}	10^{-3}	10^{-2}	10^{-1}
10^{-5}	$1.1 \cdot 10^{-5}$	$1.1 \cdot 10^{-4}$	$1.1 \cdot 10^{-3}$	$-9.8 \cdot 10^{-3}$	$-9.3 \cdot 10^{-3}$
10^{-4}	$1.1 \cdot 10^{-5}$	$1.1 \cdot 10^{-4}$	$1.1 \cdot 10^{-3}$	$-9.8 \cdot 10^{-3}$	$-9.3 \cdot 10^{-3}$
10^{-3}	$-5.7 \cdot 10^{-7}$	$-5.7 \cdot 10^{-6}$	$-5.7 \cdot 10^{-5}$	$5.1 \cdot 10^{-4}$	$4.9 \cdot 10^{-4}$
10^{-2}	$-1.2 \cdot 10^{-5}$	$-1.2 \cdot 10^{-4}$	$-1.2 \cdot 10^{-3}$	$1.1 \cdot 10^{-2}$	$1.0 \cdot 10^{-2}$
10^{-1}	$-1.6 \cdot 10^{-4}$	$-1.6 \cdot 10^{-3}$	$-1.6 \cdot 10^{-2}$	$1.4 \cdot 10^{-1}$	$1.4 \cdot 10^{-1}$

Table E.22: Obtained values for the magnetic loss tangent of the sample under test of radius 2 mm and $\mu_r' = 7$, using a reference sample with $\mu_r' = 3$ and equal radius. Permittivity is set to unity and there are no dielectric losses.

	Magnetic loss tangent of reference sample				
True value	10^{-5}	10^{-4}	10^{-3}	10^{-2}	10^{-1}
10^{-5}	$7.7 \cdot 10^{-6}$	$7.7 \cdot 10^{-5}$	$7.7 \cdot 10^{-4}$	$-7.1 \cdot 10^{-3}$	$-3.5 \cdot 10^{-3}$
10^{-4}	$7.7 \cdot 10^{-6}$	$7.7 \cdot 10^{-5}$	$7.7 \cdot 10^{-4}$	$-7.1 \cdot 10^{-3}$	$-3.5 \cdot 10^{-3}$
10^{-3}	$7.7 \cdot 10^{-6}$	$7.7 \cdot 10^{-5}$	$7.7 \cdot 10^{-4}$	$-7.1 \cdot 10^{-3}$	$-3.5 \cdot 10^{-3}$
10^{-2}	$-8.6 \cdot 10^{-6}$	$-8.6 \cdot 10^{-5}$	$-8.6 \cdot 10^{-4}$	$7.9 \cdot 10^{-3}$	$3.9 \cdot 10^{-3}$
10^{-1}	$-9.0 \cdot 10^{-5}$	$-9.0 \cdot 10^{-4}$	$-9.0 \cdot 10^{-3}$	$8.3 \cdot 10^{-2}$	$4.1 \cdot 10^{-2}$

Table E.23: Obtained values for the magnetic loss tangent of the sample under test of radius 2 mm and $\mu_r' = 7$, using a reference sample with $\mu_r' = 5$ and equal radius. Permittivity is set to unity and there are no dielectric losses.

	Magnetic loss tangent of reference sample				
True value	10^{-5}	10^{-4}	10^{-3}	10^{-2}	10^{-1}
10^{-5}	$9.2 \cdot 10^{-6}$	$9.2 \cdot 10^{-5}$	$-1.8 \cdot 10^{-2}$	$-8.3 \cdot 10^{-3}$	$-6.2 \cdot 10^{-3}$
10^{-4}	$9.2 \cdot 10^{-6}$	$9.2 \cdot 10^{-5}$	$-1.8 \cdot 10^{-2}$	$-8.3 \cdot 10^{-3}$	$-6.2 \cdot 10^{-3}$
10^{-3}	$9.2 \cdot 10^{-6}$	$9.2 \cdot 10^{-5}$	$-1.8 \cdot 10^{-2}$	$-8.3 \cdot 10^{-3}$	$-6.2 \cdot 10^{-3}$
10^{-2}	$-1.0 \cdot 10^{-5}$	$-1.0 \cdot 10^{-4}$	$2.0 \cdot 10^{-2}$	$9.3 \cdot 10^{-3}$	$7.0 \cdot 10^{-3}$
10^{-1}	$-1.1 \cdot 10^{-4}$	$-1.1 \cdot 10^{-3}$	$2.1 \cdot 10^{-1}$	$9.7 \cdot 10^{-2}$	$7.3 \cdot 10^{-2}$

Table E.24: Obtained values for the magnetic loss tangent of the sample under test of radius 2 mm and $\mu_r' = 7$, using a reference sample with $\mu_r' = 7$ and equal radius. Permittivity is set to unity and there are no dielectric losses.

	Magnetic loss tangent of reference sample				
True value	10^{-5}	10^{-4}	10^{-3}	10^{-2}	10^{-1}
10^{-5}	$1.0 \cdot 10^{-5}$	$1.0 \cdot 10^{-4}$	$1.0 \cdot 10^{-3}$	$-9.0 \cdot 10^{-3}$	$-8.6 \cdot 10^{-3}$
10^{-4}	$1.0 \cdot 10^{-5}$	$1.0 \cdot 10^{-4}$	$1.0 \cdot 10^{-3}$	$-9.0 \cdot 10^{-3}$	$-8.6 \cdot 10^{-3}$
10^{-3}	$1.0 \cdot 10^{-5}$	$1.0 \cdot 10^{-4}$	$1.0 \cdot 10^{-3}$	$-9.0 \cdot 10^{-3}$	$-8.6 \cdot 10^{-3}$
10^{-2}	$-1.1 \cdot 10^{-5}$	$-1.1 \cdot 10^{-4}$	$-1.1 \cdot 10^{-3}$	$1.0 \cdot 10^{-2}$	$9.6 \cdot 10^{-3}$
10^{-1}	$-1.2 \cdot 10^{-4}$	$-1.2 \cdot 10^{-3}$	$-1.2 \cdot 10^{-2}$	$1.0 \cdot 10^{-1}$	$1.0 \cdot 10^{-1}$

Appendix F

Tolerance tests on samples of radius 2 mm

Here we present tolerance tests on a sample of radius 2 mm.

Table F.1: Tolerance test of relative permittivity for deviating height. Sample radii are 2 mm. Errors are given in percent.

		Height h and permittivity ε_r' of reference sample							
		$h = 1.5\,\text{mm}$				$h = 1.6\,\text{mm}$			
SUT values		$\varepsilon_r' = 3$	Err.	$\varepsilon_r' = 5$	Err.	$\varepsilon_r' = 3$	Err.	$\varepsilon_r' = 5$	Err.
$h =$ 1.5 mm	$\varepsilon_r' = 3$	3.0	0.0	2.9	2.3	3.4	12.1	3.5	16.8
	$\varepsilon_r' = 5$	5.1	2.9	5.0	0.0	5.9	18.0	6.2	23.8
$h =$ 1.6 mm	$\varepsilon_r' = 3$	2.7	10.3	2.6	12.2	3.0	0.0	3.1	4.0
	$\varepsilon_r' = 5$	4.2	16.1	4.1	18.4	4.8	4.5	5.0	0.0

Table F.2: Tolerance test of dielectric loss tangent for deviating height. Sample radii are 2 mm.

		Height h and permittivity ε_r' of reference sample			
		$h = 1.5\,\text{mm}$		$h = 1.6\,\text{mm}$	
SUT values		$\varepsilon_r' = 3$	$\varepsilon_r' = 5$	$\varepsilon_r' = 3$	$\varepsilon_r' = 5$
$h = 1.5\,\text{mm}$	$\varepsilon_r' = 3$	$1.0 \cdot 10^{-3}$	$7.5 \cdot 10^{-4}$	$1.6 \cdot 10^{-3}$	$1.2 \cdot 10^{-3}$
	$\varepsilon_r' = 5$	$1.3 \cdot 10^{-3}$	$1.0 \cdot 10^{-3}$	$2.0 \cdot 10^{-3}$	$1.5 \cdot 10^{-3}$
$h = 1.6\,\text{mm}$	$\varepsilon_r' = 3$	$6.4 \cdot 10^{-4}$	$4.8 \cdot 10^{-4}$	$1.0 \cdot 10^{-3}$	$7.7 \cdot 10^{-4}$
	$\varepsilon_r' = 5$	$8.5 \cdot 10^{-4}$	$6.4 \cdot 10^{-4}$	$1.3 \cdot 10^{-3}$	$1.0 \cdot 10^{-3}$

Table F.3: Tolerance test of relative permeability for deviating height. Sample radii are 2 mm. Errors are given in percent.

		Height h and permeability μ_r' of reference sample							
		$h = 1.5\,\text{mm}$				$h = 1.6\,\text{mm}$			
SUT values		$\mu_r' = 3$	Err.	$\mu_r' = 5$	Err.	$\mu_r' = 3$	Err.	$\mu_r' = 5$	Err.
$h =$ 1.5 mm	$\mu_r' = 3$	3.0	0.0	4.1	36.4	3.1	1.7	4.2	38.5
	$\mu_r' = 5$	3.6	28.2	5.0	0.0	3.7	26.9	5.1	1.6
$h =$ 1.6 mm	$\mu_r' = 3$	2.9	1.7	4.0	33.8	3.0	0.0	4.1	35.8
	$\mu_r' = 5$	3.5	29.3	4.9	1.6	3.6	27.9	5.0	0.0

Table F.4: Tolerance test of magnetic loss tangent for deviating height. Sample radii are 2 mm.

		Height h and permeability μ_r' of reference sample			
		$h = 1.5\,\text{mm}$		$h = 1.6\,\text{mm}$	
SUT values		$\mu_r' = 3$	$\mu_r' = 5$	$\mu_r' = 3$	$\mu_r' = 5$
$h = 1.5\,\text{mm}$	$\mu_r' = 3$	$1.0 \cdot 10^{-2}$	$9.3 \cdot 10^{-3}$	$5.1 \cdot 10^{-3}$	$9.4 \cdot 10^{-3}$
	$\mu_r' = 5$	$1.1 \cdot 10^{-2}$	$1.0 \cdot 10^{-2}$	$5.6 \cdot 10^{-3}$	$1.0 \cdot 10^{-2}$
$h = 1.6\,\text{mm}$	$\mu_r' = 3$	$1.9 \cdot 10^{-2}$	$1.8 \cdot 10^{-2}$	$1.0 \cdot 10^{-2}$	$1.8 \cdot 10^{-2}$
	$\mu_r' = 5$	$1.1 \cdot 10^{-2}$	$9.9 \cdot 10^{-3}$	$5.6 \cdot 10^{-3}$	$1.0 \cdot 10^{-2}$

Table F.5: Tolerance test of relative permittivity for deviating radius. Errors are given in percent.

		Radius r and permittivity ε_r' of reference sample							
		$r = 2.0\,\text{mm}$				$r = 2.1\,\text{mm}$			
SUT values		$\varepsilon_r' = 3$	Err.	$\varepsilon_r' = 5$	Err.	$\varepsilon_r' = 3$	Err.	$\varepsilon_r' = 5$	Err.
$r =$ 2.0 mm	$\varepsilon_r' = 3$	3.0	0.0	2.9	2.3	2.9	3.8	2.8	6.2
	$\varepsilon_r' = 5$	5.1	2.9	5.0	0.0	4.9	1.9	4.8	4.8
$r =$ 2.1 mm	$\varepsilon_r' = 3$	3.1	4.1	3.0	1.6	3.0	0.0	2.9	2.5
	$\varepsilon_r' = 5$	5.4	8.2	5.3	5.1	5.2	3.1	5.0	0.0

Table F.6: Tolerance test of dielectric loss tangent for deviating radius.

		Radius r and permittivity ε'_r of reference sample			
		$r = 2.0\,\text{mm}$		$r = 2.1\,\text{mm}$	
SUT values		$\varepsilon'_r = 3$	$\varepsilon'_r = 5$	$\varepsilon'_r = 3$	$\varepsilon'_r = 5$
$r = 2.0\,\text{mm}$	$\varepsilon'_r = 3$	$1.0 \cdot 10^{-3}$	$7.5 \cdot 10^{-4}$	$9.7 \cdot 10^{-4}$	$5.7 \cdot 10^{-4}$
	$\varepsilon'_r = 5$	$1.3 \cdot 10^{-3}$	$1.0 \cdot 10^{-3}$	$1.3 \cdot 10^{-3}$	$7.6 \cdot 10^{-4}$
$r = 2.1\,\text{mm}$	$\varepsilon'_r = 3$	$1.0 \cdot 10^{-3}$	$7.7 \cdot 10^{-4}$	$1.0 \cdot 10^{-3}$	$5.8 \cdot 10^{-4}$
	$\varepsilon'_r = 5$	$1.7 \cdot 10^{-3}$	$1.3 \cdot 10^{-3}$	$1.7 \cdot 10^{-3}$	$1.0 \cdot 10^{-3}$

Table F.7: Tolerance test of relative permeability for deviating radius. Errors are given in percent.

		Radius r and permeability μ'_r of reference sample							
		$r = 2.0\,\text{mm}$				$r = 2.1\,\text{mm}$			
SUT values		$\mu'_r = 3$	Err.	$\mu'_r = 5$	Err.	$\mu'_r = 3$	Err.	$\mu'_r = 5$	Err.
$r =$ 2.0 mm	$\mu'_r = 3$	3.0	0.0	4.1	36.4	2.9	4.5	3.9	29.6
	$\mu'_r = 5$	3.6	28.2	5.0	0.0	3.4	31.7	4.7	5.3
$r =$ 2.1 mm	$\mu'_r = 3$	3.1	4.8	4.3	43.8	3.0	0.0	4.1	36.5
	$\mu'_r = 5$	3.8	24.6	5.3	5.6	3.6	28.3	5.0	0.0

Table F.8: Tolerance test of magnetic loss tangent for deviating radius.

		Radius r and permeability μ'_r of reference sample			
		$r = 2.0\,\text{mm}$		$r = 2.1\,\text{mm}$	
SUT values		$\mu'_r = 3$	$\mu'_r = 5$	$\mu'_r = 3$	$\mu'_r = 5$
$r = 2.0\,\text{mm}$	$\mu'_r = 3$	$1.0 \cdot 10^{-2}$	$9.3 \cdot 10^{-3}$	$5.0 \cdot 10^{-3}$	$9.1 \cdot 10^{-3}$
	$\mu'_r = 5$	$1.1 \cdot 10^{-2}$	$1.0 \cdot 10^{-2}$	$5.5 \cdot 10^{-3}$	$9.8 \cdot 10^{-3}$
$r = 2.1\,\text{mm}$	$\mu'_r = 3$	$2.0 \cdot 10^{-2}$	$1.9 \cdot 10^{-2}$	$1.0 \cdot 10^{-2}$	$1.8 \cdot 10^{-2}$
	$\mu'_r = 5$	$1.1 \cdot 10^{-2}$	$1.0 \cdot 10^{-2}$	$5.6 \cdot 10^{-3}$	$1.0 \cdot 10^{-2}$

Table F.9: Tolerance test of relative permittivity for deviating placement. Sample radii are 2 mm. Errors are given in percent.

		Displacement from center x and permittivity ε'_r of reference sample							
		$x = 0$ mm				$x = 1$ mm			
SUT values		$\varepsilon'_r = 3$	Err.	$\varepsilon'_r = 5$	Err.	$\varepsilon'_r = 3$	Err.	$\varepsilon'_r = 5$	Err.
$x =$ 0 mm	$\varepsilon'_r = 3$	3.0	0.0	2.9	2.3	3.0	0.3	2.9	2.1
	$\varepsilon'_r = 5$	5.1	2.9	5.0	0.0	5.2	3.3	5.0	0.3
$x =$ 1 mm	$\varepsilon'_r = 3$	3.0	0.3	2.9	2.6	3.0	0.0	2.9	2.4
	$\varepsilon'_r = 5$	5.1	2.6	5.0	0.3	5.2	3.0	5.0	0.0

Table F.10: Tolerance test of dielectric loss tangent for deviating placement. Sample radii are 2 mm.

		Displacement from center x and permittivity ε'_r of reference sample			
		$x = 0$ mm		$x = 1$ mm	
SUT values		$\varepsilon'_r = 3$	$\varepsilon'_r = 5$	$\varepsilon'_r = 3$	$\varepsilon'_r = 5$
$x = 0$ mm	$\varepsilon'_r = 3$	$1.0 \cdot 10^{-3}$	$7.5 \cdot 10^{-4}$	$1.4 \cdot 10^{-3}$	$7.5 \cdot 10^{-4}$
	$\varepsilon'_r = 5$	$1.3 \cdot 10^{-3}$	$1.0 \cdot 10^{-3}$	$1.9 \cdot 10^{-3}$	$1.0 \cdot 10^{-3}$
$x = 1$ mm	$\varepsilon'_r = 3$	$7.0 \cdot 10^{-4}$	$5.2 \cdot 10^{-4}$	$1.0 \cdot 10^{-3}$	$5.2 \cdot 10^{-4}$
	$\varepsilon'_r = 5$	$1.3 \cdot 10^{-3}$	$10.0 \cdot 10^{-4}$	$1.9 \cdot 10^{-3}$	$1.0 \cdot 10^{-3}$

Table F.11: Tolerance test of relative permeability for deviating placement. Sample radii are 2 mm. Errors are given in percent.

		Displacement from edge x and permeability μ'_r of reference sample							
		$x = 0$ mm				$x = 1$ mm			
SUT values		$\mu'_r = 3$	Err.	$\mu'_r = 5$	Err.	$\mu'_r = 3$	Err.	$\mu'_r = 5$	Err.
$x =$ 0 mm	$\mu'_r = 3$	3.0	0.0	4.1	36.4	2.8	7.2	3.7	23.9
	$\mu'_r = 5$	3.6	28.2	5.0	0.0	3.3	33.8	4.5	9.7
$x =$ 1 mm	$\mu'_r = 3$	3.2	8.1	4.5	48.9	3.0	0.0	4.0	34.8
	$\mu'_r = 5$	3.9	21.1	5.6	11.0	3.6	27.5	5.0	0.0

Table F.12: Tolerance test of magnetic loss tangent for deviating placement. Sample radii are 2 mm.

		Displacement from edge x and permeability μ_r' of reference sample			
		$x = 0\,\mathrm{mm}$		$h = 1\,\mathrm{mm}$	
SUT values		$\mu_r' = 3$	$\mu_r' = 5$	$\mu_r' = 3$	$\mu_r' = 5$
$x = 0\,\mathrm{mm}$	$\mu_r' = 3$	$1.0 \cdot 10^{-2}$	$9.3 \cdot 10^{-3}$	$3.3 \cdot 10^{-3}$	$9.0 \cdot 10^{-3}$
	$\mu_r' = 5$	$1.1 \cdot 10^{-2}$	$1.0 \cdot 10^{-2}$	$3.6 \cdot 10^{-3}$	$9.7 \cdot 10^{-3}$
$x = 1\,\mathrm{mm}$	$\mu_r' = 3$	$3.0 \cdot 10^{-2}$	$2.8 \cdot 10^{-2}$	$1.0 \cdot 10^{-2}$	$2.7 \cdot 10^{-2}$
	$\mu_r' = 5$	$1.1 \cdot 10^{-2}$	$1.0 \cdot 10^{-2}$	$3.8 \cdot 10^{-3}$	$1.0 \cdot 10^{-2}$

Index